Casimir Effect
in the Presence of Weak Gravity

Casimir-Effekt in Anwesenheit schwacher Gravitation

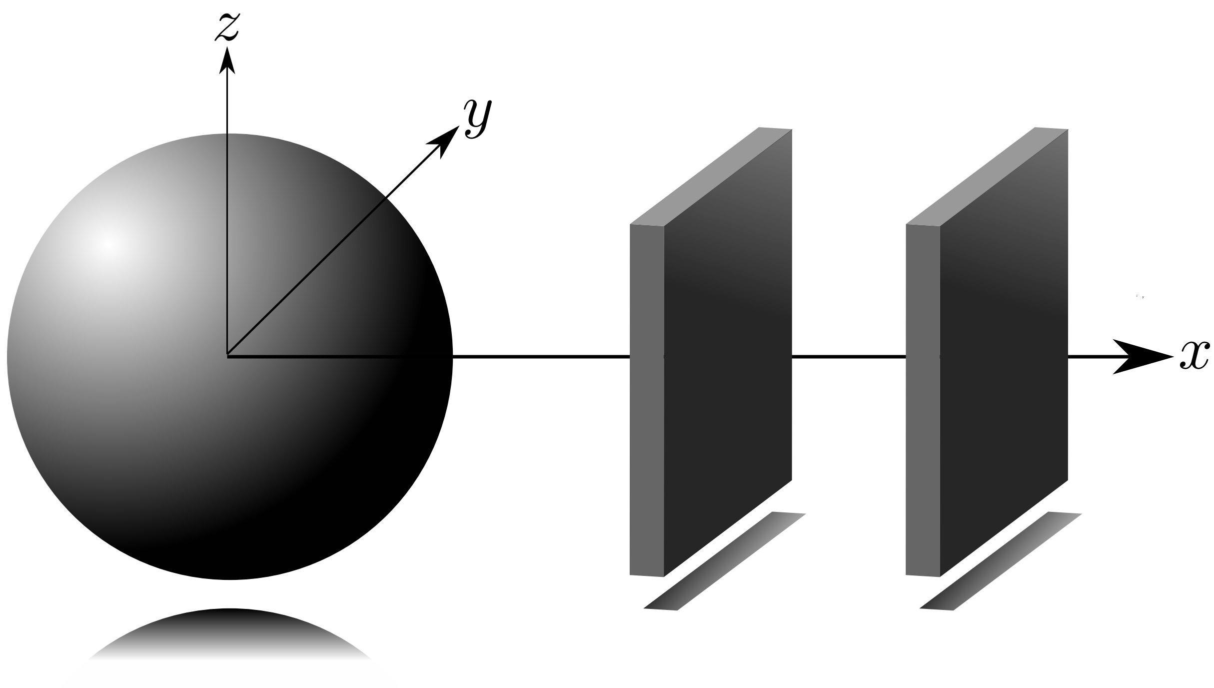

Master Thesis
written by
Lukas Martin Buß

TU Kaiserslautern,
Department of Physics,
67663 Kaiserslautern,
Germany

Examiner: Priv.-Doz. Dr. Axel Pelster
Prof. Dr. Michael Fleischhauer

October 3, 2022

This page intentionally left blank.

Declaration of Authenticity

I hereby declare that I have written the thesis with the title "Casimir Effect in the Presence of Weak Gravity" independently and without outside assistance, that I did not use any other sources apart from the ones stated in the bibliography and that I have clearly cited all passages in my work that were taken from other sources. This term paper has never been previously submitted in its current or similar form in any other course and/or degree programme [1].

Done at Kaiserslautern, October 3, 2022

Lukas Martin Buß

[1] https://www.soziologie.uni-muenchen.de/studium-und-lehre/pruefungen1/bachelor/declaration_authenticity_eng.pdf visited on 09/25/2022.

Abstract

The Casimir effect describes how quantum vacuum fluctuations produce an attractive force between two opposing, perfectly conducting plates. The Casimir force is inversely proportional to the fourth power of the plate distance and is relevant for applications in nanophotonics, nanomechanics, and chemistry [17, 24]. Studies using the Klein-Gordon theory have already shown that the Casimir effect is suitable for investigating how general relativity affects quantum electrodynamics [39, 47]. An extensive literature search revealed that the Casimir effect has not yet been investigated for electromagnetic waves based on the Maxwell theory in weak gravity.

For this purpose, a new approach is introduced to apply time-independent perturbation theory to Maxwell's equations in the presence of weak gravity. The Poincaré–Lindstedt method for solving ordinary differential equations is extended to the partial differential equations of the perturbative calculation and reproduces the results of the Klein-Gordon theory. Within this thesis, three different setups are studied, which differ by the orientation of the two plates relative to the source of gravity. Reducing the general approach to the Schwarzschild spacetime yields that the Casimir forces for all three setups can be obtained by replacing the respective lengths in the flat case with the corresponding general relativistic ones, namely the proper plate distance and the proper surface area. In literature, this heuristic rule has been found for the initial setup within the context of the Klein-Gordon theory [39, 47].

Furthermore, weak gravity's effects correspond to an effective flat model by replacing the vacuum between the plates with an anisotropic medium, whose exact characteristics depend on the chosen setup. The first-order charge and current densities must also be considered effective ones, which generally do not vanish on or between the plates.

If the source of weak gravity is allowed to rotate slowly, the Casimir energy of two setups does not change compared to the case where the source did not rotate.

Finally, initial estimates show that the measurement of these gravitational effects is challenging [47]. Therefore, two possible experimental setups are outlined, which should yield experimental evidence of the calculated effects with today's technical possibilities.

Zusammenfassung

Der Casimir-Effekt beschreibt, wie Quantenvakuumfluktuationen eine anziehende Kraft zwischen zwei gegenüberliegenden, perfekt leitenden Platten erzeugen. Die Casimir-Kraft ist umgekehrt proportional zur vierten Potenz des Plattenabstands und für Anwendungen in der Nanophotonik, Nanomechanik und Chemie unerlässlich [17, 24]. Einige Abhandlungen haben mit Hilfe der Klein-Gordon-Theorie bereits gezeigt, dass der Casimir-Effekt dazu geeignet ist, um den Einfluss allgemein-relativistischer Effekte auf die Quantenelektrodynamik zu untersuchen [39, 47]. Eine umfangreiche Literaturrecherche ergab, dass der Casimir-Effekt auf der Grundlage der Maxwell-Theorie in schwacher Gravitation bisher nicht untersucht wurde.

Zu diesem Zweck wird im Rahmen dieser Arbeit ein neuer Ansatz zur Untersuchung des Casimir-Effekts mittels der Maxwell-Theorie in Gegenwart schwacher Gravitation vorgestellt, der auf der Anwendung zeitunabhängiger Störungstheorie basiert. Dabei wird die Poincaré-Lindstedt-Methode, die zur störungstheoretischen Lösung gewöhnlicher Differenzialgleichungen geeignet ist, auf die auftretenden partiellen Differenzialgleichungen angewandt, um die Ergebnisse der Klein-Gordon-Theorie zu reproduzieren. Im Rahmen dieser Arbeit werden drei verschiedene Versuchsanordnungen genauer betrachtet, die sich durch die Orientierung der beiden Platten relativ zur Gravitationsquelle unterscheiden. Reduziert man den allgemeinen Ansatz auf die Schwarzschild-Raumzeit, so erhält man die Casimir-Kräfte für alle drei Anordnungen, indem man die jeweiligen Längen, in der für den flachen Fall gültigen Formel, durch die entsprechenden allgemein-relativistischen Längen ersetzt. Diese heuristische Regel war zuvor nur für eine der Versuchsanordnungen im Rahmen der Klein-Gordon-Theorie gefunden worden [39, 47].

Darüber hinaus kann die Wirkung der schwachen Gravitation in einem effektiven flachen Modell berücksichtigt werden, indem das Vakuum zwischen den Platten durch ein anisotropes Medium ersetzt wird, dessen genaue Eigenschaften von der gewählten Anordnung abhängen. Die Ladungs- und Stromdichten erster Ordnung müssen ebenfalls als effektive Größen betrachtet werden, die im Allgemeinen auf oder zwischen den Platten nicht verschwinden.

Erlaubt man der Quelle der schwachen Gravitation langsam zu rotieren, so ändert sich die Casimir-Energie zweier Aufbauten nicht im Vergleich zu dem Fall, in dem die Quelle nicht rotiert.

Da die Messung von Gravitationseffekten heutzutage eine Herausforderung darstellt, werden zwei vielversprechende Versuchsaufbauten skizziert [47]. Anhand dieser sollte ein experimenteller Nachweis der zu erwartende Effekte mit den heutigen technischen Messgenauigkeiten möglich sein.

This page intentionally left blank.

Contents

1. Introduction

At the beginning of this thesis, there is a historical overview of how the importance of the Casimir effect evolved from a type of van der Waals force to its relevance today. Technical applications, already of inestimable value today, deserve special attention. From a theoretical point of view, the investigation of the Casimir effect, especially in a gravitational environment, is fascinating and pushes the limits of what is experimentally possible nowadays. Gravity is the weakest of the four fundamental forces, challenging to include in any theoretical framework and even harder to measure [3, 24, 39, 47].
The introduction ends with the organization of this thesis, which briefly highlights the individual chapters and how they relate to each other.

1.1. Historical overview

According to Casimir's historical review, the physical origin of the effect named after him could be traced back to the early 19th century investigating colloidal suspensions, which were necessary for manufacturing lamps, cathode ray tubes, and other things [4]. Verwey and Overbeek achieved the first breakthrough, and one can summarize the physical part as follows [51]: Within a suspension, two particles push away from each other due to the Pauli repulsion, and for larger distances, there is an attraction between them based on the well-known van der Waals force. The advent of quantum mechanics revealed the mysteries of the van der Waals force, previously described only as a force between spontaneously induced dipoles. Consider a simple Hamiltonian for two electrically neutral particles interacting via the Van der Waals potential, the ground state energy for two electrostatic induced dipoles is given by [22, eq. (3.30)]

$$E \approx -\frac{6\hbar\bar{\omega}_{A,B}}{(4\pi\varepsilon_0)^2\, d^6}\alpha_A\alpha_B \ , \tag{1.1}$$

where $\alpha_{A,B}$ denotes the static polarizabilities respectively, $\hbar\bar{\omega}_{A,B}$ is an averaged ionization energy, ε_0 stands for the vacuum permittivity, $\hbar$ labels the reduced Planck constant, and d is the distance between the particles. It is admirable that this purely quantum electrostatic approach leads to such a simple result. However, for unique experimental setups, it could be shown by performing several experiments that the van der Waals interaction decreased more rapidly than $1/d^6$. Overbeek himself explained this discrepancy between experiment and theory. He pointed out that forces would need a finite time to propagate through space. This retardation, in the end, was the beginning of the work of Casimir and Polder. One must notice that the theory of quantum electrodynamics (QED) was new, and several techniques we use today to deal with divergences were unknown, e.g., regularization and renormalization. Thus, the treatment of the upcoming divergences was mathematically sloppy, and the calculation as a whole was „rather unwieldy“, as Evgeny Lifshitz summarized [32]. The result they got by adding the interaction of the quantized radiation field in the vacuum state for the two concerned particles was [4, eq. (4)]

$$E = -\frac{23\hbar c}{4\pi d^7}\alpha_A\alpha_B \ , \tag{1.2}$$

where c is the speed of light in vacuum. This formula agrees with the experimental data [4]. Although Lifshift's comment was much later, Casimir was aware of this issue and how they achieved their results. During a visit to Copenhagen, he met Niels Bohr and told him about his work. After Bohr's famous remark that this „must have something to do with the zero-point energy“, Casimir started an original approach [4, p. 6]. He investigated the zero-point energy, „the sum over all the half quanta of electromagnetic vibrations in a cavity“ [4, p. 6]. Casimir wrote them down in the case with and without the cavity and compared them. After having reproduced the results of the Casimir-Polder energy (1.1), he applied this method to two perfectly conducting metal plates with surface area A and obtained the Casimir energy [26, eq. (7.699)]

$$E_C = -\frac{\pi^2\hbar c A}{720 d^3} \ , \tag{1.3}$$

and the according attractive force [26, eq. (7.700)]

$$F_C = -\frac{\pi^2\hbar c A}{240 d^4} \ , \tag{1.4}$$

which represent the basis of this thesis.
Heuristically, the presence of the force can be understood by comparing the mode densities inside two different cavities, as shown in figure 1.1, and has been verified by innovative experiments [29]. Usually, a plane-plane geometry is insufficient because it is difficult to ensure the parallel alignment of the plates [48]. Instead, a plane-sphere geometry does not have this issue. The Casimir force for such a geometry, where R denotes the sphere's radius, is modified to [26, eq. (7.701)]

$$F_C^{\text{plane-sphere}} = -\frac{\pi^3\hbar c R}{360 d^3} \ . \tag{1.5}$$

Today it is possible to measure these forces with a deviation of around one percent. To this end, a sphere with radius $R = 196\ \mu$m and separations d between 0.1 to 0.9 μm are used. In this experiment, forces of the magnitude of 10^{-10} N appear [36]. According to these remarkable results and the compliance with theory, one could claim that „the existence of electromagnetic zero-point energy in a vacuum has been established beyond doubt“ [4, p. 7]. Nevertheless, to measure effects beyond the Standard Model of particle physics, in the framework of the Casimir effect, it is necessary to know the detection limit. An atomic force microscope typically used in Casimir experiments, as shown in figure 1.2, irrespective of the concrete operation mode, can resolve forces up to 10^{-13} N [31].

In the last century, physics evolved and the Casimir effect, initially a kind of van der Waals interaction, became a multidisciplinary subject. One of the most critical areas of application is found in today's micro- and nanotechnology in the use of microelectromechanical systems (MEMS) [25]. They form an indispensable technical basis for modern, innovative approaches to solutions in electronics. Many applications would not be economically feasible without MEMS. They make the application of electronic devices in automotive, medicine, safety and measurement technology, sports, logistics, and entertainment much more versatile, convenient, and intelligent [17]. A typical

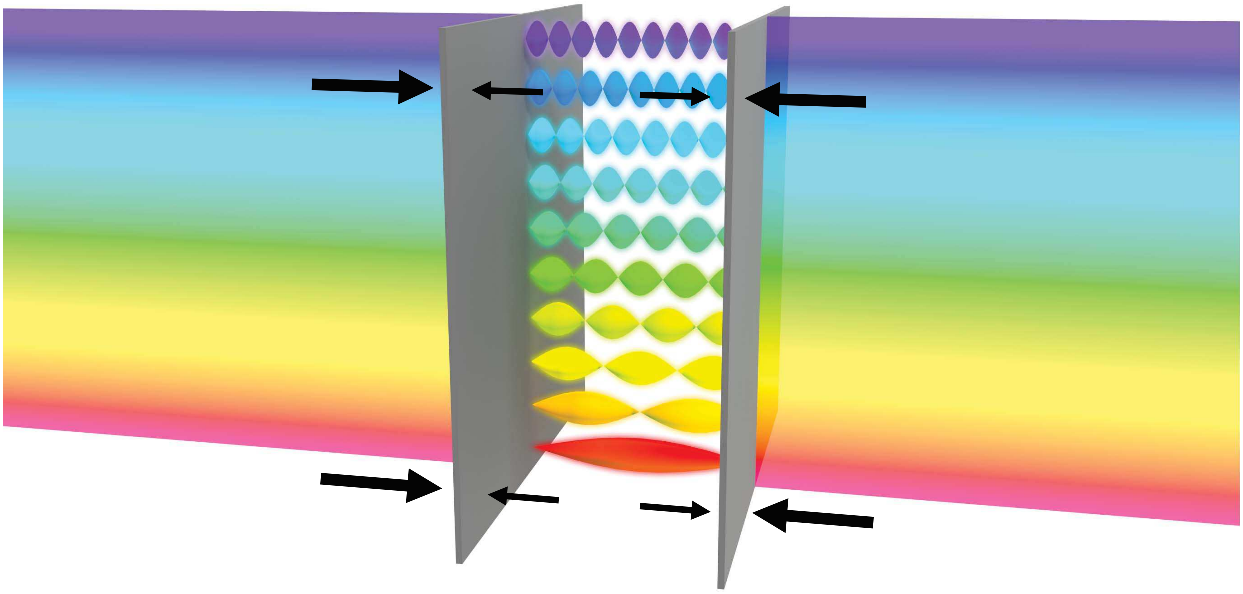

Figure 1.1.: *„In a quantum vacuum, free space is filled with electromagnetic fluctuations at all wavelengths. But in a Casimir cavity, typically composed of two perfectly conducting plates, boundary conditions allow for the existence of fluctuations only at half-integer wavelengths. That constraint lowers the energy density in the cavity relative to the energy density outside of it and produces a net attractive interaction between the plates— provided the plates are made from the same material." [48, quote & figure].*

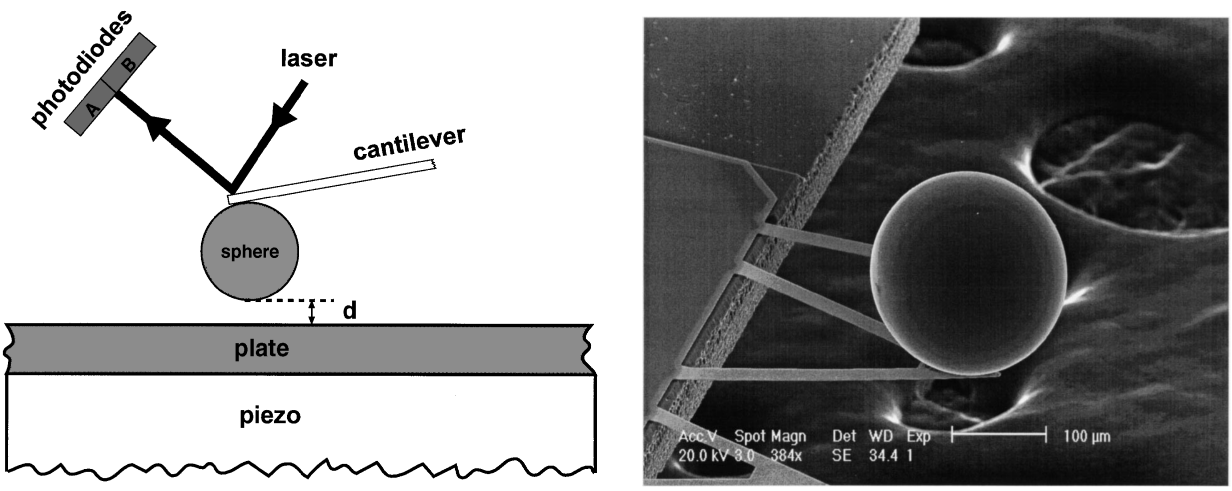

(a) *Schematic diagram of the experimental setup.*

(b) *Scanning electron microscope image of the metallized sphere mounted on an AFM cantilever.*

Figure 1.2.: *Experimental setup for measuring the Casimir force, using a plane-sphere geometry. Application of voltage to the piezo results in the movement of the plate towards the sphere. The experiments were done at a pressure of 6.6 Pa and at room temperature [36].*

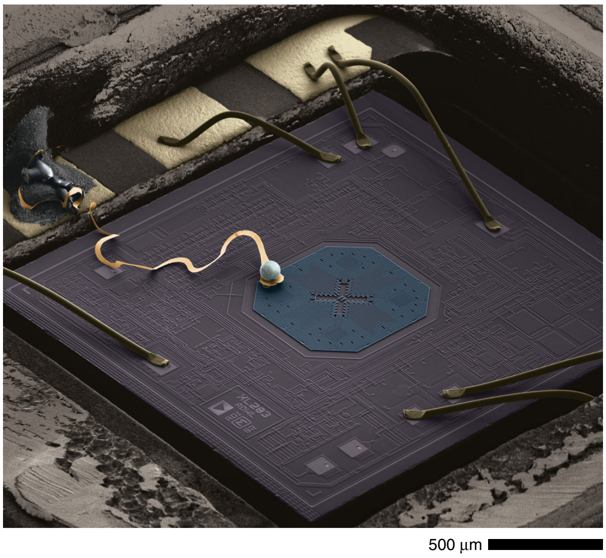

(a) *Colorized Scanning electron microscope (SEM) image of an ADXL203 sensor [49]*

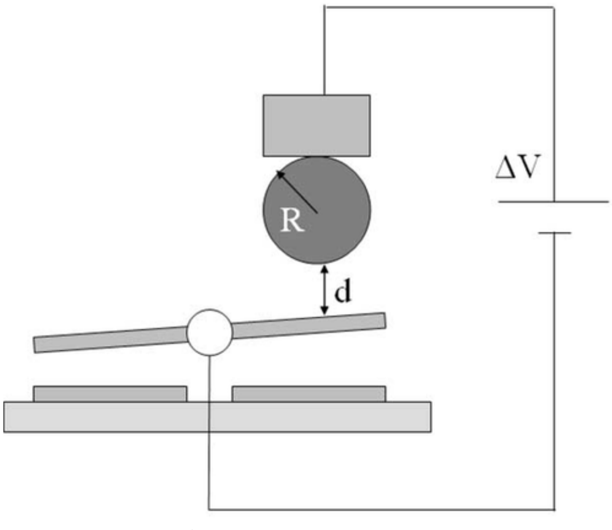

(b) *„MEMS Casimir force detection setup. Schematic of the experiment (not to scale) and scanning electron micrographs of the micromachined torsional device used for the measurement of the Casimir force with a closeup of one of the torsional rods anchored to the substrate. As the metallic sphere approaches the top plate, the Casimir force causes a rotation of the torsional rod“ [9, quote & figure].*

Figure 1.3.: *Microelectromechanical systems (MEMS).*

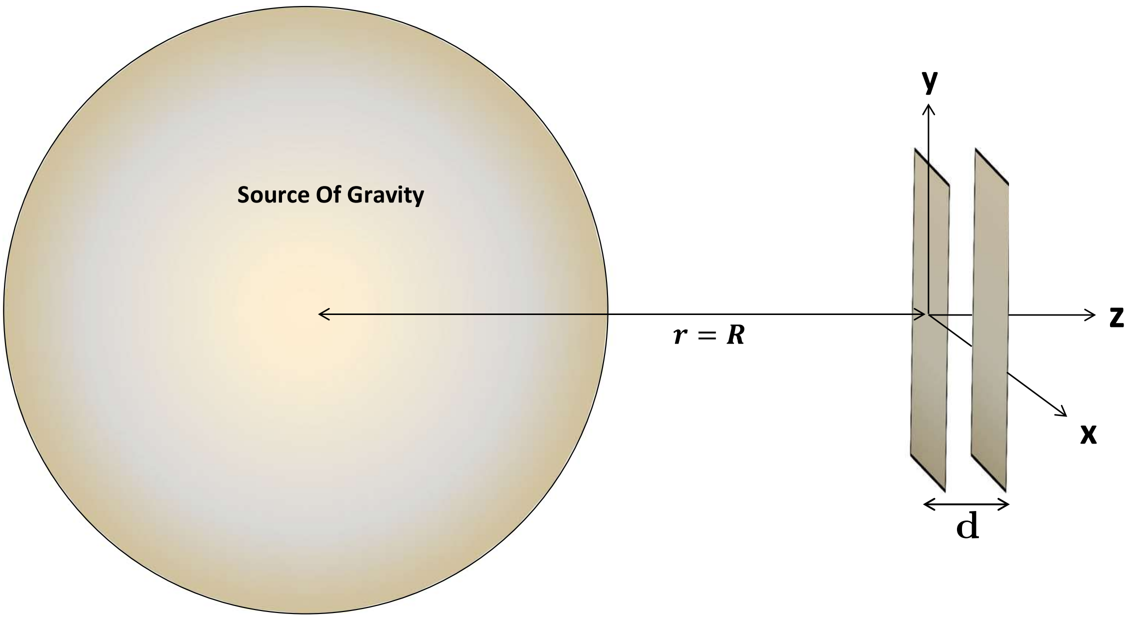

Figure 1.4.: *Schematic experimental setup assumed in the Klein-Gordon calculation from Nazari and Sorge with minor changes due to the different system of units [39]. The metal plates are far from the center of mass, therefore in a regime of weak gravity. The Cartesian z-axis coincides with the spherical r-axis in the equatorial plane, and the plates are separated by a small distance $d \ll R$.*

application of MEMS is measuring acceleration [48]. Acceleration sensors are already an essential component in some everyday products. One is detecting the horizontal or vertical state known from smartphones when rotating the display. Here, the screen display rotates with it. Another example, are the acceleration sensors in hard disks detecting when the notebook is dropped. The read/write head is automatically moved to the park position before the device hits the floor. In the park position, the read/write head is prevented from crashing into the surface of the rotating magnetic disk, scratching it, and destroying the data. Many applications of MEMS are not new. They have been used before in measurement, weapons, and space systems. Robustness, long-term stability, and consistent product quality are features of MEMS. The small size, lower price, and low power requirements are among their advantages compared to the previous applications [24]. The next step will be nanoelectromechanical systems (NEMS), which can also use quantum effects [17]. Attractive forces between the individual components become even stronger on smaller length scales, and active effort must be made to protect the components from collision or, in general, to maintain correct functionality [48].

The aim of this thesis is closely interwoven with previous investigations that used the Klein-Gordon theory [3, 39, 47]. These are just approximations to the correct results because the massless Klein-Gordon equation does not describe photons correctly since their spin is one instead of zero. So, they solve just a scalar field theory instead of a vectorial one, which is much more complicated. Literature research has revealed that no one has yet solved the Maxwell theory belonging to the Casimir effect, as shown in figure 1.4. This issue can be recognized by comparing the formula generated by Klein-Gordon theory [in SI units 47, eq. (6.24)]

$$F_C = -\left(1 - \frac{2}{3}\gamma d_p\right)\frac{\hbar c \pi^2 A_p}{480 d_p^4} \ . \tag{1.6}$$

After setting the parameter $\gamma = M/R^2 = 0$, which describes the ratio of the mass of the source of gravity M and the distance between that and the Casimir setup R, and identify the relativistically based proper lengths (and areas) with their non-relativistic counterparts $d_p = d$, $A_p = A$, to

$$F_C = -\frac{\hbar c \pi^2 A}{480 d^4} \ , \tag{1.7}$$

with the one derived by Casimir (1.4). It is noticeable that the two formulae differ by a factor of 2 due to the two types of polarization of the light, which does not occur in the scalar theory.
In particular, no comparisons between different orientations of the Casimir setups, as shown in figure 1.5, have been theoretically investigated using exactly that perturbation theory approach, although this is a fascinating question. Even if an effect like rotation or the non-constancy of the gravitational field is only measurable in one setup directly using second-order corrections, that are sufficiently small. By comparing two different experimental setups, it would be possible that such effects are already measurable in first order. This is, of course, more a question of the concrete experimental setup and its realization. However, it is an essential question because it concerns measurements at the edge of the current detection limits. For this reason, this thesis aims to use Maxwell's equations to describe electromagnetic waves inside a cavity next to a source of weak gravity. The effects that occur and change the Casimir energies, whether the gravitation source rotates or not, are explained in more detail.

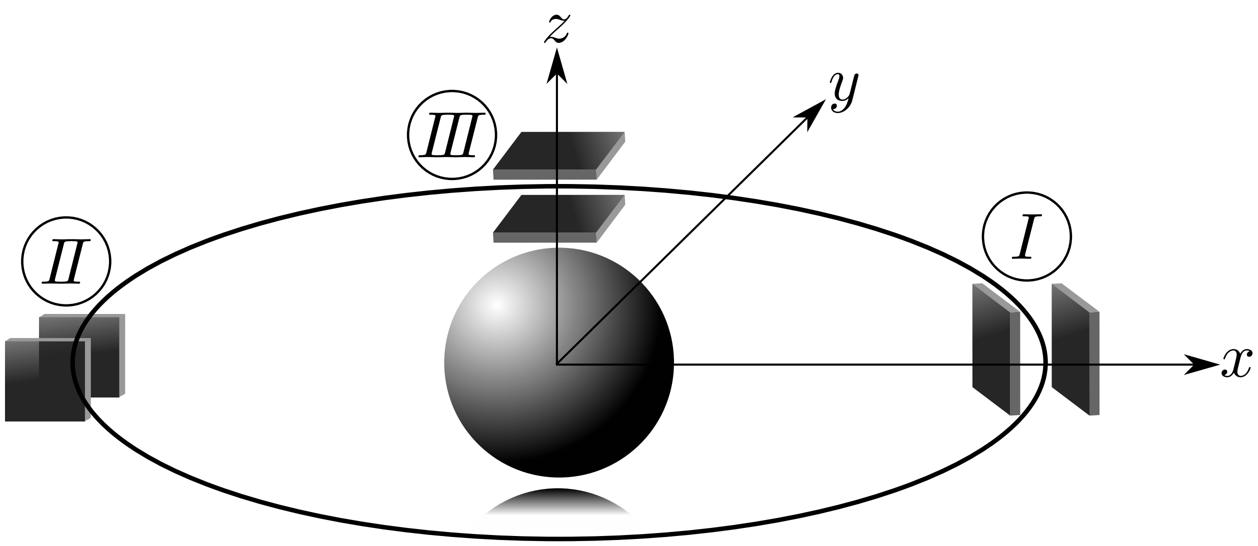

Figure 1.5.: *Three Casimir setups on a circular orbit in the equatorial plane next to a non-rotating, uncharged source of weak gravity. The setups are rotated around 90 degrees to each other around one of the coordinate axes. There is a rotation symmetry in the flat spacetime, and all three Casimir setups would have the same Casimir energy. In the general relativistic case, the spherical symmetry of the source of gravity breaks this symmetry for the electromagnetic modes. Therefore, the three setups will not have the same Casimir energy. The surface normal of setup I is parallel to the x-axis. The other two setups have a perpendicular surface normal compared to the x-axis. So, it is reasonable to assume that the first arrangement differs fundamentally from the other two because the direction of the gravitational force lies in the xy-plane in general. Indeed, the calculations will show that this assumption is correct. Although all three gravity-corrected dispersion relations will be the same, the related Casimir energies are not equal. Setups II and III show an increase in the Casimir energy in the regime of weak gravity. The first setup has a decreased Casimir energy. Degeneracy of the Casimir energies for the second and third setup occurs as predicted. Certainly, we assume that all three setups are positioned at $x = R$, $y = z = 0$. This is possible without loss of generality due to the rotational symmetry of the metric. Then the gravitational force is parallel to the x-axis. Moreover, we assume that the Casimir setups are fixed at this position, so they have zero velocity, and therefore special relativistic effects will not occur.*
Allowing the source of gravity to rotate slowly around the z-axis, while a description by the Kerr spin parameter a is viable, yields the Slow-Rotation Approximation. The dispersion relation of setup II is not trivial, and some calculation issues occur. However, the Casimir energies of setups I and III remain compared to the results of a non-rotating source of gravity. Although the source of gravity is rotating, there is no effect. Presumably, this fact is related to the direction of the surface normal to the angular momentum of the source of gravity. It shows up that these vectors are perpendicular in the case of the unaffected setups.

1.2. Organization of the thesis

This thesis is structured as follows:

In chapter 2, the Casimir effect in Minkowski spacetime will be derived as found in H. Kleinert's book [26]. For this purpose, all necessary calculations are carried out, and special features are explained. Close attention is paid to the regularization of the occurring divergences.

Chapter 3 is used as a brief introduction to Einstein's theory of general relativity. Here especially, the importance of the metric and the covariant derivative is to be emphasized. The chapter is firmly based on the book by C. W. Misner, K. S. Throne, and J. A. Wheeler [35].

Chapter 4 is devoted to how Maxwell's theory can be combined with general relativity. The more precise Maxwell-Einstein theory will be mentioned. Making a few assumptions, Maxwell's equations in curved spacetime are the equations that have to be solved in this thesis.

To prepare the perturbation theory approach to Maxwell's equations in curved spacetime, which has not been done so far, in chapter 5.1, the metric of a Schwarzschild spacetime is divided into a flat (Minkowski) and a perturbed part. Because the Casimir setups are easier to describe in Cartesian coordinates, the transformations are also done for the metric.

Then time-independent perturbation theory is applied to Maxwell's equations in curved spacetime in chapter 5.2. In the zeroth-order, the Minkowski spacetime Maxwell's equations occur, as explained in chapter 2. In the first order, inhomogeneous differential equations are obtained, given exclusively by the electromagnetic fields of the zeroth order.

Chapter 6 solves the differential equations that arise for different Casimir setups, which have zero velocity and are all fixed at the same position. The correct perturbatively usage of secular terms is presented to find suitable solutions. The results, especially the gravitational affected Casimir energies and forces, are discussed in section 6.5. Besides the the Casimir effect, the significant result of this chapter is that a Poincaré–Lindstedt method, which mainly applies to ordinary differential equations, is successfully applied to a partial differential equation.

A first extension of the model describing Casimir setups in Schwarzschild spacetime is using the so-called Slow-Rotation Approximation. The source of gravity is now allowed to rotate slowly around the z-axis. The calculations are carried out in chapter 7 for the three setups already provided in chapter 6.

The conclusion and outlook of this thesis are presented in chapters 8 and 9.

The appendix introduces the upcoming of secular terms in perturbation theory A and derives the Casimir energy with different regularization methods B. In addition, an expansion of the determinant of the sum of two matrices using elementary symmetric functions is shown in C. The appendix is completed by a short formulary that provides the most important formulae that are not elementarily D.

This page intentionally left blank.

2. The Casimir effect for two ideal-metal plates

First, a derivation of the Casimir effect in the flat (Minkowskian) case is shown. Therefore, the introduction of necessary utilities like regularization is given. In order to analyze the effect, it is auxiliary to consider the most straightforward setup, built of two perfectly conducting plane-parallel metal plates with surface area A at a distance d, see figure 2.1. To this end, suppose the plates are located at $x = 0$ and $x = d$, and the thickness of the plates is negligible. For this purpose, Maxwell's equations have to be solved.

2.1. Maxwell theory in confined geometries

The differential form of Maxwell's equations in SI units is given by

$$\boldsymbol{\nabla} \cdot \mathbf{E} = \frac{\rho}{\varepsilon_0} \, , \tag{2.1}$$

$$\boldsymbol{\nabla} \cdot \mathbf{B} = 0 \, , \tag{2.2}$$

$$\boldsymbol{\nabla} \times \mathbf{E} = -\frac{\partial \mathbf{B}}{\partial t} \, , \tag{2.3}$$

$$\boldsymbol{\nabla} \times \mathbf{B} = \mu_0 \left(\mathbf{j} + \varepsilon_0 \frac{\partial \mathbf{E}}{\partial t} \right) \tag{2.4}$$

with the nabla operator $\boldsymbol{\nabla} = \left(\frac{\partial}{\partial x}, \frac{\partial}{\partial y}, \frac{\partial}{\partial z} \right)$ in Cartesian coordinates, the electric field $\mathbf{E}$, the magnetic induction field $\mathbf{B}$, the electric charge density ρ, the electric current density $\mathbf{j}$, the permittivity of free space ε_0, the permeability of free space μ_0, and the speed of light $c = \frac{1}{\sqrt{\varepsilon_0 \mu_0}}$. It is possible to obtain for both electromagnetic fields $\mathbf{E}$ and $\mathbf{B}$ a wave equation by combining Maxwell's equations (2.1)–(2.4) using theorems of vector calculus:

$$\Box \mathbf{E} = \frac{1}{c^2} \frac{\partial^2 \mathbf{E}}{\partial t^2} - \nabla^2 \mathbf{E} = -\partial_t \mathbf{j} - \boldsymbol{\nabla} \frac{\rho}{\varepsilon_0} \, , \tag{2.5}$$

$$\Box \mathbf{B} = \frac{1}{c^2} \frac{\partial^2 \mathbf{B}}{\partial t^2} - \nabla^2 \mathbf{B} = \mu_0 \boldsymbol{\nabla} \times \mathbf{j} \, . \tag{2.6}$$

After we restrict to the vacuum case with $\rho = \mathbf{j} = 0$, the inhomogeneous Maxwell's equations reduce to homogeneous wave equations:

$$\Box \mathbf{E} = 0 \, , \tag{2.7}$$

$$\Box \mathbf{B} = 0 \, . \tag{2.8}$$

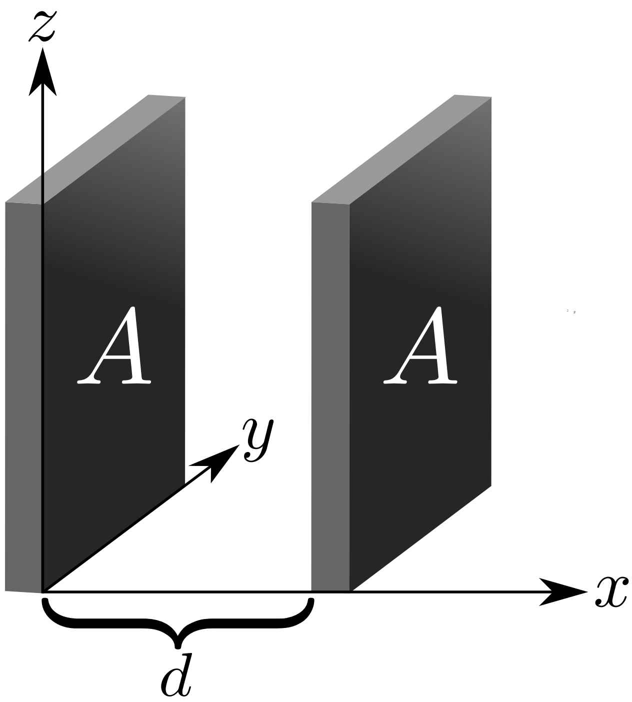

Figure 2.1.: *Setup is similar to setup I figure 1.5 for the Casimir effect: Two plane-parallel ideal-metal plates of surface area A at distance d. The thickness of the plates is exaggerated and is assumed to be negligible.*

Both equations must be fulfilled at the same time. Solutions, like plane waves, must accomplish the interface conditions, namely [41, eqs. (2.187), (2.188)]

$$\mathbf{e}_x \cdot \mathbf{B} = 0, \quad \text{for } x = 0 \text{ and } x = d\,, \tag{2.9}$$

$$\mathbf{e}_x \times \mathbf{E} = 0, \quad \text{for } x = 0 \text{ and } x = d\,. \tag{2.10}$$

Accordingly, the boundary value problem (2.7)-(2.10) gives rise to two independent classes of standing wave solutions. The corresponding transversal wave vector reads $\mathbf{k}_\perp = k_y \mathbf{e}_y + k_z \mathbf{e}_z$ and leads to $\mathbf{k}_\perp \cdot \mathbf{r} = k_y y + k_z z \equiv \mathbf{k}_\perp \cdot \mathbf{r}_\perp$.

- Transversal electric (TE) modes, i.e. $\mathbf{e}_x \cdot \mathbf{E} = 0$ [41, eqs. (2.189), (2.190)]:

$$\begin{aligned} \mathbf{E}\,(t,x,y,z) &= \mathrm{N}_{\mathrm{TE}} \mathrm{i}\omega \sin(k_x x) \mathbf{e}_x \times \mathbf{k}_\perp \exp(\mathrm{i}\,[k_y y + k_z z - \omega t])\,, \\ \mathbf{B}\,(t,x,y,z) &= \mathrm{N}_{\mathrm{TE}} \left[\mathrm{i}k_\perp^2 \sin(k_x x) \mathbf{e}_x - k_x \cos(k_x x) \mathbf{k}_\perp\right] \exp(\mathrm{i}\,[k_y y + k_z z - \omega t])\,. \end{aligned} \tag{2.11}$$

  Due to the interface conditions from equations (2.9) and (2.10) the x-component of the wave vector $\mathbf{k}$ has discrete values

$$0 = \sin(k_x x)\Big|_{x=0} = \sin(k_x x)\Big|_{x=d} \quad \Longrightarrow \quad k_x = \frac{\pi}{d} n, \quad n = 1, 2, 3, \ldots \tag{2.12}$$

Note that $n = 0$, more precisely $k_x = 0$, is not allowed since the electric field would vanish but the magnetic would not, which contradicts Faraday's law (2.3).

- Transversal magnetic (TM) modes, i.e. $\mathbf{e}_x \cdot \mathbf{B} = 0$ [41, eqs. (2.192), (2.193)]:

$$\begin{aligned} \mathbf{B}(t,x,y,z) &= \mathrm{N}_{\mathrm{TM}} \frac{\omega}{c^2} \cos(k_x x) \mathbf{e}_x \times \mathbf{k}_\perp \exp(\mathrm{i}\,[k_y y + k_z z - \omega t]) \ , \\ \mathbf{E}(t,x,y,z) &= \mathrm{N}_{\mathrm{TM}} \left[\mathrm{i} k_x \sin(k_x x) \mathbf{k}_\perp - k_\perp^2 \cos(k_x x) \mathbf{e}_x\right] \exp(\mathrm{i}\,[k_y y + k_z z - \omega t]) \ . \end{aligned} \tag{2.13}$$

Here, the interface conditions (2.9) and (2.10) lead to

$$0 = \sin(k_x x)\Big|_{x=0} = \sin(k_x x)\Big|_{x=d} \quad \Longrightarrow \quad k_x = \frac{\pi}{d} n, \quad n = 0, 1, 2, 3, \ldots \tag{2.14}$$

It is remarkable that in this case, the $n = 0$ quantum number is allowed, and no contradiction to any of Maxwell equations (2.1)–(2.4) occurs. Additionally, n is not an integer since the solutions concerning the negative numbers are linearly dependent on those that apply to the natural numbers. For both solution classes, the dispersion relation reads

$$\omega_{\mathbf{k}} = c|\mathbf{k}| = c\sqrt{k_x^2 + \mathbf{k}_\perp^2} \ . \tag{2.15}$$

Assuming the transversal lengths L_y and L_z are much larger than the longitudinal distance between the plates d, the quantization of these transversal momenta becomes negligible. It is crucial to perform the transition into the continuum correctly. Therefore, use periodic boundary conditions for the transversal vector components and write:

$$\exp(ik_j j)\Big|_{j=0} = \exp(ik_j j)\Big|_{j=d} \quad \Longrightarrow \quad k_j = \frac{2\pi}{L_j} n_j, \quad n_j \in \mathbb{Z}, \quad j = y, z \ . \tag{2.16}$$

This means that changing the mode number in both transversal directions by one amount

$$1 = \Delta n_j = \frac{L_j}{2\pi} \, \mathrm{d}k_j \ , \quad j = y, z \tag{2.17}$$

gives a minor alteration. In the thermodynamic limit of infinitely large L_y, L_z with nearly a continuous set of states, it is allowed to replace the sums with integrals

$$\sum_{n_j=-\infty}^{\infty} 1 = L_j \int_{-\infty}^{\infty} \frac{\mathrm{d}k_j}{2\pi}, \quad j = y, z \ . \tag{2.18}$$

Further, by introducing the plate area $A = L_y L_z$ and identifying $A \big/ (2\pi)^2$ with the transverse density of states, the vacuum energy between the metal plates is given by the sum over the ground state energy $\hbar\omega_{\mathbf{k}}/2$ of all modes [41, eq. (2.199)]

$$E_{\text{plates}}^{\text{inside}} = 2\sum_{n=0}^{\infty}\left(1-\frac{1}{2}\delta_{n,0}\right) A \int \frac{\mathrm{d}^2 k_\perp}{(2\pi)^2}\frac{1}{2}\hbar c\sqrt{\frac{\pi^2 n^2}{d^2}+\mathbf{k}_\perp^2}\ , \tag{2.19}$$

where the prefactor of 2 is due to the two polarization directions of light. Correspondingly, the wave vectors are not restricted outside the two metal plates, yielding for a length $L_x \gg d$ the vacuum energy [41, eq. (2.200)]

$$E_{\text{plates}}^{\text{outside}} = 2\,(L_x - d)\,A\int_{-\infty}^{\infty}\frac{\mathrm{d}k_x}{2\pi}\int\frac{\mathrm{d}^2 k_\perp}{(2\pi)^2}\frac{1}{2}\hbar c\sqrt{\frac{\pi^2 n^2}{d^2}+\mathbf{k}_\perp^2}\ . \tag{2.20}$$

In the absence of metal plates, the total vacuum energy in the box with volume $L_x A$ would read [41, eq. (2.201)]

$$E_{\text{total}} = 2L_x A\int_{-\infty}^{\infty}\frac{\mathrm{d}k_x}{2\pi}\int\frac{\mathrm{d}^2 k_\perp}{(2\pi)^2}\frac{1}{2}\hbar c\sqrt{\mathbf{k}_x^2+\mathbf{k}_\perp^2}\ . \tag{2.21}$$

Installing the metal plates, thus, leads to the following change of the vacuum energy, namely the Casimir energy E_C [41, eq. (2.202)]

$$E_C = E_{\text{plates}}^{\text{inside}} + E_{\text{plates}}^{\text{outside}} - E_{\text{total}}\ . \tag{2.22}$$

Inserting therein the concrete formulae from equation (2.19)–(2.21) leads to

$$E_C = \hbar c A\left[\sum_{n=0}^{\infty}\left(1-\frac{1}{2}\delta_{n,0}\right) - \int_0^{\infty}\mathrm{d}n\right]\int\frac{\mathrm{d}^2 k_\perp}{(2\pi)^2}\sqrt{\frac{\pi^2 n^2}{d^2}+\mathbf{k}_\perp^2}\ . \tag{2.23}$$

After introducing the abbreviation [41, eq. (2.204)]

$$\sum_{n=0}^{\infty}{}' f_n = \sum_{n=0}^{\infty} f_n - \frac{1}{2}f_0\ , \tag{2.24}$$

which formally considers that the respected TE and TM modes are enumerated differently, the Casimir energy is given by [41, eq. (2.203)]

$$E_C = \hbar c A\left(\sum_{n=0}^{\infty}{}' - \int_0^{\infty}\mathrm{d}n\right)\int\frac{\mathrm{d}^2 k_\perp}{(2\pi)^2}\sqrt{\frac{\pi^2 n^2}{d^2}+\mathbf{k}_\perp^2}\ . \tag{2.25}$$

2.2. Regularization

In order to evaluate equation (2.25), the two infinities must be tamed by introducing some regularization procedure. The first infinity that appears is called ultra-violet divergence, which occurs at the upper boundary of the integral. The second one emerges from the difference between a series and an integral. Note that any physically relevant calculation must lead to a finite result independent of the regularization method.

2.2.1. Regularization methods

There exist several different regularization techniques to evaluate the diverging integral. Some important ones are:

- Dimensional regularization is used in theoretical physics. It uses the analytic continuation of the Gamma function to grant the convergence of a series or an integral. More explicitly, a calculation is performed in an arbitrary dimension D, but the result is evaluated for the dimension of interest [26, chapter 7.14].
- Zeta function regularization is applied in both mathematics and theoretical physics. It is based on the same principle as dimensional regularization, with the significant difference being that a series or integral does not converge due to the dimension change. Instead, it does this by applying properties of the zeta function directly [26, chapter 7.13].
- Causal regularization is almost exclusively used in mathematics. The essential advantage to the other methods is that this method is well defined from the mathematical point of view, even in curvilinear coordinates, which are used in general relativity. Nevertheless, it is an unhandy calculation method that is not often used in physics [45].

Derivations for the Casimir energy using dimensional- or zeta function regularization can be found in the book of H. Kleinert [26].

2.2.2. Regularization of the difference between a series and an integral

For suitable functions and conditions, the evaluation can be carried out, for instance, by applying the „Abel–Plana Summation Formula“ (APSF) [7, eq. (1.5)]

$$\sum_{n=0}^{\infty} f(n) - \int_0^{\infty} f(x)\,\mathrm{d}x = \frac{1}{2} f(0) + \mathrm{i} \int_0^{\infty} \frac{f(\mathrm{i}y) - f(-\mathrm{i}y)}{\exp(2\pi y) - 1}\,\mathrm{d}y \ . \tag{2.26}$$

Using the abbreviation (2.24), this leads to

$$\left(\sum_{n=0}^{\infty}{}' - \int_0^{\infty} \mathrm{d}n \right) f(n) = \mathrm{i} \int_0^{\infty} \frac{f(\mathrm{i}t) - f(-\mathrm{i}t)}{\exp(2\pi t) - 1}\,\mathrm{d}t \ . \tag{2.27}$$

The APSF is of great importance because it allows efficient calculations. For this purpose, some useful formulae are necessary D. There are multiple ways to calculate the difference (2.25). In appendix B the Euler-Maclaurin Summation Formula (EMSF) and the Poisson Summation Formula (PSF) will also be mentioned, together with an according derivation of the Casimir energy. No matter what regularization is chosen, the result stays unchanged [41, chapter 2.17.2].

2.3. Casimir energy

This section shows a step-by-step calculation for the Casimir energy in Minkowski spacetime.

2.3.1. Integral transformation

The energy (2.25) contains an integral over the dispersion relation

$$f(k_x) \equiv \int \sqrt{k_x^2 + k_\perp^2}\, \mathrm{d}^2 k_\perp = \int_{-\infty}^{\infty} \mathrm{d}k_y \int_{-\infty}^{\infty} \mathrm{d}k_z \sqrt{k_x^2 + k_y^2 + k_z^2}\ . \tag{2.28}$$

First, $f(k_x)$ represents a two-dimensional integral over all four quadrants of a Cartesian coordinate system. According to the symmetry of the k_y and k_z axes, it is possible to evaluate just an integral over one quadrant of four times the value:

$$f(k_x) = 4 \int_0^{\infty} \mathrm{d}k_y \int_0^{\infty} \mathrm{d}k_z \sqrt{k_x^2 + k_y^2 + k_z^2}\ . \tag{2.29}$$

It is beneficial to transform into polar coordinates, as follows

$$k_y = k \sin(\varphi)\ , \tag{2.30}$$
$$k_z = k \cos(\varphi)\ , \tag{2.31}$$

which yields

$$f(k_x) = 4 \int_0^{\frac{\pi}{2}} \mathrm{d}\varphi \int_0^{\infty} \sqrt{k_x^2 + k^2}\ k\, \mathrm{d}k = \int_0^{2\pi} \mathrm{d}\varphi \int_0^{\infty} \sqrt{k_x^2 + k^2}\ k\, \mathrm{d}k\ \ . \tag{2.32}$$

After applying the substitution $u = \frac{d}{\pi}\sqrt{k_x^2 + k^2}$ with $\pi^2 u\, \mathrm{d}u = d^2 k\, \mathrm{d}k$ and $k_x = \pi n/d$ this leads to

$$f(n) = 2\frac{\pi^4}{d^3} \int_{|n|}^{\infty} u^2\, \mathrm{d}u\ \ . \tag{2.33}$$

2.3.2. Abel-Plana Summation Formula

Starting from equation (2.25) and inserting the transformation (2.33), the Casimir energy reads

$$E_C = \hbar c A \frac{1}{2}\frac{\pi^2}{d^3} \left(\sum_{n=0}^{\infty}{}' - \int_0^{\infty} \mathrm{d}n \right) \int_{|n|}^{\infty} u^2\, \mathrm{d}u\ \ . \tag{2.34}$$

Evaluating the last integral with the APSF from equation (2.27), by dropping the absolute value because n is an integer according to (2.12) and (2.14), leads to

$$E_C = \hbar c A \frac{1}{2}\frac{\pi^2}{d^3}\ \mathrm{i} \int_0^{\infty} \frac{\int_{\mathrm{i}t}^{\infty} u^2\, \mathrm{d}u - \int_{-\mathrm{i}t}^{\infty} u^2\, \mathrm{d}u}{\exp(2\pi t) - 1}\, \mathrm{d}t = \hbar c A \frac{1}{2}\frac{\pi^2}{d^3}\ \mathrm{i} \int_0^{\infty} \frac{\int_{\mathrm{i}t}^{-\mathrm{i}t} u^2\, \mathrm{d}u}{\exp(2\pi t) - 1}\ . \tag{2.35}$$

Calculating the primitive integral and insert the boundaries, this reduces to

$$E_C = \hbar c A \frac{1}{2}\frac{\pi^2}{d^3}\ \mathrm{i} \int_0^{\infty} \frac{\frac{2}{3}\mathrm{i}t^3}{\exp(2\pi t) - 1}\, \mathrm{d}t\ \ . \tag{2.36}$$

The integral in (2.36) is a Bernoulli kind integral, as shown in (D.6), and corresponds to the Bernoulli number $B_4 = -1/30$ from (D.7):

$$E_C = -\hbar c A \frac{1}{2}\frac{\pi^2}{d^3}\,\frac{2}{3}\frac{|B_4|}{8} = -\frac{\hbar c \pi^2 A}{720 d^3} \equiv E_C^{\text{flat}} \,. \tag{2.37}$$

This agrees with the result that Casimir originally found and is explicitly given in equation (1.3). The Casimir force is calculated as the negative derivative of the Casimir energy with respect to the plate distance d:

$$F_C = -\frac{\partial E_C(d)}{\partial d} = -\frac{\hbar c \pi^2 A}{240 d^4} \equiv F_C^{\text{flat}} \,. \tag{2.38}$$

An important result can be achieved by comparing (2.34) and (1.3):

$$\left(\sum_{n=0}^{\infty}{}' - \int_0^\infty \mathrm{d}n \right) \int_{|n|}^{\infty} u^2 \, \mathrm{d}u = -\frac{1}{360} \,, \tag{2.39}$$

which will be used later in the general relativistic case.

This page intentionally left blank.

3. General relativity in a nutshell

For a basic introduction to the concepts of general relativity, especially in the field of differential geometry, I recommend reading the textbook „Gravitation“ by C. W. Misner, K. S. Throne, and J. A. Wheeler [35]. It is the standard reference for anyone who uses general relativity – both beginners and advanced researchers – and the subsequent chapters are mainly based on it. For German readers, the book „Allgemeine Relativitätstheorie“ by T. Fließbach is concisely written but does not cover all details [15].
The essential concepts of general relativity needed to understand this thesis are covered in the following sections.

3.1. Tensors in brief

To measure distances, the introduction of the metric tensor $\mathbf{g}$ is necessary. It is intimately connected to the scalar product, and every tensor index can be shifted to its dual one by applying the metric tensor. In a local Lorentz frame, the metric tensor can be defined via [35, eq. (13.2)]

$$g_{\alpha\beta} = \mathbf{g}(\mathbf{e}_\alpha, \mathbf{e}_\beta) = \mathbf{e}_\alpha \cdot \mathbf{e}_\beta \ , \tag{3.1}$$

where $\mathbf{e}_\alpha, \mathbf{e}_\beta$ represent basis vectors of a Lorentz frame, and „$\cdot$“ denotes the corresponding scalar product. Further, the following relation for the Kronecker delta [35, eq. (13.11)]

$$\delta^\alpha{}_\beta = g^\alpha{}_\beta = g_{\gamma\beta} g^{\gamma\alpha} = \sum_\gamma g_{\gamma\beta} g^{\gamma\alpha} \tag{3.2}$$

holds, showing how to rise or lower indices using the metric tensor and assuming Einstein's summation convention. The „downstairs“ indices are called the „covariant components“, and the „upstairs“ ones are named „contravariant“ components. In the case of the metric tensor, the contravariant part can be interpreted as the inverse of the covariant one. At this point, it should be mentioned that the Euclidean metric is a straightforward one because the covariant- and contravariant metric tensors are the same, according to

$$g_{ij} = \delta_{ij} \ , \tag{3.3}$$

hence the metric tensor is just the identity matrix. The flat Minkowski vector space describes a four-dimensional spacetime without gravitation. Using the metric signature $(+, -, -, -)$, here and anywhere else in this thesis, the metric tensor reads in any Lorentz frame [35, eq. (2.10)]

$$\eta_{\mu\nu} = \begin{pmatrix} 1 & 0 & 0 & 0 \\ 0 & -1 & 0 & 0 \\ 0 & 0 & -1 & 0 \\ 0 & 0 & 0 & -1 \end{pmatrix} \tag{3.4}$$

and has the useful properties

$$\eta^{\alpha\beta} = \eta_{\alpha\beta} \quad \text{for all } \alpha, \beta \; , \tag{3.5}$$

$$\eta \equiv \det(\eta_{\mu\nu}) = -1 \; . \tag{3.6}$$

The square of the infinitesimal separation $\mathrm{d}s$ to measure e.g., arc lengths, sometimes called „line element“, is given by [35, eq. (13.3)]

$$\mathrm{d}s^2 = g_{\alpha\beta}\, \mathrm{d}x^\alpha\, \mathrm{d}x^\beta \; . \tag{3.7}$$

Separations can be classified into „timelike“ ($\mathrm{d}s^2 > 0$), „spacelike“ ($\mathrm{d}s^2 < 0$), and „lightlike“ ($\mathrm{d}s^2 = 0$), due to the chosen sign convention. It is necessary to realize that every object is an object of a form [35, chapter 9]. Especially even every integral is an integral of a form, which has intriguing consequences for integral theorems (e.g., divergence theorem) in general [35, Box 5.4]. Examples of objects and their forms are curves, vectors, tensors, 1-forms, and more. This will no longer be emphasized in the following, but it can generally be recognized from the number of indices. Note that if a bold letter appears in the body text, and is related to a vector, it usually indicates a direction. If it appears only in normal type, the absolute value of a vector or the determinant of a matrix is indicated.

A vector has one index $\mathbf{v} = v_\alpha$; similarly, a tensor has two indices $\mathbf{T} = T_{\mu\nu}$, using covariant forms as an example. Especially for second-order tensors, the components can be split up into a symmetric (round brackets) and an antisymmetric (square brackets) part [35, eqs. (3.46), (3.47)]:

$$A_{\mu\nu} = A_{(\mu\nu)} + A_{[\mu\nu]} \; , \tag{3.8}$$

$$A_{(\mu\nu)} = \frac{1}{2} \left(A_{\mu\nu} + A_{\nu\mu} \right) \; , \tag{3.9}$$

$$A_{[\mu\nu]} = \frac{1}{2} \left(A_{\mu\nu} - A_{\nu\mu} \right) \; . \tag{3.10}$$

A similar relation does not hold for tensors higher than second-order in general. The last tensor, which is of great importance, is a fourth-order complete antisymmetric tensor called the „Levi-Civita tensor“ ϵ. The most general definition one can give is [35, eq. (3.50a)]:

$$\epsilon\left(\mathbf{n}, \mathbf{u}, \mathbf{v}, \mathbf{w}\right) \text{ changes sign when any two of vectors are interchanged.} \tag{3.11}$$

This can be specified to arbitrary n-dimensional Lorentz frames, with $\mathbf{e}_0$ pointing towards the positive time-axis (the future) and with $\mathbf{e}_1, \mathbf{e}_2, \ldots, \mathbf{e}_n$ representing a right-handed set of spatial basis vectors, to [35, eqs. (3.50d), (3.50e)]

$$\epsilon_{12\ldots n} = \epsilon\left(\mathbf{e}_1, \mathbf{e}_2, \ldots, \mathbf{e}_n\right) \qquad = \begin{cases} 0 & \text{unless } \mathbf{e}_1, \mathbf{e}_2, \ldots, \mathbf{e}_n \text{ are all different,} \\ +1 & \text{for even permutations of the basis vectors,} \\ -1 & \text{for odd permutations.} \end{cases} \tag{3.12}$$

The Laplace expansion to express the determinant of a matrix $\mathbf{\Lambda}$ can be rewritten using this particular tensor in the following way [35, eq. (3.50g)]

$$\epsilon^{\alpha\beta\gamma\delta}\Lambda^0{}_\alpha\Lambda^1{}_\beta\Lambda^2{}_\gamma\Lambda^3{}_\delta = -\det(\Lambda^\mu{}_\nu)\ . \tag{3.13}$$

This relation is helpful because there are only complicated formulae to express the determinant of a sum of arbitrary matrices, namely $\det(\mathbf{A}+\mathbf{B})$ [33]. It can be shown, in a straightforward way, for instance, by writing out the whole determinant and reordering the terms that [13]

$$\det(\mathbf{A}+\mathbf{B}) = \det(\mathbf{A}) + \det(\mathbf{B}) + \det(\mathbf{A}) \cdot \mathrm{Tr}\left(\mathbf{A}^{-1}\mathbf{B}\right) \tag{3.14}$$

holds for the simple case of 2×2 matrices. In general, such simple formulae do not exist, but at least the case of 4×4 matrices is necessary for a complete treatment of general relativity. Appendix C shows how an exact and approximate result for the determinant of sums of 4×4 matrices can be obtained using elementary symmetric functions (C.29).

3.2. Einstein's equivalence principle

The equivalence principle is the core of general relativity and represents a tool to mesh non-gravitational laws of physics with gravity. With its assistance, all the special relativistic laws of physics can be generalized to curved spacetime. General relativity is valid even for strong gravity, implying large spacetime curvatures. Only at the endpoint of a gravitational collapse, namely inside black holes, and at the beginning of the universe, often called the „big bang", Einstein's equivalence principle is supposed to break down.
There are several definitions of the equivalence principle, and every textbook uses the one that fits best for its readership. However, all these definitions are at least distinguishable in two categories: A weak and a strong version [35]:

- **Weak equivalence principle** [35, p. 1050]**:**
„The path [the trajectory] through spacetime of a freely falling, neutral test body [depends on its position and velocity, but] is independent of its structure and composition."

- **Strong equivalence principle** [35, p. 386]**:**
„In any and every local Lorentz frame, anywhere and anytime in the universe, all the (non-gravitational) laws of physics must take on their familiar special-relativistic forms."
Equivalently: „There is no way, by experiments confined to infinitesimally small regions of spacetime, to distinguish one local Lorentz frame in one region of spacetime from any other local Lorentz frame in the same or any other region."
Equivalently: „The laws of physics, written in abstract geometric form, differ in no way whatsoever between curved spacetime and flat spacetime."

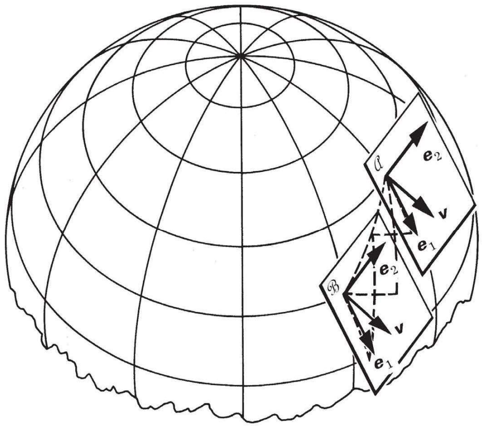

Figure 3.1.: *The parallel-transport law links tangent spaces at neighboring points (events). The parallel transport of* $\mathbf{e}_1$ *is shown in the figure using Schild's ladder. The concept of parallel transport provides a unique and complete way to link algebraic objects in different tangent spaces as long as they are arbitrarily close to each other. Otherwise, the result of parallel transport depends on the selected path. The differences decrease by a factor of 4 each time the affine-parameter distance between the two events is cut in half, so even as an approximation, this concept is acceptable [35, p. 252].*

3.3. Covariant derivatives of tensors

Comparing different trajectories using the concept of parallel transport, especially the construction of „Schild's Ladder", it is possible to give a first-order approach for approximating the correct parallel transport of a vector, see Figure 3.1 [35, Box 10.2]. Skipping these things because executing complex calculations necessitates a component approach leads to introducing the covariant derivative in the following way.
First, assume a set of basis vectors $\{\mathbf{e}_\alpha\}$ and the dual set of basis 1-forms $\{\omega^\alpha\}$ is given. Two bases are needed to quantify the possible twisting and turning of „field" basis vectors. To examine the changes in vector fields along a basis vector $\mathbf{e}_\beta$, abbreviating

$$D_{\mathbf{e}_\beta} \equiv D_\beta \;, \tag{3.15}$$

and especially the rate of change of some basis vector: $D_\beta \mathbf{e}_\alpha$. The rate of change is itself a vector, so it can be expanded in terms of the basis [35, eq. (10.13)]:

$$D_\beta \mathbf{e}_\alpha = \mathbf{e}_\mu \Gamma^\mu{}_{\alpha\beta} \tag{3.16}$$

and the resultant „connection coefficients" $\Gamma^\mu{}_{\alpha\beta}$ can be calculated via a projection on the basis 1-forms [35, eq. (10.16)]:

$$\langle \omega^\mu, D_\beta \mathbf{e}_\alpha \rangle = \Gamma^\mu{}_{\alpha\beta} \;. \tag{3.17}$$

More useful formulae related to the metric and only valid in coordinate frames are [35, eq. (13.23)]:

$$\Gamma_{\mu\alpha\beta} = \Gamma_{\mu\beta\alpha} = \frac{1}{2}\left(\frac{\partial g_{\mu\alpha}}{\partial x^\beta} + \frac{\partial g_{\mu\beta}}{\partial x^\alpha} - \frac{\partial g_{\alpha\beta}}{\partial x^\mu}\right) , \tag{3.18}$$

$$\Gamma^\mu{}_{\alpha\beta} = \Gamma^\mu{}_{\beta\alpha} = g^{\mu\nu}\Gamma_{\nu\alpha\beta} . \tag{3.19}$$

Note that these result from the relation [35, eq. (8.33), Box 8.6]:

$$D_\gamma g_{\alpha\beta} \equiv g_{\alpha\beta;\gamma} = 0 \tag{3.20}$$

which holds in arbitrary frames and means the metric is covariantly constant. The connection coefficients $\Gamma^\mu{}_{\alpha\beta}$, called Christoffel symbols, are symmetric in the indices α and β. They can also be used to calculate the components of the gradient of an arbitrary tensor $\mathbf{S}$ using the flat-space method, plus a correction applied to each index more accurately to each basis vector [35, eq. (10.18)]:

$$D_\delta S^\alpha{}_{\beta\gamma} \equiv S^\alpha{}_{\beta\gamma;\delta} = S^\alpha{}_{\beta\gamma,\delta} + S^\mu{}_{\beta\gamma}\Gamma^\alpha{}_{\mu\delta} - S^\alpha{}_{\mu\gamma}\Gamma^\mu{}_{\beta\delta} - S^\alpha{}_{\beta\mu}\Gamma^\mu{}_{\gamma\delta} . \tag{3.21}$$

Note that the gradient operation „;“ „obeys the standard partial-differentiation chain rule of ordinary calculus“ [35, p. 260]. Another quite valuable property to evaluate the divergence of vectors is the contraction of the upper index with either of the lower indices [35, eq. (8.51a)]

$$\Gamma^\mu{}_{\nu\mu} = \frac{\partial}{\partial x^\nu}\ln\left(\sqrt{-g}\right) , \tag{3.22}$$

where $g = \det(g_{\mu\nu})$ denotes the determinant of the metric tensor.
The relevant expressions needed for actual calculations read:

$$D_\beta V^\alpha = V^\alpha{}_{;\beta} = \frac{\partial V^\alpha}{\partial x^\beta} + \Gamma^\alpha{}_{\lambda\beta}V^\lambda , \tag{3.23}$$

$$D_\beta V_\alpha = V_{\alpha;\beta} = \frac{\partial V_\alpha}{\partial x^\beta} - \Gamma^\lambda{}_{\beta\alpha}V_\lambda , \tag{3.24}$$

$$D_\alpha A^{\mu\nu} = A^{\mu\nu}{}_{;\alpha} = \frac{\partial A^{\mu\nu}}{\partial x^\alpha} + \Gamma^\mu{}_{\lambda\alpha}A^{\lambda\nu} + \Gamma^\nu{}_{\rho\lambda}A^{\mu\rho} , \tag{3.25}$$

$$D_\alpha A_{\mu\nu} = A_{\mu\nu;\alpha} = \frac{\partial A_{\mu\nu}}{\partial x^\alpha} - \Gamma^\lambda{}_{\mu\alpha}A_{\lambda\nu} - \Gamma^\lambda{}_{\nu\alpha}A_{\mu\lambda} , \tag{3.26}$$

$$D_\alpha A^\mu_\nu = A^\mu{}_{\nu;\alpha} = \frac{\partial A^\mu_\nu}{\partial x^\alpha} + \Gamma^\lambda{}_{\mu\alpha}A^\lambda_\nu - \Gamma^\lambda{}_{\nu\alpha}A^\mu_\lambda . \tag{3.27}$$

The derivation of the geodesic equation, which describes the trajectories of particles in spacetime, can be done by using Einstein's equivalence principle directly [54, p. 70-72], by using variation calculus, Hamilton's principle [54, p. 73-77] or the concept of parallel transport [35, chapter 8.5 & 11][44, chapter 5]. The component version of the geodesic equation $D_{\mathbf{u}}\mathbf{u} = 0$ for a given coordinate system $\{x^\alpha\}$, which induces basis vectors $\mathbf{e}_\alpha = \frac{\partial}{\partial x^\alpha}$ into the tangent space, and connection coefficients $\Gamma^\alpha{}_{\beta\gamma}$ for this basis, becomes a differential equation for the geodesic $x^\alpha(\lambda)$ [35, eq. (10.27)]:

$$D_{\mathbf{u}}\mathbf{u} = 0 \iff \frac{\mathrm{d}^2 x^\alpha}{\mathrm{d}\lambda^2} + \Gamma^\alpha{}_{\gamma\beta}\frac{\mathrm{d}x^\gamma}{\mathrm{d}\lambda}\frac{\mathrm{d}x^\beta}{\mathrm{d}\lambda} = 0 . \tag{3.28}$$

This formula is known as the „geodesic equation of motion“ and is mainly used to calculate, e.g., orbits of celestial bodies. Depending on the type of object described, it must be distinguished between objects with and without rest mass. In the first case, the parameter λ changes to the proper time τ. In the second case, it remains an arbitrary orbit parameter. However, geodesics can be interpreted as world lines of extremal proper time [35, chapter 13.4, Box 13.2]. This idea leads to the „world line formalism“, which is nowadays a powerful calculation tool that can be applied to the Casimir effect, for instance [53].

3.4. Einstein's field equations

The expression „curved spacetime“ is often used, and the fact that there are major differences to the flat case has been mentioned several times. But what is this curvature? Is there a way to measure it? An appropriate method is often: „Curvature first, understanding second“ [35, p. 334]; let us start this way.

In one dimension, curvature describes the deviation of a curve to a straight line, and in two dimensions, it means the deviation of an object to a plane. An example of (intrinsic) curvature for a two-dimensional object is the curvature of a spherical surface, see figure 3.2. In general relativity, already in dimensions higher than two, such comparisons are not useful. Instead, the curvature depends even on the choice of a direction on the surface or generally manifold. Riemann introduced a rigorous way to define curvature for manifolds.

In any coordinate basis $\{\mathbf{e}_\alpha\} = \{\frac{\partial}{\partial x^\alpha}\}$, with commutation coefficients $c_{\alpha\beta}{}^{\gamma} = 0$ (holonomic), the components of the Riemann curvature tensor $R^\alpha{}_{\beta\gamma\delta}$ are given by [35, eq. (8.44)]

$$R^\alpha{}_{\beta\gamma\delta} = \Gamma^\alpha{}_{\beta\delta,\gamma} - \Gamma^\alpha{}_{\beta\gamma,\delta} + \Gamma^\alpha{}_{\mu\gamma}\Gamma^\mu{}_{\beta\delta} - \Gamma^\alpha{}_{\mu\delta}\Gamma^\mu{}_{\beta\gamma} \tag{3.29}$$

and for any vector A^α this yields

$$R^\alpha{}_{\beta\gamma\lambda}A^\beta = D_\gamma D_\lambda A^\beta - D_\lambda D_\gamma A^\beta \equiv [D_\gamma, D_\lambda]A^\beta \; . \tag{3.30}$$

With a contraction on indexes one and three of Riemann curvature tensor $R_{\mu\nu}$, one gets the Ricci curvature tensor [35, eq. (8.47)]

$$R_{\mu\nu} = R^\alpha{}_{\mu\alpha\nu} = \Gamma^\alpha{}_{\mu\nu,\alpha} - \Gamma^\alpha{}_{\mu\alpha,\nu} + \Gamma^\alpha{}_{\beta\alpha}\Gamma^\beta{}_{\mu\nu} - \Gamma^\alpha{}_{\beta\nu}\Gamma^\beta{}_{\mu\alpha} \; . \tag{3.31}$$

Further, the contraction of the Ricci tensor leads to the Riemann curvature scalar R [35, eq. (8.48)]

$$R = R^\alpha{}_\alpha = g^{\alpha\beta}R_{\alpha\beta} \; . \tag{3.32}$$

The quantity of interest, in the end, is the Einstein tensor $G_{\mu\nu}$. This object is formed by successive contractions of the Riemann tensor [35, eq. (17.5)]:

$$G_{\mu\nu} = R^\alpha{}_{\mu\alpha\nu} - \frac{1}{2}g_{\mu\nu}g^{\sigma\tau}R^\alpha{}_{\sigma\alpha\tau} \; . \tag{3.33}$$

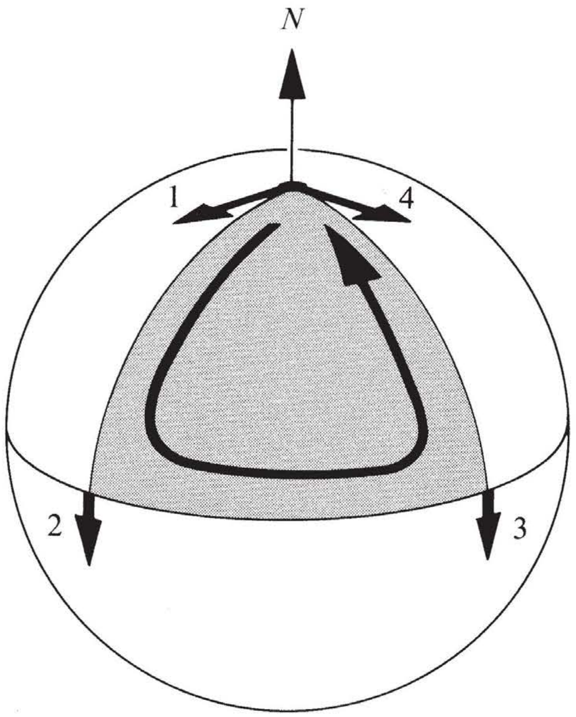

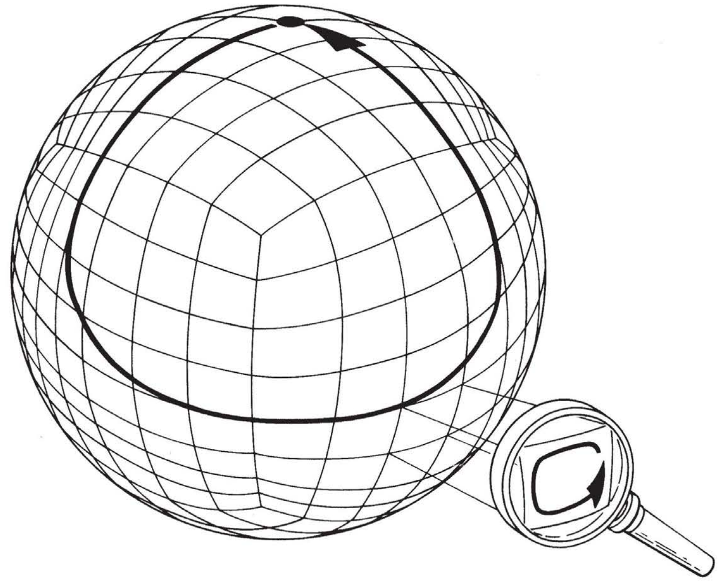

(a) *„The rotation of a vector transported parallel to itself around a closed loop provides a definition of curvature", namely the Gaussian curvature. For a sphere the Gaussian curvature's value is $1/a^2$ where a denotes the radius of the sphere. This curvature can be measured intrinsically by comparing the angle turned through and the area circumnavigated. [quote & figure 35, p. 337]*

(b) *The „box-like structure" should emphasise that the sphere is interpreted as a 2-form, a curved two-dimensional manifold as it is often seen in general relativity. The scheme stays basically the same. The two major differences are: The angle is directly given by the number of boxes enclosed any give way, „the fact if a box is counted as positive or negative depends on whether the sense of the arrow marked on it agrees or disagrees withe the sense of circumnavigation of the route."[quote & figure 35, p. 337]*

Figure 3.2.: *Different perspectives on curvature using the surface of a sphere as an example. The general way to calculate is given by: $g_{\mu\nu} \to \Gamma_{\mu\alpha\beta} \to \Gamma^{\mu}{}_{\alpha\beta} \to R^{\mu}{}_{\nu\alpha\beta} \to R_{\alpha\beta} \to R$.
The explicit formulae can be found in sections 3.3 and 3.4.
First, use the metric for the two-dimensional surface of a sphere of radius a:
$\mathrm{d}s^2 = a^2\left[\mathrm{d}\vartheta^2 + \sin^2(\vartheta)\,\mathrm{d}\varphi^2\right]$, and after executing the calculations, get the six Christoffel symbols, four of them are zero. More relevant are the non-zero components of the Riemann curvature tensor: $R^{\vartheta}{}_{\varphi\vartheta\varphi} = \sin^2(\vartheta), R^{\vartheta\varphi}{}_{\vartheta\varphi} = \frac{1}{a^2}$ and the Ricci tensors: $R^{\vartheta}{}_{\vartheta} = R^{\varphi}{}_{\varphi} = \frac{1}{a^2}$.
After further contractions, the Riemann curvature scalar is given by: $R = \frac{2}{a^2}$
It is possible to introduce an orthonormal frame in this manifold and transform the curvature tensor. After an additional normalization, the two non-vanishing components of the curvature tensor are the same, with the concrete value of $\frac{1}{a^2}$. The last step is optional and only necessary if the calculation should be done in a concrete reference frame, in this case, a diagonal metric. [35, Box 14.1, Box 14.2].*

This can be simplified using the Ricci tensor (3.31) and the Riemann curvature scalar (3.32) to

$$G_{\mu\nu} = R_{\mu\nu} - \frac{1}{2} g_{\mu\nu} R \,. \tag{3.34}$$

The Einstein tensor $G_{\mu\nu}$ must fulfill Bianchis identities [35, eq. (8.46), Box 8.6]

$$R^{\alpha}{}_{\beta[\mu\nu;\lambda]} = 0 \tag{3.35}$$

and taking into account (3.20) this leads to the so-called „contracted Bianchi identities“ [35, eq. (8.50), Box 8.6]

$$G^{\alpha\beta}{}_{;\beta} = 0 \,. \tag{3.36}$$

Indeed, Bianchi's identities are a powerful tool to calculate conserved momenta in general relativity. Additionally, they can be used to identify quantities that stay unchanged by the influence of gravity, like the homogeneous Maxwell equations.
A typical sentence is that „mass is the source of gravity “ [35, p. 404]. More precisely, one has to say that „mass-energy generates curvature“ [35, p. 404]. The density of mass-energy ρ measured by any observer with four-velocity $\mathbf{u}$ is [35, p. 404]

$$\rho = \mathbf{u} \cdot \mathbf{T} \cdot \mathbf{u} = u^{\alpha} T_{\alpha\beta} u^{\beta} \,. \tag{3.37}$$

The stress-energy tensor $\mathbf{T}$ appears as a frame-independent geometric object that acts as the source of gravity. Of course, the momentum-energy is a conserved quantity, so it must fulfill [35, p. 405]

$$\boldsymbol{\nabla} \cdot \mathbf{T} = 0 \,. \tag{3.38}$$

Therefore the object $\mathbf{T}$ must be a symmetric, divergence-free tensor. Geometrically it must be an object purely built out of spacetime geometry, given by the metric tensor, and nothing else [35, p. 405]. Great efforts are required to meet these conditions. First, a not necessarily symmetric but canonical (Hilbert) energy-momentum tensor must be calculated using Noether's theorem and a Lagrange density. Second, to use this tensor in Einstein's theory of gravity, a symmetrization of the previous energy-momentum tensor is necessary. Therefore, a Belinfante–Rosenfeld modification must be applied [40, chapter 7.8]. Putting together (3.36) and (3.38), applying the introduced abbreviations, and assuming that the stress-energy tensor already exists in the necessary form, Einstein's field equations are given by

$$G_{\mu\nu} = -\frac{8\pi G}{c^4} T_{\mu\nu} \,, \tag{3.39}$$

where the prefactor is defined via the comparison to Newtonian's theory of gravity [35, p. 407].
Today, it may be out of date to derive Einstein's field equations using the axioms of general relativity. In the book of Misner et al., six different derivation paths are described [35, Box 17.2]. The most concise derivation goes back to David Hilbert (1915), who used the calculus of variations.

One question remains: How is special relativity included in the general one? Provided the spacetime or any other manifold is flat, there exists a coordinate system $\{x^\alpha(\mathcal{P})\}$ in which all geodesics appear straight. This happens if all connection coefficients in the geodesic equation of motion (3.28) expressed in the same coordinate system vanish:

$$\Gamma^\beta{}_{\mu\nu} = 0. \tag{3.40}$$

From the vanishing of these connection coefficients, it follows immediately (3.29) that all the components of the Riemann curvature tensor are zero:

$$R^\beta{}_{\gamma\mu\nu} = 0 \tag{3.41}$$

and Einstein's field equations (3.39) simplify to

$$G_{\mu\nu} = 0\ . \tag{3.42}$$

Geometrically, one could say: „For all geodesics to be straight in a given coordinate system means that initially, parallel geodesics preserve their separation; the geodesic deviation is zero; therefore, the curvature vanishes“ [35, p. 283]. The most famous case where the Riemann curvature tensor is equal to zero is the one of special relativity, namely the manifold connected to the Minkowski metric $\eta_{\mu\nu}$. Even the opposite of the last statement is true: If the Riemann curvature implies the existence of a coordinate system in which all geodesics appear straight in it, the spacetime is flat, and the Minkowski metric is the relevant one [35, p. 283].
Finally, some limiting cases of general relativity are shown [35, Box 17.1]:

- Special relativity: There are two possibilities for recovering this case from general relativity.
  - If the curvature vanishes, $R^\beta{}_{\gamma\mu\nu} = 0$ ($g_{\mu\nu} = \eta_{\mu\nu}$), a global inertial frame can be introduced.
  - If one particular point in spacetime is fixed, the equivalence principle demands that the laws of physics take on their special relativistic form in any local inertial frame.
- Newtonian theory: In the limit of weak gravitational fields, low velocities, and small pressures [details see 35, chapter 17].
- Post-Newtonian theory: It is similar to Newtonian theory but contains „first-order relativistic corrections“ [details see 35, chapter 39].
- Linearized theory of gravity: In the limit of weak gravitational fields but arbitrary large velocities and pressures, general relativity reduces to this case [details see 35, chapter 18].

Solving (3.39) is not always possible analytically, even in a limiting case. Therefore, a numerical solution to the differential equations could be practical. However, these simulations require enormous computational power, which is only an option if the necessary resources are available. For instance, a simulation of the Casimir Effect in an Alcubierre metric was performed on „660 2.40 GHz Intel Skylake CPUs“ in 2021 [56].

3.5. The Schwarzschild solution

Solving Einstein's field equations (3.39) is a rather challenging task because, on the left-hand side, there is the Einstein curvature tensor strongly related to the metric. The stress-energy tensor is on the right-hand side, including all other fields. To understand the circularity, the dependence of the left-hand side on the right-hand and vice versa, let us assume an object with (large) mass M compared to a single beam of light with a (small) mass equivalent m. This object gives the vast majority of the spacetime curvature. The light beam itself, however, leads locally to a slight deviation. This shows why it is reasonable to assume for small energy that the feedback can be neglected since otherwise, the resulting time-dependent problem can quickly become difficult to solve. Today, many metrics are known to solve Einstein's field equations, so one usually fixes the metric and then looks more closely at the problem. Of course, this approach will not yield a complete result, but it is a convenient ansatz for first investigations. In particular, the charge can often be neglected when looking at astronomical objects like stars since the matter is generally uncharged. That is the reason why in particular, two metrics are essential. The Schwarzschild metric describes the gravitational field of a spherical non-rotating, non-charged mass

$$\mathrm{d}s^2_{\text{Schwarzschild}} = c^2 \left(1 - \frac{r_s}{r}\right) \mathrm{d}t^2 - \frac{1}{1 - \frac{r_s}{r}} \mathrm{d}r^2 - r^2 \,\mathrm{d}\vartheta^2 - r^2 \sin^2(\vartheta)\, \mathrm{d}\varphi^2 \ , \tag{3.43}$$

where $r_s = 2GM/c^2$ denotes the Schwarzschild radius, more popular, the event horizon. The distance r to the object's center, supplemented by the polar angle ϑ and the azimuthal angle φ, is given as three-dimensional spherical coordinates. The spacetime geometry of a star in Schwarzschild spacetime is shown in figure 3.3. Similarly, using „Boyer–Lindquist coordinates“ and the $(+,-,-,-)$ signature, and assuming that there is an additional angular momentum, the Kerr metric reads [derived from Kerr-Newmann metric 35, Box 33.2]

$$\mathrm{d}s^2_{\text{Kerr}} = \frac{\Delta}{\rho^2} \left[c\, \mathrm{d}t - a \sin^2(\vartheta)\, \mathrm{d}\varphi\right]^2 - \rho^2 \left(\frac{\mathrm{d}r^2}{\Delta} - \mathrm{d}\vartheta^2\right) - \frac{\sin^2(\vartheta)}{\rho^2} \left[\left(r^2 + a^2\right) \mathrm{d}\varphi - ac\, \mathrm{d}t\right]^2 \ , \tag{3.44}$$

where M denotes the mass of the gravitation source, a stands for the Kerr spin parameter, $J = |\mathbf{J}|$ labels the magnitude of angular momentum, and the abbreviations which give the typical length scales are:

$$a = \frac{J}{Mc} \ , \tag{3.45}$$

$$\chi = \frac{ac^2}{MG} \ , \tag{3.46}$$

$$\rho^2 = r^2 + a^2 \cos^2(\vartheta) \ , \tag{3.47}$$

$$\Delta = r^2 - r_s r + a^2 \ . \tag{3.48}$$

Adding a charge parameter $r_Q^2 = Q^2G/4\pi\varepsilon_0 c^4$ to the Δ parameter, one gets the complete Kerr-Newmann metric, which also includes the charge Q.
The overlap of both metrics forms the so-called „Slow-Rotation approximation“ (SRA). This follows from a perturbation theory approach of the Kerr metric for the dimensionless spin parameter χ.

Up to first-order, it reads [second-order terms dropped, in SI units 1, eq. (2)]

$$\mathrm{d}s^2_{\mathrm{SRA}} = c^2 \left(1 - \frac{r_s}{r}\right) \mathrm{d}t^2 + 2\frac{r_s}{r} a \sin^2(\vartheta) c \,\mathrm{d}t \,\mathrm{d}\varphi - \frac{1}{1 - \frac{r_s}{r}} \,\mathrm{d}r^2 - r^2 \left[\mathrm{d}\vartheta^2 + \sin^2(\vartheta) \,\mathrm{d}\varphi^2\right] \ . \tag{3.49}$$

Note that the SRA (3.49) is equal to the Schwarzschild metric (3.43) in the case $a = 0$. Thus, the main attribute investigated in this thesis is how the mass M of a source of gravity influences the Casimir setup at a considerable distance R. The first extension is provided by the SRA, which allows the analysis of a small angular momentum a. In cases where rotational effects like Lense–Thirring precession can be neglected, the system of reference can approximately be changed to one where the source of gravity is fixed, and the Casimir setup is in a circular orbit. This case is much more relevant because any real mission using a space probe will not stand still next to the source of gravity. However, since nowadays, even the most modern orbiter, like the Parker Solar Probe (PSP), reach only fractions ($v^{\mathrm{PSP}}_{\mathrm{max}} \approx 10^{-4} c \Rightarrow a^{\mathrm{PSP}}_{\mathrm{max}} \approx 10^{-23}$ m) of the speed of light, the approximation of a slow orbit of the central body is justified [50] [more details about Lense–Thirring precession, also called frame dragging, see 35, chapters 19.2, 21.12, 33, 40].

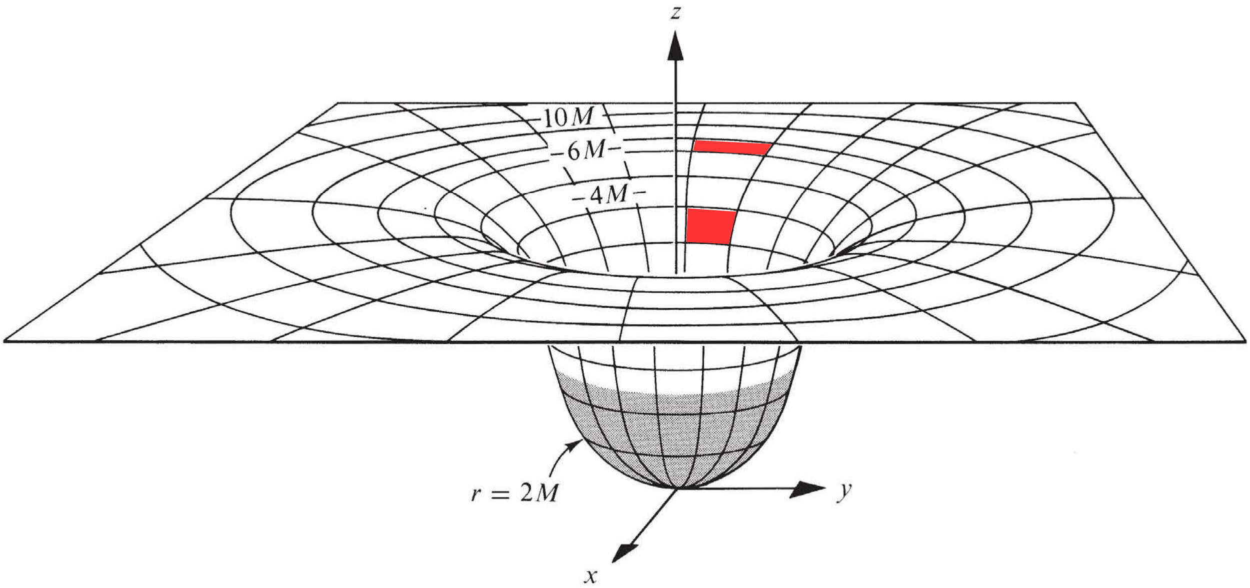

Figure 3.3.: *„Geometry within (grey) and around (white) a star of radius $R = 2.66M$, schematically displayed. The star is in hydrostatic equilibrium and has zero angular momentum (spherical symmetry). The two-dimensional geometry $\mathrm{d}s^2 = (1 - 2m(r)/r)^{-1}\,\mathrm{d}r^2 + r^2\,\mathrm{d}\varphi^2$ of an equatorial slice through the star ($\vartheta = \pi/2$, t = constant) is represented as embedded in Euclidean 3-space, in such a way that distances between any two nearby points (r, φ) and $(r + \mathrm{d}r\,, \varphi + \mathrm{d}\varphi)$ are correctly reproduced. Distances measured off the curved surface have no physical meaning; points off that surface have no physical meaning; and the Euclidean 3-space itself has no physical meaning. Only the curved 2-geometry has meaning. A circle of Schwarzschild coordinate radius r has proper circumference $2\pi r$ (attention limited to equatorial plane of star, $\vartheta = \pi/2$). Replace this circle by a sphere of proper area $4\pi r^2$, similarly for all the other circles, in order to visualize the entire 3-geometry in and around the star at any chosen moment of Schwarzschild coordinate time t. The factor $(1 - 2m(r)/r)^{-1}$ develops no singularity as r decreases within $r = 2M$, because $m(r)$ decreases sufficiently fast with decreasing r.“ [quote & figure 35, p. 614]*
Note the use of geometric units to get SI units. In the case of distances, multiply them by a factor of G/c^2 .
Furthermore, the effect of „spaghettification“ can be seen by comparing the (red) disks. Towards the center of mass, the radial length increases, whereas the perpendicular length decreases. The disk further away is approximately stretched to a square. Arbitrarily close to the center of mass, the disk has an infinite length but a width of zero.

4. Maxwell theory

This chapter first uses Maxwell's equations as an illustrative example for applying Einstein's equivalence principle from section 3.2. To this end, the equations in both the Minkowski and in curved spacetime are explained. The latter will be discussed in more detail, and a form will be derived suitable for analyzing the Casimir effect. Here the focus lies on the inhomogeneous Maxwell equations since it is shown that the homogeneous ones are formally unaffected by the underlying spacetime geometry.

4.1. Flat spacetime

Writing down Maxwell's equations in flat spacetime in a Lorentz covariant form and taking into account the $(+,-,-,-)$ sign convention from (3.4), the electromagnetic field tensor $F_{\mu\nu}$ reads [35, eq. (3.7)]

$$F_{\mu\nu} = \begin{pmatrix} 0 & E_x/c & E_y/c & E_z/c \\ -E_x/c & 0 & -B_z & B_y \\ -E_y/c & B_z & 0 & -B_x \\ -E_z/c & -B_y & B_x & 0 \end{pmatrix} , \tag{4.1}$$

where E_i denotes the components of the electric field and B_i the components of the magnetic induction field for $i = x, y, z$. Raising and lowering indices work by using the Mikowski metric and its inverse. For instance, the contravariant electromagnetic field tensor is defined according to

$$F^{\mu\nu} = g^{\alpha\mu} g^{\beta\nu} F_{\alpha\beta} . \tag{4.2}$$

The inhomogeneous Maxwell's equations (2.1)–(2.4) are then summarized in SI units as follows [35, eq. (3.36), eq. (3.49b)]

$$\text{inhomogeneous:} \quad F^{\mu\nu}{}_{,\mu} = \mu_0 j^\nu , \tag{4.3}$$

$$\text{homogeneous:} \quad F_{[\alpha\beta,\gamma]} = F_{\alpha\beta,\gamma} + F_{\beta\gamma,\alpha} + F_{\gamma\alpha.\beta} = 0 . \tag{4.4}$$

In order to obtain the corresponding equations in curved spacetime, Einstein's equivalence principle, as introduced in section 3.2, must be applied.

4.2. Curved spacetime

A self-consistent description of electromagnetic fields in a curved spacetime background would need the Einstein-Maxwell equations. To this end, consider the stress-energy tensor of the electromagnetic field $T^{(EM)}_{\alpha\beta}$, which has to be inserted at the right-hand side of (3.39) [35, eq. (22.21)]

$$T^{(EM)}_{\alpha\beta} = -\frac{1}{\mu_0}\left(F_{\alpha\mu}F_{\beta}{}^{\mu} - \frac{1}{4}F_{\mu\nu}F^{\mu\nu}g_{\alpha\beta}\right) . \tag{4.5}$$

Let us assume that an electromagnetic field exists and an object with a large mass M, e.g., a star. The electromagnetic field would primarily follow a geodesic induced by the source of gravity. The Maxwell-Einstein equations would describe the interplay of how spacetime influences the geodesics of this field. The electromagnetic field itself contains energy that is equivalent to a specific mass according to $m = E/c^2$ [35, Box 2.2], and this mass bends the spacetime again and changes the spacetime geometry locally. This changed spacetime geometry will produce different geodesics for the electromagnetic field. This circular, time-dependent problem is rather hard to solve analytically. Assuming that the mass of the electromagnetic field is much smaller than the mass of the central object $m \ll M$, as in the case of a star and a Casimir setup orbiting around, its influence gets neglected, and the metric is stationary. In that situation, the equations to deal with are just Maxwell's equations in a given curved spacetime.
As in classical electrodynamics, a vector potential A_μ is introduced, which replaces the electromagnetic field tensor $F_{\mu\nu}$. Applying Einstein's equivalence principle leads to the definition [35, eq. (22.19a)]

$$F_{\mu\nu} \equiv A_{\nu;\mu} - A_{\mu;\nu} . \tag{4.6}$$

Inserting (3.26) into (4.6) yields

$$F_{\mu\nu} = \partial_\mu A_\nu - \partial_\nu A_\mu . \tag{4.7}$$

Thus, the covariant electromagnetic tensor does not change its form in any other coordinate system. That is why the electric and the magnetic induction fields can be fixed as entries of this specific tensor, leading to the following definitions [8, eqs. (3.4), (3.5)]

$$F_{0k} = \frac{1}{c}\partial_t A_k - \partial_k A_0 \equiv \frac{E_k}{c} , \tag{4.8}$$

$$F_{jk} = \partial_j A_k - \partial_k A_j \equiv -B_{jk} = -\epsilon_{ijk}B^i . \tag{4.9}$$

A particular point is remarkable for the magnetic field components. An antisymmetric 3×3 submatrix of the covariant electromagnetic tensor contains its components by applying the Levi-Civita symbol to the contravariant magnetic field components. Generalizing equations (4.3) and (4.4) from special to general relativity reads [8, eq. (3.7)][35, eqs. (3.32), (3.36)]

$$\text{inhomogeneous:} \quad F^{\mu\nu}{}_{;\mu} = \mu_0 j^\nu , \tag{4.10}$$

$$\text{homogeneous:} \quad F_{[\beta\gamma;\alpha]} = 0 . \tag{4.11}$$

This set of equations (4.10) and (4.11) is compatible with charge conservation and magnetic flux conservation in curved spacetime [8].
„Compare the component versions [(4.3) and (4.4) with (4.10) and (4.11)], they differ only in one way: the comma (partial derivative; flat-spacetime gradient) is replaced by a semicolon (covariant derivative; curved-spacetime gradient)“ [35, p. 387]. „The laws of physics, written in component form, change on passage from flat spacetime to curved spacetime by a mere replacement of all commas by semicolons (no change at all physically or geometrically; change only due to switch in reference frame from Lorentz to non-Lorentz)“ [35, p. 387]. That is why some people call this the „comma-goes-to-semicolon rule“. Although the transition seems trivial, the consequences are not because it implies that gravity is associated with all the laws of physics. By introducing the covariant derivative in curved spacetime, gravity enters in an essential and mathematically elegant way.
It is also important to note that the inhomogeneous equations (4.10) assume local, linear, homogeneous, and isotropic constitutive relations without explicit reference. The homogeneous (4.11) and inhomogeneous equations (4.10), which build a set of 8 equations, are connected to the spacetime geometry by the covariant derivative [8, eq. (3.8)]. The latter ones explicitly read

$$F^{\mu\nu}{}_{;\mu} = \partial_\mu F^{\mu\nu} + \Gamma^\mu{}_{\alpha\mu} F^{\alpha\nu} + \Gamma^\nu{}_{\alpha\mu} F^{\mu\alpha} \; . \tag{4.12}$$

First, recognize that the third term in (4.12) vanishes because the Christoffel symbol $\Gamma^\nu{}_{\alpha\mu}$ is symmetric in indexes two and three, and the electromagnetic tensor is antisymmetric, so the summations over α and μ lead to a zero. For the second term, use equation (3.22), which can be combined with the divergence of any antisymmetric tensor $S^{\mu\nu}$ given by [8, eq. (3.9)][35, eq. (8.51c)]

$$S^{\mu\nu}{}_{;\mu} = \frac{1}{\sqrt{-g}} \partial_\mu \left(\sqrt{-g} S^{\mu\nu} \right) \; . \tag{4.13}$$

Therefore, the inhomogeneous Maxwell equations (4.10) reduce to [8, eq. (3.10)]

$$\partial_\mu F^{\mu\nu} + \frac{1}{\sqrt{-g}} \partial_\mu \left(\sqrt{-g} \right) F^{\mu\nu} = \mu_0 j^\nu \; . \tag{4.14}$$

Reexpressing the contravariant with the covariant electromagnetic field strength tensor in (4.14) yields [8, eq. (3.11)]

$$g^{\alpha\mu} g^{\beta\nu} \partial_\mu F_{\alpha\beta} + F_{\alpha\beta} \left[\partial_\mu \left(g^{\beta\nu} g^{\alpha\mu} \right) + g^{\alpha\mu} g^{\beta\nu} \frac{1}{\sqrt{-g}} \partial_\mu \left(\sqrt{-g} \right) \right] = \mu_0 j^\nu \; . \tag{4.15}$$

More explicitly, using the product rule and the electric- and magnetic components as defined in equations (4.8) and (4.9), the inhomogeneous Maxwell equations read [8, eq. (3.12)]

$$\begin{aligned} &\frac{1}{c} \partial_\mu E_j \left(g^{0\mu} g^{j\nu} - g^{j\mu} g^{0\nu} \right) + \frac{1}{c} E_j \left[\partial_\mu \left(g^{0\mu} g^{j\nu} - g^{j\mu} g^{0\nu} \right) + \frac{1}{\sqrt{-g}} \partial_\mu \left(\sqrt{-g} \right) \left(g^{0\mu} g^{j\nu} - g^{j\mu} g^{0\nu} \right) \right] \\ &- \partial_\mu B^k g^{m\mu} g^{n\nu} \epsilon_{kmn} - B^k \epsilon_{kmn} \left[\partial_\mu \left(g^{m\mu} g^{n\nu} \right) + \frac{1}{\sqrt{-g}} \partial_\mu \left(\sqrt{-g} \right) g^{m\mu} g^{n\nu} \right] = \mu_0 j^\nu \; . \end{aligned} \tag{4.16}$$

To get the Gauss law in curved spacetime, also called extended Gauss law, specialize $\nu = 0$ in (4.16) [8, eq. (3.13)]

$$\partial_\mu E_j \left(g^{0\mu} g^{j0} - g^{j\mu} g^{00}\right) + E_j \left[\partial_\mu \left(g^{0\mu} g^{j0} - g^{j\mu} g^{00}\right) + \frac{1}{\sqrt{-g}} \partial_\mu \left(\sqrt{-g}\right) \left(g^{0\mu} g^{j0} - g^{j\mu} g^{00}\right)\right]$$
$$-\partial_\mu B^k c g^{m\mu} g^{n0} \epsilon_{kmn} - B^k c \epsilon_{kmn} \left[\partial_\mu \left(g^{m\mu} g^{n0}\right) + \frac{1}{\sqrt{-g}} \partial_\mu \left(\sqrt{-g}\right) \left(g^{m\mu} g^{n0}\right)\right] = \frac{\rho}{\varepsilon_0} \; . \tag{4.17}$$

This equation conforms to the generalization of Gauss' law known from equation (2.1) in the way that new electromagnetic phenomena get predicted in the presence of sufficiently strong gravitational fields. Assuming the charge density ρ vanishes in (4.17), the presence of electric fields is allowed, although there exist only static magnetic induction fields; this is extraordinary since such terms do not occur in the Minkowski case. These magnetic fields vanish if the off-diagonal metric components g^{n0} are zero, corresponding to the gravitomagnetic potential components defined in a weak field (linear) approximation of gravity [8, p. 10].
In this case, $\nu = 1, 2, 3$ equation (4.16) reduces to the extended Maxwell-Ampère law in curved spacetime [8, eq. (3.17)]

$$\frac{1}{c} \partial_\mu E_j \left(g^{0\mu} g^{ji} - g^{j\mu} g^{0i}\right) + \frac{1}{c} E_j \left[\partial_\mu \left(g^{0\mu} g^{ji} - g^{j\mu} g^{0i}\right) + \frac{1}{\sqrt{-g}} \partial_\mu \left(\sqrt{-g}\right) \left(g^{0\mu} g^{ji} - g^{j\mu} g^{0i}\right)\right]$$
$$-\partial_\mu B^k \epsilon_{kmn} g^{m\mu} g^{ni} - B^k \epsilon_{kmn} \left[\partial_\mu \left(g^{m\mu} g^{ni}\right) + \frac{1}{\sqrt{-g}} \partial_\mu \left(\sqrt{-g}\right) \left(g^{m\mu} g^{ni}\right)\right] = \mu_0 j^i \; . \tag{4.18}$$

In the Maxwell-Ampère law (4.18), a coupling is related to every metric entry, while in Gauss' law, these parts vanish for diagonal metrics. The extended Ampère law is even more intertwined than the extended Gauss' law. For non-stationary spacetimes, two terms will come together and induce a time-varying electric field via Gauss' law. It is expected that gravitational waves produce direct effects in magnetic fields. The term proportional to the electric field vanishes for stationary spacetimes, but time-dependent ones can still occur. All in all, new predictions emerge due to curvature [8, p. 10].
The homogeneous Maxwell equations (4.11) are given by [8, eq. (3.26)]

$$F_{\beta\gamma;\alpha} + F_{\gamma\alpha;\beta} + F_{\alpha\beta;\gamma} = \partial_\alpha F_{\beta\gamma} + \partial_\beta F_{\gamma\alpha} + \partial_\gamma F_{\alpha\beta} - F_{\beta\gamma} {\Gamma^\lambda}_{[\gamma\alpha]} - F_{\alpha\lambda} {\Gamma^\lambda}_{[\beta\gamma]} - F_{\gamma\lambda} {\Gamma^\lambda}_{[\alpha\beta]} = 0 \; . \tag{4.19}$$

Therefore, even in a spacetime with Riemann geometry, these equations reduce to the usual Faraday law

$$\partial_t B^i = -\epsilon^{ijk} \partial_j E_k \tag{4.20}$$

and Gauss' law for magnetism

$$\partial_j B^j = 0 \; . \tag{4.21}$$

They both stay unchanged and can be used to simplify the extended Gauss law and the extended Ampère's law in exceptional cases.

5. Perturbation theory

This chapter deals with the perturbation theory approach and the necessary assumptions. The main components are the extension of all physical meaningful quantities and the extension of the inhomogeneous Maxwell equations in curved spacetime (4.16) by inserting an extension of the metric in Cartesian coordinates. Furthermore, the validity of this approach for several objects in our solar system ist discussed. Finally, the continuity equation, which is often used together with Maxwell's equation, is satisfied by the first-order charge- and current density.

Weak gravitational fields can be dealt with by applying perturbation theory. To this end, the following definitions are used

$$\begin{aligned} g^{\mu\nu} &= \eta^{\mu\nu} + h^{\mu\nu} \; , \\ g_{\mu\nu} &= \eta_{\mu\nu} + h_{\mu\nu} \; . \end{aligned} \tag{5.1}$$

In other words, the spacetime metric deviates slightly from the Minkowski metric. This is, of course, only true as long as the entries of the perturbative metric $h^{\mu\nu}$ are at least in the order of λ

$$\begin{aligned} |h^{\mu\nu}|, |h_{\mu\nu}| &\propto \lambda \; , \\ \lambda &= \frac{r_s}{r} \ll 1 \; , \end{aligned} \tag{5.2}$$

which describes the ratio of the Schwarzschild radius r_s compared to the distance to the source of gravity r. Similar to (5.1) the electromagnetic fields are expanded in a power series for small λ:

Table 5.1.: *The first-order gravitational perturbation with respect to the Minkowski metric for several objects in our solar system. Values were calculated using [43, 50].*

Object	r_s/R_{surface}	$r_{s\ \text{Sun}}/R_{\text{mean Sun}}$
Sun	$4.25 \cdot 10^{-6}$	not defined
Mercury	$2.01 \cdot 10^{-10}$	$5.10 \cdot 10^{-5}$
Venus	$1.19 \cdot 10^{-9}$	$2.73 \cdot 10^{-5}$
Earth	$1.39 \cdot 10^{-9}$	$1.97 \cdot 10^{-5}$
PSP	$8.48 \cdot 10^{-25}$	$4.80 \cdot 10^{-4}$

$$
\begin{aligned}
E_k &= E_k^{(0)} + \lambda E_k^{(1)} + \mathcal{O}\big(\lambda^2\big) \ , \\
B^k &= B^{k(0)} + \lambda B^{k(1)} + \mathcal{O}\big(\lambda^2\big) \ , \\
\rho &= \rho^{(0)} + \lambda \rho^{(1)} + \mathcal{O}\big(\lambda^2\big) \ , \\
j^\nu &= j^{\nu(0)} + \lambda j^{\nu(1)} + \mathcal{O}\big(\lambda^2\big) \ .
\end{aligned}
\tag{5.3}
$$

For several objects in our solar system, the values of λ are provided in table 5.1. The key message of this table is that the Sun's gravitational force is much stronger than any other object in the solar system. This fact is quantified by two variables: $r_{s\ \mathrm{Sun}}/R_{\mathrm{mean\ Sun}}$ and r_s/R_{surface}.
The first parameter $r_{s\ \mathrm{sun}}/R_{\mathrm{mean\ Sun}}$ describes the influence of the Sun's gravitational force on an object at its mean distance $R_{\mathrm{mean\ Sun}}$. Note that $R_{\mathrm{mean\ Sun}}$ differs from object to object.
The second one r_s/R_{surface} denotes the gravitational influence of the object on another object located on the surface. As shown in figure 1.5, executing experiments means measuring effects based on the Sun's gravity because $r_{s\ \mathrm{Sun}}/R_{\mathrm{mean\ Sun}} \gg r_s/R_{\mathrm{surface}}$ holds for any object in the solar system.
The closer an object is to the Sun, the stronger the Sun's gravitational attraction becomes, and thus the parameter r_s/R increases. The Parker Solar Probe of NASA, denoted as „PSP" is an artificial object that uses seven Venus flybys to reduce its distance to the Sun continuously. The closest approach to the Sun ever achieved by a manufactured object with a distance of about 6.16 million kilometers will happen in 2024 [50].

5.1. Perturbed metrics

This section extends the metric tensor of the SRA (3.49) into a Minkowski part plus a perturbation. Additionally, a metric transformation into Cartesian coordinates is done since these are more suitable for describing the Casimir effect between two plane-parallel than spherical coordinates.

For reasons of generality, the „Slow-Rotation Approximation" (SRA) of the Kerr metric, see (3.49) is the starting point of this calculation. The SRA reduces to the Schwarzschild metric if the Kerr spin a parameter vanishes. The contravariant total differentials for spherical coordinates $x^\mu = (ct, r, \varphi, \vartheta)$ read

$$
\mathrm{d}x^\mu = (c\,\mathrm{d}t\,, \mathrm{d}r\,, \mathrm{d}\varphi\,, \mathrm{d}\vartheta) \ , \tag{5.4}
$$

so the covariant total differentials are [dual of natural local tetrad 37, chapter 2.1.3]

$$
\mathrm{d}x_\mu = g_{\mu\nu}\,\mathrm{d}x^\nu = \big(c\,\mathrm{d}t\,, \mathrm{d}r\,, r^2\,\mathrm{d}\varphi\,, r^2\sin^2(\varphi)\,\mathrm{d}\vartheta\big) \ . \tag{5.5}
$$

Starting with the metric from equation (3.49), using the abbreviation λ for the smallness parameter (5.2) and apply (3.7) leads to

$$
\mathrm{d}s^2 = c^2\,\mathrm{d}t^2\,(1-\lambda) + 2\lambda a c\,\mathrm{d}t\,\mathrm{d}\varphi - \frac{1}{1-\lambda}\,\mathrm{d}r^2 - r^2\left[\mathrm{d}\vartheta^2 + \sin^2(\vartheta)\,\mathrm{d}\varphi^2\right] \ . \tag{5.6}
$$

Remember the Kerr spin parameter a from (3.49), which must be small compared to the maximal angular momentum $a_{\max}$. The existence of such an upper limit of the angular momentum is claimed by the „cosmic censorship hypothesis" which states that singularities are hidden within event horizons, so no naked singularity exists [35, Box 34.2]. From this assumption, it can be derived that there must be a maximum angular momentum with the value $a_{\max} = \pm\, MG/c^2$ [35, p. 935]. The according covariant metric tensor for rotations around the z-axis, see figure 1.5, reads

$$g_{\mu\nu} = \begin{pmatrix} 1-\lambda & 0 & \lambda a \sin^2(\vartheta) & 0 \\ 0 & -\frac{1}{1-\lambda} & 0 & 0 \\ \lambda a \sin^2(\vartheta) & 0 & -r^2 \sin^2(\vartheta) & 0 \\ 0 & 0 & 0 & -r^2 \end{pmatrix} . \tag{5.7}$$

In Maxwell's equations (4.16), the contravariant metric tensor occurs several times. According to (3.2), the contravariant metric tensor is given by

$$g^{\mu\nu} = \begin{pmatrix} \frac{r^2}{\lambda^2 a^2 \sin^2(\vartheta) - r^2(\lambda-1)} & 0 & \frac{\lambda a}{\lambda^2 a^2 \sin^2(\vartheta) - r^2(\lambda-1)} & 0 \\ 0 & -(1-\lambda) & 0 & 0 \\ \frac{\lambda a}{\lambda^2 a^2 \sin^2(\vartheta) - r^2(\lambda-1)} & 0 & \frac{(\lambda-1)\csc^4(\vartheta)}{\lambda^2 a^2 - r^2(\lambda-1)\csc^2(\vartheta)} & 0 \\ 0 & 0 & 0 & -\frac{1}{r^2} \end{pmatrix} . \tag{5.8}$$

In first-order perturbation theory, using a Taylor expansion for the parameter λ, both tensors are decomposed into a Minkowski part $\eta^{\mu\nu}$ plus a correction $h^{\mu\nu} \propto \lambda$, see (5.1), as follows:

$$g_{\mu\nu} = \begin{pmatrix} 1 & 0 & 0 & 0 \\ 0 & -1 & 0 & 0 \\ 0 & 0 & -r^2 \sin^2(\vartheta) & 0 \\ 0 & 0 & 0 & -r^2 \end{pmatrix} + \lambda \begin{pmatrix} -1 & 0 & a \sin^2(\vartheta) & 0 \\ 0 & -1 & 0 & 0 \\ a \sin^2(\vartheta) & 0 & 0 & 0 \\ 0 & 0 & 0 & 0 \end{pmatrix} + \mathcal{O}\big(\lambda^2\big) , \tag{5.9}$$

$$g^{\mu\nu} = \begin{pmatrix} 1 & 0 & 0 & 0 \\ 0 & -1 & 0 & 0 \\ 0 & 0 & -\frac{1}{r^2 \sin^2(\vartheta)} & 0 \\ 0 & 0 & 0 & -\frac{1}{r^2} \end{pmatrix} + \lambda \begin{pmatrix} 1 & 0 & \frac{a}{r^2} & 0 \\ 0 & 1 & 0 & 0 \\ \frac{a}{r^2} & 0 & 0 & 0 \\ 0 & 0 & 0 & 0 \end{pmatrix} + \mathcal{O}\big(\lambda^2\big) . \tag{5.10}$$

Cartesian coordinates $x^\mu = (ct, x, y, z)$ are preferred in describing Casimir setups. First, the Cartesian coordinates are connected to spherical coordinates via [derived from 37, eq. (1.6.1)]

$$
\begin{aligned}
r &= \sqrt{x^2+y^2+z^2}\ , && (5.11)\\
\vartheta &= \arccos\left(\frac{z}{\sqrt{x^2+y^2+z^2}}\right) = \arccos\left(\frac{z}{r}\right)\ , && (5.12)\\
\varphi &= \arctan\left(\frac{y}{x}\right)\ . && (5.13)
\end{aligned}
$$

The total differentials of spherical coordinates are represented by

$$
\begin{aligned}
\mathrm{d}r &= \frac{x}{\sqrt{x^2+y^2+z^2}}\,\mathrm{d}x + \frac{y}{\sqrt{x^2+y^2+z^2}}\,\mathrm{d}y + \frac{z}{\sqrt{x^2+y^2+z^2}}\,\mathrm{d}z\ , && (5.14)\\
\mathrm{d}\varphi &= -\cos^2(\varphi)\left(\frac{y}{x^2}\,\mathrm{d}x + \frac{1}{x}\,\mathrm{d}y\right)\ , && (5.15)\\
\mathrm{d}\theta &= -\frac{1}{r^3\sin(\theta)}\ \big(-xz\,\mathrm{d}x - yz\,\mathrm{d}y + (x^2+y^2)\,\mathrm{d}z\big)\ . && (5.16)
\end{aligned}
$$

Their squares, which are necessary for the metric conversion, can be obtained by simple calculations and using the trigonometric identities $\sin^2(\vartheta) = 1-\cos^2(\vartheta) = 1-(z/r)^2$ and $\cos^2(\varphi) = 1/\big(1+\tan^2(\varphi)\big)$:

$$
\begin{aligned}
\mathrm{d}r^2 =& \frac{1}{r^2}\left(x^2\,\mathrm{d}x^2 + 2xy\,\mathrm{d}x\,\mathrm{d}y + 2xz\,\mathrm{d}x\,\mathrm{d}z + y^2\,\mathrm{d}y^2 + 2yz\,\mathrm{d}y\,\mathrm{d}z + z^2\,\mathrm{d}z^2\right) && (5.17)\\
\mathrm{d}\varphi^2 =& \frac{x^4}{(r^2-z^2)^2}\left(\frac{y^2}{x^4}\,\mathrm{d}x^2 - 2\frac{y}{x^3}\,\mathrm{d}x\,\mathrm{d}y + \frac{1}{x^2}\,\mathrm{d}y^2\right) && (5.18)\\
\mathrm{d}\theta^2 =& \frac{r^2}{r^2-z^2}\frac{1}{r^6}\big(x^2z^2\,\mathrm{d}x^2 + 2xyz^2\,\mathrm{d}x\,\mathrm{d}y - 2x^3z\,\mathrm{d}x\,\mathrm{d}z - 2xy^2z\,\mathrm{d}x\,\mathrm{d}z + y^2z^2\,\mathrm{d}y^2\\
& - 2x^2yz\,\mathrm{d}y\,\mathrm{d}z - 2y^3z\,\mathrm{d}y\,\mathrm{d}z + x^4\,\mathrm{d}z^2 + 2x^2y^2\,\mathrm{d}z^2 + y^4\,\mathrm{d}z^2\big)\ . && (5.19)
\end{aligned}
$$

In this way, the perturbation matrices $h^{\mu\nu}$ and $h_{\mu\nu}$ from (5.9) and (5.10) in Cartesian coordinates $x^\mu = (ct,x,y,z)$ read

$$
h_{\mu\nu} = -\lambda\begin{pmatrix}
1 & -a\frac{y}{r^2-z^2} & a\frac{x}{r^2-z^2} & 0\\
-a\frac{y}{r^2-z^2} & \frac{x^2}{r^2} & \frac{xy}{r^2} & \frac{xz}{r^2}\\
a\frac{x}{r^2-z^2} & \frac{xy}{r^2} & \frac{y^2}{r^2} & \frac{yz}{r^2}\\
0 & \frac{xz}{r^2} & \frac{yz}{r^2} & \frac{z^2}{r^2}
\end{pmatrix}\ , \tag{5.20}
$$

$$
h^{\mu\nu} = \lambda\begin{pmatrix}
1 & a\frac{y}{r^2-z^2} & -a\frac{x}{r^2-z^2} & 0\\
a\frac{y}{r^2-z^2} & \frac{x^2}{r^2} & \frac{xy}{r^2} & \frac{xz}{r^2}\\
-a\frac{x}{r^2-z^2} & \frac{xy}{r^2} & \frac{y^2}{r^2} & \frac{yz}{r^2}\\
0 & \frac{xz}{r^2} & \frac{yz}{r^2} & \frac{z^2}{r^2}
\end{pmatrix}\ . \tag{5.21}
$$

The perturbation tensors related to the Schwarzschild metric can be obtained by setting the Kerr spin parameter to zero: $a = 0$. Then the off-diagonal elements vanish, and according to the discussion in section 4.2, the Schwarzschild case should be much easier to solve than the case with rotation. Restricting the perturbed metric from (5.10) in spherical coordinates to a fixed distance $r = R = const$ inside the equatorial plane $\vartheta = \frac{\pi}{2}$ corresponds to the conditions $\sqrt{x^2 + y^2} = R = const$ and $z = 0$ for the perturbed metric (5.21) in Cartesian coordinates. In this case, the perturbed metric has only nine entries, which are not equal to zero.
Since in (4.16) not only the metric tensor $g_{\mu\nu}$ but also its determinant g appears, a first-order expansion for the determinant is carried out in Appendix C.2 and yields

$$\det(\eta_{\mu\nu} + h_{\mu\nu}) \approx -1 - h_{11} + h_{22} + h_{33} + h_{44} \; . \tag{5.22}$$

Assuming that the Casimir setup is fixed at location $\mathbf{r} = (R, 0, 0)^T$ this converts to $h_{11} = h_{22} = \lambda$ and $h_{33} = h_{44} = 0$, see (5.21), the expression $h_{11} - h_{22} - h_{33} - h_{44}$ is zero, so the first-order approximation of the determinant of the SRA (5.9) is given by

$$\det\left(g_{\mu\nu}^{\mathrm{SRA}}\right) = -1 + \mathcal{O}\left(\lambda^2\right) = \det(\eta_{\mu\nu}) \; . \tag{5.23}$$

This means that the determinant of the relevant expression is just the same real number as in the case of Minkowski spacetime up to second-order perturbations. Since Maxwell's equations are evaluated only up to the first order, this result is sufficient for the determinant.

5.2. Perturbed Maxwell's equations

The assumptions made in (5.3) are applied to the inhomogeneous Maxwell's equations (4.16) to get perturbative equations for the zeroth- and the first order. Higher orders are not taken into account in this thesis.

Therefore, introduce the abbreviations

$$\begin{aligned} G^{0j\mu\nu} &\equiv g^{0\mu} g^{j\nu} - g^{j\mu} g^{0\nu} \\ &= \left(\eta^{0\mu} + h^{0\mu}\right)\left(\eta^{j\nu} + h^{j\nu}\right) - \left(\eta^{j\mu} + h^{j\mu}\right)\left(\eta^{0\nu} + h^{0\nu}\right) \\ &= \eta^{0\mu}\eta^{j\nu} + \eta^{0\mu}h^{j\nu} + \eta^{j\nu}h^{0\mu} + h^{0\mu}h^{j\nu} - \eta^{j\mu}\eta^{0\nu} - \eta^{j\mu}h^{0\nu} - \eta^{0\nu}h^{j\mu} - h^{j\mu}h^{0\nu} \\ &= \underbrace{\eta^{0\mu}\eta^{j\nu} - \eta^{j\mu}\eta^{0\nu}}_{\equiv \xi^{0j\mu\nu}} \underbrace{+ \eta^{0\mu}h^{j\nu} + \eta^{j\nu}h^{0\mu} - \eta^{j\mu}h^{0\nu} - \eta^{0\nu}h^{j\mu}}_{\equiv \lambda\zeta^{0j\mu\nu}} + \mathcal{O}\left(\lambda^2\right) \; , \end{aligned} \tag{5.24}$$

and

$$\begin{aligned} H^{mn\mu\nu} &\equiv g^{m\mu} g^{n\nu} \\ &= \left(\eta^{m\mu} + h^{m\mu}\right)\left(\eta^{n\nu} + h^{n\nu}\right) \\ &= \eta^{m\mu}\eta^{n\nu} + \eta^{n\nu}h^{m\mu} + \eta^{m\mu}h^{n\nu} + h^{m\mu}h^{n\nu} \\ &= \underbrace{\eta^{m\mu}\eta^{n\nu}}_{\equiv \tau^{mn\mu\nu}} \underbrace{+ \eta^{n\nu}h^{m\mu} + \eta^{m\mu}h^{n\nu}}_{\equiv \lambda\sigma^{mn\mu\nu}} + \mathcal{O}\left(\lambda^2\right) \; , \end{aligned} \tag{5.25}$$

where just terms up to first order are taken into account. The determinant is generally expanded as follows

$$g = g^{(0)} + \lambda g^{(1)} + \mathcal{O}(\lambda^2) = \eta + \lambda g^{(1)} = -1 + \lambda g^{(1)} \;, \tag{5.26}$$

$$\sqrt{-g} \equiv g^{\star(0)} + \lambda g^{\star(1)} + \mathcal{O}(\lambda^2) = 1 + \lambda g^{\star(1)}, \quad g^{\star(0)} = 1 \;, \tag{5.27}$$

$$\begin{aligned} \frac{\partial_\mu \sqrt{-g}}{\sqrt{-g}} &= \frac{\partial_\mu \left(g^{\star(0)} + \lambda g^{\star(1)}\right)}{g^{\star(0)} + \lambda g^{\star(1)}} + \mathcal{O}(\lambda^2) = \frac{\partial_\mu g^{\star(0)}}{g^{\star(0)} + \lambda g^{\star(1)}} + \lambda \frac{\partial_\mu g^{\star(1)}}{g^{\star(0)} + \lambda g^{\star(1)}} + \mathcal{O}(\lambda^2) \\ &= \frac{\partial_\mu g^{\star(0)}}{g^{\star(0)} + \lambda g^{\star(1)}} + \lambda \frac{\partial_\mu g^{\star(1)}}{g^{\star(0)}} + \mathcal{O}(\lambda^2) = \lambda \partial_\mu g^{\star(1)} + \mathcal{O}(\lambda^2) \;. \end{aligned} \tag{5.28}$$

In general this leads to the fact, that equation (4.16) simplifies to

$$\begin{aligned} &\frac{1}{c} G^{0j\mu\nu} \partial_\mu E_j + \frac{1}{c} E_j \left[\partial_\mu G^{0j\mu\nu} + \frac{1}{\sqrt{-g}} G^{0j\mu\nu} \left(\partial_\mu \sqrt{-g}\right)\right] \\ -H^{mn\mu\nu} \epsilon_{kmn} \partial_\mu B^k - \epsilon_{kmn} B^k &\left[\partial_\mu H^{mn\mu\nu} + \frac{1}{\sqrt{-g}} H^{mn\mu\nu} \left(\partial_\mu \sqrt{-g}\right)\right] = \mu_0 j^\nu \;, \end{aligned} \tag{5.29}$$

or equivalently

$$\begin{aligned} \mu_0 \left(j^{\nu(0)} + \lambda j^{\nu(1)}\right) = &\frac{1}{c} \left(\xi^{0j\mu\nu} + \lambda \zeta^{0j\mu\nu}\right) \partial_\mu \left(E_j^{(0)} + \lambda E_j^{(1)}\right) \\ &+ \frac{1}{c} \left(E_j^{(0)} + \lambda E_j^{(1)}\right) \left[\partial_\mu \left(\xi^{0j\mu\nu} + \lambda \zeta^{0j\mu\nu}\right) + \left(\xi^{0j\mu\nu} + \lambda \zeta^{0j\mu\nu}\right) \lambda \partial_\mu g^{\star(1)}\right] \\ &- \left(\tau^{mn\mu\nu} + \lambda \sigma^{mn\mu\nu}\right) \epsilon_{kmn} \partial_\mu \left(B^{k(0)} + \lambda B^{k(1)}\right) \\ &- \epsilon_{kmn} \left(B^{k(0)} + \lambda B^{k(1)}\right) \left[\partial_\mu \left(\tau^{mn\mu\nu} + \lambda \sigma^{mn\mu\nu}\right) + \left(\tau^{mn\mu\nu} + \lambda \sigma^{mn\mu\nu}\right) \lambda \partial_\mu g^{\star(1)}\right] . \end{aligned} \tag{5.30}$$

Sorting by equal orders, the zeroth-order reads

$$\mu_0 j^{\nu(0)} = \frac{1}{c} \xi^{0j\mu\nu} \partial_\mu E_j^{(0)} + \frac{1}{c} E_j^{(0)} \partial_\mu \xi^{0j\mu\nu} - \tau^{mn\mu\nu} \epsilon_{kmn} \partial_\mu B^{k(0)} - \epsilon_{kmn} B^{k(0)} \partial_\mu \tau^{mn\mu\nu} \;. \tag{5.31}$$

Substituting back the former expressions for (5.24) and (5.25), (5.31) reduces to

$$\mu_0 j^{\nu(0)} = \frac{1}{c} \partial_\mu E_j^{(0)} \left(\eta^{0\mu} \eta^{j\nu} - \eta^{j\mu} \eta^{0\nu}\right) - \epsilon_{kmn} \partial_\mu B^{k(0)} \left(\eta^{m\mu} \eta^{n\nu}\right) \;. \tag{5.32}$$

Specializing this formula further to $\nu = 0$, which corresponds to Gauss' law, yields

$$\frac{1}{c} \partial_\mu E_j^{(0)} \left(\eta^{0\mu} \eta^{j0} - \eta^{j\mu} \eta^{00}\right) - \partial_\mu B^{k(0)} \epsilon_{kmn} \eta^{m\mu} \eta^{n0} = \mu_0 j^{0(0)} \;. \tag{5.33}$$

Decomposing the index μ into $\mu = 0$ and $\mu = k$ leads to

$$\frac{1}{c}\partial_k E_j^{(0)}\left(\underbrace{\eta^{0k}\eta^{j0}}_{=0}-\eta^{jk}\eta^{00}\right)-\partial_\mu B^{k(0)}\epsilon_{kmn}\eta^{m\mu}\underbrace{\eta^{n0}}_{=0}=\mu_0 j^{0(0)}\ , \tag{5.34}$$

which finally results the Gauss' law in Minkowski spacetime (2.1)

$$\boldsymbol{\nabla}\cdot\mathbf{E}^{(0)}=\frac{\rho}{\varepsilon_0}\ . \tag{5.35}$$

Analogously for $\nu = l = 1,2,3$ equation (5.31) transforms into Ampère's law via

$$\frac{1}{c}\partial_\mu E_j^{(0)}\left(\underbrace{\eta^{0\mu}}_{=0,\mu\neq 0}\eta^{jl}-\eta^{j\mu}\underbrace{\eta^{0l}}_{=0}\right)-\partial_\mu B^{k(0)}\epsilon_{kmn}\left(\eta^{m\mu}\eta^{nl}\right)=\mu_0 j^{l(0)}\ . \tag{5.36}$$

Decomposing again the index μ into $\mu = 0$ and $\mu = k$ yields Ampère's law in Minkowski spacetime (2.4)

$$\boldsymbol{\nabla}\times\mathbf{B}^{(0)}=\frac{1}{c^2}\partial_t\mathbf{E}^{(0)}+\mu_0\mathbf{j}^{(0)}\ . \tag{5.37}$$

As expected, Maxwell's equations in Minkowski spacetime (2.1)–(2.4) have been reproduced in zeroth-order perturbation theory.

The first-order correction terms, which include the effect of weak gravity, following from, (5.30) read

$$\begin{aligned}\mu_0 j^{\nu(1)}=&\frac{1}{c}\left[\xi^{0j\mu\nu}\partial_\mu E_j^{(1)}+\zeta^{0j\mu\nu}\partial_\mu E_j^{(0)}\right]+\frac{1}{c}E_j^{(0)}\left[\partial_\mu\zeta^{0j\mu\nu}+\xi^{0j\mu\nu}\partial_\mu g^{\star(1)}\right]\\&+\frac{1}{c}E_j^{(1)}\partial_\mu\xi^{0j\mu\nu}-\epsilon_{kmn}B^{k(1)}\partial_\mu\tau^{mn\mu\nu}\\&-\epsilon_{kmn}\sigma^{mn\mu\nu}\partial_\mu B^{k(0)}-\epsilon_{kmn}\tau^{mn\mu\nu}\partial_\mu B^{k(1)}-\epsilon_{kmn}B^{k(0)}\left[\partial_\mu\sigma^{mn\mu\nu}+\tau^{mn\mu\nu}\partial_\mu g^{\star(1)}\right]\ .\end{aligned} \tag{5.38}$$

After evaluating every single expression the first-order of the extended Gauss' law yields

$$\begin{aligned}\mu_0 j^{0(1)}=\frac{\rho^{(1)}}{\varepsilon_0}=\frac{1}{c}&\left[\sum_j\partial_j E_j^{(1)}+h^{j0}\partial_0 E_j^{(0)}+h^{00}\sum_j\partial_j E_j^{(0)}-h^{j\mu}\partial_\mu E_j^{(0)}\right]\\&+\frac{1}{c}\left[E_j^{(0)}\delta^{jl}\partial_l h^{00}-E_j^{(0)}\partial_l h^{jl}+E_j^{(0)}\delta^{jl}\partial_l g^{\star(1)}\right]\\&+\sum_m\epsilon_{kmn}h^{n0}\partial_m B^{k(0)}+\epsilon_{kmn}B^{k(0)}\delta^{ml}\partial_l h^{n0}\ .\end{aligned} \tag{5.39}$$

In the vacuum case the charge density $\rho^{(1)}$ in (5.39) vanishes.

Furthermore, reading off the property $\partial_j g^{\star(1)} = 0$ from (5.23). This is possible in two ways: First, if the determinant is $-1 + \mathcal{O}(\lambda^2)$ then all derivatives must vanish. Second, it was shown that the first-order correction, corresponding to $g^{\star(1)}$ is zero. Analog, the derivative of a constant vanishes. Equation (5.39) then simplifies to

$$\begin{aligned}\sum_j \partial_j E_j^{(1)} = &- \left[h^{00} \sum_j \partial_j E_j^{(0)} + \sum_j E_j^{(0)} \partial_j h^{00} \right] + \left[h^{jl} \partial_l E_j^{(0)} + E_j^{(0)} \partial_l h^{jl} \right] \\ &- c \sum_m \epsilon_{kmn} \left[h^{n0} \partial_m B^{k(0)} + B^{k(0)} \partial_m h^{n0} \right] .\end{aligned} \tag{5.40}$$

Correspondingly, the the first-order of the extended Ampère law is given by

$$\begin{aligned}\mu_0 j^{p(1)} = &- \frac{1}{c} \partial_0 E_p^{(1)} - \sum_m \epsilon_{kmp} \partial_m B^{k(1)} \\ &+ \frac{1}{c} \left[h^{jp} \partial_0 E_j^{(0)} + h^{0p} \sum_j \partial_j E_j^{(0)} + \sum_j E_j^{(0)} \partial_j h^{0p} \right] \\ &- \frac{1}{c} \left[h^{00} \partial_0 E_p^{(0)} + h^{0l} \partial_l E_p^{(0)} + E_p^{(0)} \partial_l h^{0l} \right] \\ &+ \epsilon_{kmp} h^{m\mu} \partial_\mu B^{k(0)} + \sum_m \epsilon_{kmn} h^{np} \partial_m B^{k(0)} \\ &+ \epsilon_{kmp} B^{k(0)} \partial_l h^{ml} + \sum_m \epsilon_{kmn} B^{k(0)} \partial_m h^{np} - \sum_m \epsilon_{kmp} B^{k(0)} \partial_m g^{\star(1)} .\end{aligned} \tag{5.41}$$

Generalizing to the vacuum $j^{p(1)} = 0$ and adding $\partial_m g^{\star(1)} = 0$ from (5.23) the formula (5.41) reduces to

$$\begin{aligned}\frac{1}{c} \partial_0 E_p^{(1)} + \sum_m \epsilon_{kmp} \partial_m B^{k(1)} = &\frac{1}{c} \left[h^{jp} \partial_0 E_j^{(0)} + h^{0p} \sum_j \partial_j E_j^{(0)} + \sum_j E_j^{(0)} \partial_j h^{0p} \right] \\ &- \frac{1}{c} \left[h^{00} \partial_0 E_p^{(0)} + h^{0l} \partial_l E_p^{(0)} + E_p^{(0)} \partial_l h^{0l} \right] \\ &+ \epsilon_{kmp} h^{m\mu} \partial_\mu B^{k(0)} + \sum_m \epsilon_{kmn} h^{np} \partial_m B^{k(0)} \\ &+ \epsilon_{kmp} B^{k(0)} \partial_l h^{ml} + \sum_m \epsilon_{kmn} B^{k(0)} \partial_m h^{np} .\end{aligned} \tag{5.42}$$

At this point, it should be mentioned that the left-hand side of equation (5.40) corresponds to the divergence of the first-order electric vector field $\mathbf{E}^{(1)}$, formally similar to what is calculated in Minkowski spacetime just with the zeroth-order (2.1). The left-hand side of equation (5.42) is, except for a minus sign due to sign convention, also similar to the zeroth-order (2.4), if the sum over m is identified with the curl of the first-order magnetic induction field $\mathbf{B}^{(1)}$.
Identifying the right-hand sides of equations (5.40) and (5.42) with an effective first-order charge density $\rho_{\text{eff}}^{(1)} = \rho^{(1)}(\mathbf{E}^{(0)}, \mathbf{B}^{(0)})$ and a first-order current density $\mathbf{j}_{\text{eff}}^{(1)} = \mathbf{j}^{(1)}(\mathbf{E}^{(0)}, \mathbf{B}^{(0)})$, describing

the influence of weak gravity, it can be stated that these are exclusively given by the zeroth-order electric field $\mathbf{E}^{(0)}$ and the zeroth-order magnetic induction field $\mathbf{B}^{(1)}$. Since the properties of the vacuum do not change with or without gravity, it is convenient to change the notation and drop the term effective for the following quantities:

$$\begin{aligned} \sum_j \partial_j E_j^{(1)} &= \frac{\rho^{(1)}}{\varepsilon_0} , \\ \frac{1}{c}\partial_0 E_p^{(1)} + \sum_m \epsilon_{kmp}\partial_m B^{k(1)} &= -\mu_0 \mathbf{j}^{(1)} . \end{aligned} \tag{5.43}$$

Note that (5.43) are again Maxwell equations, but this time of the first order, considering the effects of weak gravity. Summarizing (5.39), (5.41), and (5.43), this means the first-order electric- and magnetic fields are given via inhomogeneities, which result from the zeroth-order solutions. This recursive structure is typical for perturbation theory [10, chapter 11].
Using identities of vector calculus, the according inhomogeneous wave equations are given by

$$\begin{aligned} \Box\mathbf{E}^{(1)} &= -\mu_0\partial_t\mathbf{j}^{(1)} - \frac{1}{\varepsilon_0}\boldsymbol{\nabla}\cdot\rho^{(1)} , \\ \Box\mathbf{B}^{(1)} &= \mu_0\boldsymbol{\nabla}\times\mathbf{j}^{(1)} , \end{aligned} \tag{5.44}$$

similar to those commonly used in the Minkowski case.
Equation (5.44) reveals that the presence of effective charge- and current densities correspond to the presence of weak gravity in Minkowski spacetime.

5.3. Continuity equation for first-order Maxwell's equations

The continuity equation is often combined with Maxwell's equations and corresponds to the charge conservation. It is sufficient to test its validity because an interpretation of the first-order charge- and current density as meaningful physical quantities, which can be used for experiments, is valid.

In general relativistic the continuity equation reads

$$\partial_\mu j^\mu = \partial_0 j^0 + \boldsymbol{\nabla}\cdot\mathbf{j} = 0 , \tag{5.45}$$

where $j^\mu = (c\rho, \mathbf{j})$ denotes the four-current density with the contravariant current density $\mathbf{j}$. Explicitly, this yields

$$\partial_t\rho^{(1)} - \boldsymbol{\nabla}\cdot\mathbf{j}^{(1)} = 0 , \tag{5.46}$$

where $\mathbf{j}^{(1)}$ denotes the (effective) covariant current density according to (5.43).
Let us have a look onto (5.42) and (5.40) for

$$\partial_\alpha h^{\beta\gamma} = 0 , \tag{5.47}$$

so all derivatives of the perturbation matrix $h^{\mu\nu}$ are equal to zero. This is satisfied as long as the perturbed metric is constant in time and space. For the SRA (3.49) this is true as long as the evaluation is performed at a fixed point $\mathbf{r} = R = const$ in the spacetime and the angular momentum a does not change. Then the parameter λ from (5.2) can be written as $\lambda = r_s/R$ for a constant distance to the source of gravity R. In this case, Gauss's law is given by

$$\frac{\rho^{(1)}}{\varepsilon_0} = -h^{00}\sum_j \partial_j E_j^{(0)} + h^{jl}\partial_l E_j^{(0)} - c\sum_m \epsilon_{kmn} h^{n0}\partial_m B^{k(0)} \ , \tag{5.48}$$

and Ampère's law simplifies to

$$\begin{aligned} -\mu_0 \mathbf{j}^{(1)} = &\frac{1}{c} h^{jp}\partial_0 E_j^{(0)} + h^{0p}\sum_j \partial_j E_j^{(0)} - \frac{1}{c} h^{00}\partial_0 E_p^{(0)} - h^{0l}\partial_l E_p^{(0)} \\ &+ \epsilon_{kmp} h^{m0}\partial_0 B^{k(0)} + \epsilon_{kmp} h^{ml}\partial_l B^{k(0)} + \sum_m \epsilon_{kmn} h^{np}\partial_m B^{k(0)} \ . \end{aligned} \tag{5.49}$$

The corresponding partial derivatives read

$$\partial_0 \frac{\rho^{(1)}}{\varepsilon_0} = \frac{1}{c}\partial_t \frac{\rho^{(1)}}{\varepsilon_0} = -h^{00}\partial_0 \sum_j \partial_j E_j^{(0)} + h^{jl}\partial_0\partial_l E_j^{(0)} - c\sum_m \epsilon_{kmn} h^{n0}\partial_0\partial_m B^{k(0)} \ , \tag{5.50}$$

$$\begin{aligned} -\sum_p \mu_0 \partial_p j_p^{(1)} = &\frac{1}{c} h^{jp}\partial_0\partial_p E_j^{(0)} + h^{0p}\partial_p \sum_j \partial_j E_j^{(0)} - \frac{1}{c} h^{00}\partial_0 \sum_p \partial_p E_p^{(0)} - \sum_p h^{0l}\partial_l\partial_p E_p^{(0)} \\ &+ \sum_p \epsilon_{kmp} h^{m0}\partial_0\partial_p B^{k(0)} + \sum_p \epsilon_{kmp} h^{ml}\partial_p\partial_l B^{k(0)} + \sum_m \epsilon_{kmn} h^{np}\partial_p\partial_m B^{k(0)} \ . \end{aligned} \tag{5.51}$$

First, it is shown that two terms of Ampère's law cancel each other in pairs

$$h^{0p}\partial_p \sum_j \partial_j E_j^{(0)} - \sum_p h^{0l}\partial_l\partial_p E_p^{(0)} = 0 \ . \tag{5.52}$$

Rename the indices in the second term, what is always allowed as long the indices does not appear twice due to the relabeling, and replace the coordinates $l \to p$, $p \to j$ leads to

$$h^{0p}\partial_p \sum_j \partial_j E_j^{(0)} - h^{0p}\partial_p \sum_j \partial_j E_j^{(0)} = 0 \ . \tag{5.53}$$

Obviously, this is true. In the same way it can be shown that

$$\sum_p \epsilon_{kmp} h^{ml}\partial_p\partial_l B^{k(0)} + \sum_m \epsilon_{kmn} h^{np}\partial_p\partial_m B^{k(0)} = 0 \ . \tag{5.54}$$

To this end, replace $m \to p$, $p \to l$, $n \to m$ and use that $\epsilon_{kmp} = -\epsilon_{kpm}$ and this relations is fulfilled as well.
Inserting the remaining terms into (5.46), considering the correct signs, prefactors, and relabeling if necessary, the continuity equation (5.45) is satisfied. Take special care of the fact that $c^2 = \frac{1}{\mu_0 \varepsilon_0}$.

The essence of this calculation is to show that $\rho^{(1)}$ and $\mathbf{j}^{(1)}$ are physically well-defined and no pseudo quantities that only occur due to perturbation theory. This leads to the idea that the first-order charge density and the first-order current density could act as relevant measurement variables to demonstrate the influence of gravity on the Casimir effect. A concrete experimental setup based on these quantities is unclear at the moment. However, assuming the generation of those is possible on and between the plates in the flat case, it is assumed that a change of the electromagnetic fields occurs, which corresponds to the influence a source of weak gravity would have.

This page intentionally left blank.

6. Casimir effect for fixed setups in weak gravity

In this chapter, the perturbed Maxwell equations, derived in chapter 5.2, are solved for the three setups shown in figure 1.5, assuming that those are fixed at position $\mathbf{r}$, which will be specified later, and do not move at all. The inhomogeneities of the wave equations (5.44) are given by the solutions in the flat Minkowskian case via (5.39) and (5.41). The TE and TM mode solutions for setup I are presented in (2.11) and (2.13). Since measurable effects are expected to be identified with the real part of these solutions, only those will be considered. Both solutions fulfill the property

$$\nabla \cdot \mathbf{E}^{(0)} = 0 \, , \tag{6.1}$$

which helps to simplify the inhomogeneities of (5.39) and (5.41) by a few terms. For setups II and III, the solutions for the flat case can be obtained from (2.11) and (2.13) by suitably permuting the involved components of coordinates, the electric field, and the magnetic induction field. The zeroth-order solutions can always be found below at the beginning of the respective section.

The simplest metric for investigating the influence of weak gravity on the Casimir effect is the Schwarzschild metric. Nevertheless, a description that is as general as possible is also desirable. Therefore, we consider a generalization of the Slow-Rotation Approximation. According to (5.21), in the equatorial plane, it reads

$$h^{\mu\nu} = \begin{pmatrix} h^{00} & h^{01} & h^{02} & 0 \\ h^{10} & h^{11} & h^{21} & 0 \\ h^{20} & h^{12} & h^{22} & 0 \\ 0 & 0 & 0 & 0 \end{pmatrix} \, . \tag{6.2}$$

A reduction to the Schwarzschild metric in the equatorial plane and Cartesian coordinates is possible by setting the Kerr spin parameter in (5.21) to zero, i.e., $a = 0$, which corresponds to setting $h^{10} = h^{01} = h^{20} = h^{02} = 0$ and additionally demanding $h^{22} = 0$ leads to

$$h^{\mu\nu} = \begin{pmatrix} h^{00} & 0 & 0 & 0 \\ 0 & h^{11} & 0 & 0 \\ 0 & 0 & 0 & 0 \\ 0 & 0 & 0 & 0 \end{pmatrix} \, . \tag{6.3}$$

Putting $h^{22} = 0$ is justified by the assumption that all three setups are evaluated at the same position in Cartesian coordinates, namely

$$\mathbf{r} = \begin{pmatrix} R \\ 0 \\ 0 \end{pmatrix} \text{ for const} = R \gg r_s \ . \tag{6.4}$$

In this case, the following relations from (5.21) simplify to

$$\frac{x^2}{r^2} = 1 \ , \tag{6.5}$$

$$\lambda = \frac{r_s}{R} = \text{const} \ , \tag{6.6}$$

which are useful to grant the validity of a time-independent perturbation theory approach. Further, as long as the perturbed metric components $h^{\mu\nu}$ stay constant, any other metric can also be investigated as long as it fits (6.3).
The assumption (6.4) is valid for the following two cases:

1. The Casimir setup and the gravitating object are fixed at their respective locations, having the distance R to each other, and are not moving.
2. The Casimir setup and the source of gravity are fixed at their positions, but the gravitation source rotates slowly around the z-axis.
   For small angular momentum, this is approximately similar to the case that the Casimir setup rotates in a circular orbit with a distance R around the fixed source of gravity.

Having a closer look at figure 1.5 and considering condition (6.4), it can be seen that the surface normal of setup I is the only one parallel to the x-axis, which is also parallel to the gravitational force. The surface normals for setups II and III are perpendicular to the gravitational force. Since the potential energy in the gravitational field of a body constantly changes only along the (parallel) field lines, it is expected that the Casimir energy of setup I will change. In contrast, what will happen for setups II and III is unclear. Note that the Casimir force in the case of weak gravity was already calculated for setup I using a scalar Klein-Gordon theory [39, 47]. For the Maxwell theory, however, the two transversal degrees of freedom have to be taken into account, so we expect an additional factor of two compared to the Klein-Gordon theory, as already discussed in chapter 1.

6.1. Setup I

This section investigates the Casimir effect of setup I in figure 1.5 under the condition that it is located at (6.4) and not moving at all. New methods are introduced here, and calculations are detailed.

6.1.1. Transversal electric modes

According to the case in Minkowski spacetime from section 2.1, two independent solutions of the zeroth-order Maxwell equations must be inserted separately in the first order, starting with the transversal electric (TE) modes. To treat all three setups clearly and concisely, the abbreviations

$$\begin{aligned}
\sigma &\equiv \mathbf{k}_\perp \cdot \mathbf{r}_\perp - \omega t \ , \\
\Delta\sigma &\equiv \frac{h^{00}\frac{\omega^2}{c^2} + h^{11}k_x^2}{2k_\parallel^2}\sigma \ , \\
|\mathbf{k}| &= \sqrt{\mathbf{k}_\parallel^2 + \mathbf{k}_\perp^2} = \sqrt{k_x^2 + k_y^2 + k_z^2}
\end{aligned} \tag{6.7}$$

are introduced. Here $\mathbf{k}_\parallel$ denotes the direction parallel to the surface normal, more precise the direction in which quantization of the modes occurs. Accordingly, $\mathbf{k}_\perp$ denotes the direction perpendicular to these where the modes are continuous.
First, the $\mathbf{k}$ vector components have to be set. For setup I the correct identifications are

$$\begin{aligned}
\mathbf{k}_\perp \cdot \mathbf{r}_\perp &= k_y y + k_z z \ , \\
k_\parallel &= k_x \ .
\end{aligned} \tag{6.8}$$

The real part of the components of the complex unperturbed solutions (2.11) reads

$$\mathbf{E}^{(0)} = \mathrm{N_{TE}}\omega \begin{pmatrix} 0 \\ k_z \\ -k_y \end{pmatrix} \sin(k_x x)\sin(\sigma) \ , \tag{6.9}$$

$$\mathbf{B}^{(0)} = -\mathrm{N_{TE}} \begin{pmatrix} k_\perp^2 \sin(k_x x)\sin(\sigma) \\ k_x k_y \cos(k_x x)\cos(\sigma) \\ k_x k_z \cos(k_x x)\cos(\sigma) \end{pmatrix} \ . \tag{6.10}$$

Look up Gauss'- and Ampère's laws for the metric (6.3) by simplifying the general expressions (5.40) and (5.42) and insert therein the unperturbed solutions (6.9) and (6.10), yielding the charge density

$$\rho^{(1)} = h^{11}\partial_1 E_1 = 0 \ , \tag{6.11}$$

and the current density

$$\mathbf{j}^{(1)} = -\frac{1}{\mu_0} \begin{pmatrix} -\frac{1}{c}h^{00}\partial_0 E_1^{(0)} \\ -\frac{1}{c}h^{00}\partial_0 E_2^{(0)} + h^{11}\partial_1 B^{3(0)} \\ -\frac{1}{c}h^{00}\partial_0 E_3^{(0)} h^{11}\partial_1 B^{2(0)} \end{pmatrix} \tag{6.12}$$

$$= -\frac{1}{\mu_0} \begin{pmatrix} 0 \\ \mathrm{N_{TE}} k_z \sin(k_x x)\cos(\sigma)\left(\frac{\omega^2}{c^2}h^{00} + k_x^2 h^{11}\right) \\ -\mathrm{N_{TE}} k_y \sin(k_x x)\cos(\sigma)\left(\frac{\omega^2}{c^2}h^{00} + k_x^2 h^{11}\right) \end{pmatrix} \ . \tag{6.13}$$

Surprisingly, the (effective) current density does not vanish at the plate surfaces according to the $\sin(k_x x)$ terms in (6.13), considering the boundary conditions of the TE modes (2.12). As a result, an eddy current in the metal plates must occur reproducing the effect of weak gravity in Minkowski spacetime. Further, this current is not limited to the plates since it also appears between them. This seems to be challenging to build for an experimental realization. Nevertheless, the charge density (6.11) vanishes completely as it is expected in the flat case.
The wave equations for the first-order correction terms, according to (5.44), are then given by

$$\Box\mathbf{E}^{(1)} = \mathrm{N}_{\mathrm{TE}}\omega\left(h^{00}\frac{\omega^2}{c^2}+h^{11}k_x^2\right)\begin{pmatrix}0\\ k_z\sin(k_x x)\sin(\sigma)\\ -k_y\sin(k_x x)\sin(\sigma)\end{pmatrix}\ , \tag{6.14}$$

$$\Box\mathbf{B}^{(1)} = -\mathrm{N}_{\mathrm{TE}}\left(h^{00}\frac{\omega^2}{c^2}+h^{11}k_x^2\right)\begin{pmatrix}k_\perp^2\sin(k_x x)\sin(\sigma)\\ k_x k_y\cos(k_x x)\cos(\sigma)\\ k_x k_z\cos(k_x x)\cos(\sigma)\end{pmatrix}\ . \tag{6.15}$$

Note that (6.14) and (6.15) describe inhomogeneous wave equations where the right-hand side is exclusively given by the zeroth-order solutions (6.9) and (6.10). That is why an appropriate ansatz leads to so-called secular terms, which diverge in both the transversal spatial coordinates and time. Consequently, the resulting solution no longer satisfies the conservation of energy. Using a suitable renormalization, however, it is possible to combine the terms of the zeroth order and the secular terms of the first order so that a bound solution with a new dispersion relation is obtained. The solutions of (6.14) and (6.15) read

$$\mathbf{E}^{(1)} = \begin{pmatrix}0\\ -k_z\\ k_y\end{pmatrix}\frac{1}{2k_x^2}\mathrm{N}_{\mathrm{TE}}\omega\sigma\sin(k_x x)\cos(\sigma)\left(h^{00}\frac{\omega^2}{c^2}+h^{11}k_x^2\right)\ , \tag{6.16}$$

$$\mathbf{B}^{(1)} = \mathrm{N}_{\mathrm{TE}}\frac{1}{2k_x^2}\left(h^{00}\frac{\omega^2}{c^2}+h^{11}k_x^2\right)\begin{pmatrix}k_\perp^2\cos(\sigma)\sigma\sin(k_x x)\\ -k_x k_y\left[\sigma\sin(\sigma)+\cos(\sigma)\right]\cos(k_x x)\\ -k_x k_z\left[\sigma\sin(\sigma)+\cos(\sigma)\right]\cos(k_x x)\end{pmatrix}\ . \tag{6.17}$$

Note that Maxwell's equations (2.1)–(2.4) applied to the first order turn out to be automatically fulfilled by (6.16) and (6.17). The secular term that occurs in (6.16) is $\sigma\cos(\sigma)$ because σ diverges in the case of k_y, k_z, or ω going to infinity, see (6.7) and (6.8), while $\cos(\sigma)$ is a bounded function. The same term can also be found in the x-component of the magnetic induction field (6.17). In the y and z-component, the secular terms read $\sigma\sin(\sigma)$. For the simple case of the Duffing oscillator, the handling of secular terms is provided in Appendix A. The significant difference between the Duffing oscillator and the calculation here is that Maxwell's equations are partial differential equations instead of ordinary ones, like in the case of a Duffing oscillator.

Moreover, in the transversal components of (6.17), there can be found the term $\cos(\sigma)$, which corresponds to homogeneous solutions of the wave equations (5.44). These are necessary since the original equations that must be solved are Gauss' (5.40) and Ampère's law (5.42). This is achievable only by considering the homogeneous solutions, which generally read

$$\mathbf{E}^{(1)}_{\text{homo}} = \mathbf{A}\sin\big(\mathbf{k}_\parallel \cdot \mathbf{r}_\parallel\big)\sin(\sigma) + \mathbf{B}\cos\big(\mathbf{k}_\parallel \cdot \mathbf{r}_\parallel\big)\cos(\sigma)\ , \tag{6.18}$$

$$\mathbf{B}^{(1)}_{\text{homo}} = \mathbf{C}\sin\big(\mathbf{k}_\parallel \cdot \mathbf{r}_\parallel\big)\sin(\sigma) + \mathbf{D}\cos\big(\mathbf{k}_\parallel \cdot \mathbf{r}_\parallel\big)\cos(\sigma)\ , \tag{6.19}$$

where **A**, **B**, **C**, and **D** denote constant vectorial prefactors. According to (6.14) and (6.15), the only homogeneous solution needed is the one proportional to the prefactor **D**. It is fixed via (6.11) and (6.13).

The electric field obtained from perturbation theory is the sum of the zeroth order and the first order, namely

$$\mathbf{E}^{\text{curved}}_{\text{TE}} \approx \mathbf{E}^{(0)} + \mathbf{E}^{(1)} \tag{6.20}$$

$$= \mathrm{N}_{\text{TE}}\omega\sin(k_x x)\begin{pmatrix} 0 \\ -k_z \\ k_y \end{pmatrix}\left\{-\sin(\sigma) + \frac{h^{00}\frac{\omega^2}{c^2} + h^{11}k_x^2}{2k_x^2}\sigma\cos(\sigma)\right\}\ . \tag{6.21}$$

Providing Taylor expansions inside the curly brackets for $\cos(\Delta\sigma) \approx 1$, $\Delta\sigma \approx \sin(\Delta\sigma)$, and $\Delta\sigma$ is a small parameter because it is proportional to the small parameters h^{00} and h^{11}, see (6.7). This leads to

$$\mathbf{E}^{\text{curved}}_{\text{TE}} \approx \mathrm{N}_{\text{TE}}\omega\sin(k_x x)\begin{pmatrix} 0 \\ -k_z \\ k_y \end{pmatrix}\{-\sin(\sigma)\cos(\Delta\sigma) + \sin(\Delta\sigma)\cos(\sigma)\}\ . \tag{6.22}$$

Apply the addition theorem $\sin(\sigma)\cos(\Delta\sigma) \pm \sin(\Delta\sigma)\cos(\sigma) = \sin(\sigma \pm \Delta\sigma)$ and get

$$\mathbf{E}^{\text{curved}}_{\text{TE}} = \mathrm{N}_{\text{TE}}\omega\sin(k_x x)\begin{pmatrix} 0 \\ k_z \\ -k_y \end{pmatrix}\sin(\sigma - \Delta\sigma)\ . \tag{6.23}$$

The renormalization is performed as follows: Define

$$\tilde{\lambda} \equiv \frac{\Delta\sigma}{\sigma} = \frac{h^{00}\frac{\omega^2}{c^2} + h^{11}k_x^2}{2k_x^2} \tag{6.24}$$

and rewrite the argument of $\sin(\sigma - \Delta\sigma)$ in (6.23) as

$$\sigma - \Delta\sigma = \sigma\left(1 - \tilde{\lambda}\right) \tag{6.25}$$

Introduce changes of the wave vector components included in $\sigma = k_y y + k_z z - \omega t$ and k_x by

$$\Delta k_y = -\tilde{\lambda} k_y \Longrightarrow {k_y}' = k_y + \Delta k_y = k_y\left(1 - \tilde{\lambda}\right) \ , \tag{6.26}$$

$$\Delta k_z = -\tilde{\lambda} k_z \Longrightarrow {k_z}' = k_z + \Delta k_z = k_z\left(1 - \tilde{\lambda}\right) \ , \tag{6.27}$$

$$\Delta \omega = -\tilde{\lambda} \omega \Longrightarrow \omega' = \omega + \Delta \omega = \omega\left(1 - \tilde{\lambda}\right) \ , \tag{6.28}$$

$$\Delta k_x = 0 \Longrightarrow {k_x}' = k_x \ , \tag{6.29}$$

and rewrite the old dispersion relation

$$\omega\left(\mathbf{k}\right) = c|\mathbf{k}| = c\sqrt{k_x^2 + k_y^2 + k_z^2} \ , \tag{6.30}$$

by replacing the old wave vector components by the new ones

$$\omega\left(\mathbf{k}\right) = \frac{\omega'}{1 - \tilde{\lambda}} = c\sqrt{{k'_x}^2 + \frac{{k'_y}^2}{\left(1 - \tilde{\lambda}\right)^2} + \frac{{k'_z}^2}{\left(1 - \tilde{\lambda}\right)^2}} \ . \tag{6.31}$$

For the renormalized angular frequency ω', which depends on the new wave vector components, this yields

$$\omega'\left(\mathbf{k}'\right) = c\sqrt{{k'_x}^2\left(1 - \tilde{\lambda}\right)^2 + {k'_y}^2 + {k'_z}^2} \ . \tag{6.32}$$

Applying a Taylor expansion now for the new frequency ω' in $\tilde{\lambda} \approx 0$ to obtain

$$\omega'\left(\mathbf{k}'\right) = c\sqrt{{k'_x}^2 + {k_y}'^2 + {k_z}'^2} - \frac{c{k'_x}^2\tilde{\lambda}}{\sqrt{{k'_x}^2 + {k_y}'^2 + {k_z}'^2}} + \mathcal{O}\left(\tilde{\lambda}^2\right) \ . \tag{6.33}$$

According to (6.7), both square roots in (6.33) can be identified with $|\mathbf{k}'| = \sqrt{{k'_x}^2 + {k_y}'^2 + {k_z}'^2}$. In addition, the notation is changed, and the „′" signs are dropped for the wave vector components. This is allowed since the renormalization process leads to new physical relevant quantities, which must be used instead of the old ones:

$$\omega\left(\mathbf{k}\right) = c|\mathbf{k}|\left(1 - \frac{k_x^2\tilde{\lambda}}{|\mathbf{k}|^2} + \mathcal{O}\left(\tilde{\lambda}^2\right)\right) \ . \tag{6.34}$$

Taking (6.24) into account, and substituting back $\tilde{\lambda}$, yields

$$\omega(\mathbf{k}) = c|\mathbf{k}| \left[1 - \frac{1}{2}\left(h^{00} + h^{11}\frac{k_x^2}{|\mathbf{k}|^2}\right)\right] + \mathcal{O}(\lambda^2) \ . \tag{6.35}$$

Before continuing with the calculation, it should be noted that in (6.32) there can be seen the influence of gravity on the wave vector components. Remind that these behave reciprocally to the spatial coordinates because they are linked via a Fourier transform. The compression of the longitudinal wave vector component k_x by the factor $\left(1 - \tilde{\lambda}\right)$ is therefore related to a stretching of the corresponding spatial coordinate x. Moreover, there occurs no change along the transversal directions k_y and k_z. Thus, the y and z directions are not influenced. This is an interesting phenomenon because it shows parts of „the fate of a man who falls into the singularity“ [35, p. 860]. In a popular scientific way often called „spaghettification“. The effect can be summarized as follows: Assume an astrophysicist, representative of any object, falls into a black hole, and his feet are closer to the event horizon than his head. The gravitational force is distance-dependent and increases rapidly for smaller distances, therefore occurs, a tidal force between the astrophysicist's head and his feet, stretching him in the radial direction. Simultaneously, the astrophysicist's body compresses in the tangential direction since the attractive forces acting on the object's different parts are directed to the same center of mass. The height would diverge in the limit that he touches the event horizon, whereas the width would vanish. The effect is illustrated in figure 3.3.
Only the radial effect occurs in (6.32), and the perpendicular effect is not because the plates must not bend to ensure they are parallel, see figures 1.1, 1.5, and 2.1. The plate distance does not influence the plate alignment and can be treated as a variable.

Analogously, the new magnetic induction field is given by

$$\mathbf{B}_{\mathrm{TE}}^{\mathrm{curved}} \approx \mathbf{B}^{(0)} + \mathbf{B}^{(1)} \ . \tag{6.36}$$

Splitting up the x-component and the y, z-components since they have different prefactors $\sin(k_x x)$ and $\cos(k_x x)$ leads to

$$\begin{aligned} B_{\mathrm{TE};x}^{\mathrm{curved}} &\approx B_x^{(0)} + B_x^{(1)} && (6.37)\\ &= -\mathrm{N}_{\mathrm{TE}} k_\perp^2 \sin(k_x x)\left\{\sin(\sigma) - \frac{h^{00}\frac{\omega^2}{c^2} + h^{11}k_x^2}{2k_x^2}\sigma\cos(\sigma)\right\} && (6.38)\\ &\approx -\mathrm{N}_{\mathrm{TE}} k_\perp^2 \sin(k_x x)\left\{\sin(\sigma)\cos(\Delta\sigma) - \cos(\sigma)\sin(\Delta\sigma)\right\} && (6.39)\\ &= -\mathrm{N}_{\mathrm{TE}} k_\perp^2 \sin(k_x x)\sin(\sigma - \Delta\sigma) \ , && (6.40) \end{aligned}$$

$$\begin{aligned} B_{\mathrm{TE};y,z}^{\mathrm{curved}} &\approx B_{y,z}^{(0)} + B_{y,z}^{(1)} && (6.41)\\ &= -\mathrm{N}_{\mathrm{TE}} k_{y,z} k_x \cos(k_x x)\left\{\cos(\sigma) + \frac{h^{00}\frac{\omega^2}{c^2} + h^{11}k_x^2}{2k_x^2}\left[\sigma\sin(\sigma) + \cos(\sigma)\right]\right\} && (6.42)\\ &= -\mathrm{N}_{\mathrm{TE}} k_{y,z} k_x \cos(k_x x)\left\{\left(1 + \tilde{\lambda}\right)\cos(\sigma)\cos(\Delta\sigma) + \sin(\sigma)\sin(\Delta\sigma)\right\} \ . && (6.43) \end{aligned}$$

Adding up a term proportional to $\mathcal{O}\left(\tilde{\lambda}^2\right)$, treated as a zero in first-order perturbation theory, makes it possible to rewrite the expression to

$$B^{\text{curved}}_{\text{TE};y,z} \approx -\text{N}_{\text{TE}} k_{y,z} k_x \cos(k_x x) \left\{ \left(1+\tilde{\lambda}\right)\cos(\sigma)\cos(\Delta\sigma) + \left(1+\tilde{\lambda}\right)\sin(\sigma)\sin(\Delta\sigma) \right\} \tag{6.44}$$

$$= -\text{N}_{\text{TE}} k_{y,z} k_x \cos(k_x x) \left(1+\tilde{\lambda}\right) \cos\left(\sigma - \Delta\sigma\right) \ . \tag{6.45}$$

The homogeneous solution only changes the amplitude of the new magnetic induction field in the transversal directions by a factor $\tilde{\lambda}$. It does not affect on the renormalization process, which is vital for the Casimir energy. Therefore, these are only important if one is interested in the energy conservation of the system consisting of the Casimir setup, surrounding vacuum, and the source of gravity, see figure 1.5. This shifted amplitude in the transversal directions of either the electric field or the magnetic induction field occurs throughout the subsequent calculations without mentioning it separately since, from a mathematical point of view, the sum of the homogeneous and particular solution always corresponds to the total solution of an inhomogeneous differential equation.

Due to the same argument of the $\cos\left(\sigma - \Delta\sigma\right)$ and $\sin\left(\sigma - \Delta\sigma\right)$ functions, the same dispersion relation (6.35) occurs.

Determining the Casimir energy, the dispersion relation from equation (6.35) must be integrated over the transversal vector components $\mathbf{k}_\perp$, as in the flat case (2.25). First, notice that the first correction term proportional to h^{00} gives a simple shift of the flat case energy in the form $E_C^{h^{00}} = E_C^{\text{flat}}\left(1 - \frac{h^{00}}{2}\right)$, but the second term gives rise to new, more complicated terms. Therefore, an integral must be solved, and a regularization must be performed. The complete first-order corrected Casimir energy will be $E_C^{\text{curved}} = E_C^{h^{00}} + E_C^{h^{11}}$. The scheme presented in section 2.3 is applied to evaluate the integral:

$$E_C^{h^{11}} = \hbar c A \left({\sum_{n=0}^{\infty}}' - \int_0^\infty \mathrm{d}n \right) \int \frac{\mathrm{d}^2\mathbf{k}_\perp}{(2\pi)^2} \left(-\frac{h^{11}}{2} \frac{k_x^2}{\sqrt{k_x^2 + k_\perp^2}} \right) \tag{6.46}$$

$$= -\frac{h^{11}}{2} \hbar c A \left({\sum_{n=0}^{\infty}}' - \int_0^\infty \mathrm{d}n \right) 4 \int_0^\infty \int_0^\infty \frac{\mathrm{d}k_y\,\mathrm{d}k_z}{(2\pi)^2} \frac{k_x^2}{\sqrt{k_x^2 + k_\perp^2}} \ . \tag{6.47}$$

Transform to polar coordinates:

$$E_C^{h^{11}} = -\frac{h^{11}}{2} \hbar c A \left({\sum_{n=0}^{\infty}}' - \int_0^\infty \mathrm{d}n \right) 4 \frac{\pi}{2} \int_0^\infty \frac{1}{(2\pi)^2} \frac{k_x^2 k\,\mathrm{d}k}{\sqrt{k_x^2 + k^2}} \ . \tag{6.48}$$

Substitute $u = \frac{d}{\pi}\sqrt{k_x^2 + k^2} = \frac{d}{\pi}\sqrt{\frac{\pi^2 n^2}{d^2} + k^2}$ with $\mathrm{d}u = \frac{d^2}{\pi^2}\frac{k}{u}\,\mathrm{d}k$:

$$E_C^{h^{11}} = -\frac{h^{11}}{4} \hbar c A \frac{\pi^2}{d^3} \left({\sum_{n=0}^{\infty}}' - \int_0^\infty \mathrm{d}n \right) \int_{|n|}^\infty n^2\,\mathrm{d}u \ . \tag{6.49}$$

Applying the APSF from (2.27) now and recognize again that the absolute value can be dropped:

$$E_C^{h^{11}} = -\frac{h^{11}}{4}\hbar c A \frac{\pi^2}{d^3}\mathrm{i}\int_0^\infty \frac{1}{\exp(2\pi t)-1}\left[\int_{\mathrm{i}t}^\infty (\mathrm{i}t)^2\,\mathrm{d}u - \int_{-\mathrm{i}t}^\infty (-\mathrm{i}t)^2\,\mathrm{d}u\right]\mathrm{d}t \ . \tag{6.50}$$

Evaluating the u-integrals yields

$$E_C^{h^{11}} = \frac{h^{11}}{2}\hbar c A \frac{\pi^2}{d^3}\int_0^\infty \frac{t^3}{\exp(2\pi t)-1}\,\mathrm{d}t \ . \tag{6.51}$$

Use the relation of the integral to the Bernoulli numbers B_n from equation (D.6) and the exact values of those from (D.7) to get

$$E_C^{h^{11}} = h^{11}\hbar c A \frac{\pi^2}{d^3}\frac{1}{480} \ . \tag{6.52}$$

Taking the flat Casimir energy (1.3) into account leads to

$$E_C^{h^{11}} = -\frac{3}{2}h^{11}E_C^{\text{flat}} \ . \tag{6.53}$$

In particular keep in mind

$$\left(\sum_{n=0}^{\infty}{}' - \int_0^\infty \mathrm{d}n\right)\int_{|n|}^\infty n^2\,\mathrm{d}u = -\frac{1}{120} \ , \tag{6.54}$$

represents an important side result needed below.

The first-order corrected Casimir reads

$$E_C^{\text{curved}} = E_C^{\text{flat}}\left[1 - \frac{1}{2}\left(h^{00} + 3h^{11}\right)\right] \ , \tag{6.55}$$

which simplifies in the particular case of a Schwarzschild spacetime $h^{00} = h^{11} = \lambda = r_s/R$ to

$$E_C^{\text{curved}} = E_C^{\text{flat}}\left(1 - 2\lambda\right) \ . \tag{6.56}$$

To check if the replacement rule claimed by Klein-Gordon theory is valid, look at the proper distance d_p between the plates, connected to the metric via

$$d_p = \sqrt{-g_{11}}d \ , \tag{6.57}$$

due to the sign convention of (3.49). Use the metric component $g_{11} = -(1+\lambda)$ from (5.9) and apply several Taylor series for the following expressions

$$\begin{aligned}
\frac{1}{d_p^3} &= \frac{1}{d^3\sqrt{g_{11}^3}} \approx \frac{1-\frac{3\lambda}{2}}{d^3}\ , \\
\frac{1}{d_p^4} &= \frac{1}{d^4\sqrt{g_{11}^4}} \approx \frac{1-2\lambda}{d^4}\ .
\end{aligned} \tag{6.58}$$

The area of the plates A does not need any correction concerning the proper area A_p because the thickness of the plates is assumed to tend to zero. Further, the edge lengths are perpendicular to the direction of the gravitational force. In other words, the surface area would get corrections related to the g_{22} and g_{33} elements of the metric, which are, according to (5.9), the same as in the Minkowski spacetime (3.4), leading to $A = A_p$. Remind that the Minkowski metric (3.4) stays the same in any Lorentz frame. Therefore the prefactors of the line elements in spherical coordinates have to be respected, namely $\mathrm{d}s^{2\ \text{spherical}}_{\text{Minkowski}} = c^2\,\mathrm{d}t^2 - \mathrm{d}r^2 + r^2\left(\mathrm{d}\vartheta^2 + \sin^2(\vartheta)\,\mathrm{d}\varphi^2\right)$ [37, chapter 2.1.3]. However, for setups II and III, the surface area must be adjusted since, in those cases, the edge lengths of the plates are affected by gravitation. The perturbed Casimir energy E_C^{curved} and the perturbed Casimir force F_C^{curved} read

$$\begin{aligned}
E_C^{\text{curved}} &= E_C^{\text{flat}}\,(1-2\lambda) = -\hbar c A_p \frac{\pi^2}{d_p^3}\frac{1}{720} + \Delta E \neq E_C^{\text{flat}}(d_p, A_p)\ , \\
F_C^{\text{curved}} &= F_C^{\text{flat}}\,(1-2\lambda) = -\hbar c A_p \frac{\pi^2}{d_p^4}\frac{1}{240} \qquad\qquad = F_C^{\text{flat}}(d_p, A_p)\ .
\end{aligned} \tag{6.59}$$

First, compare these two equations to the unperturbed results in equations (1.3) and (1.4) and notice that the perturbed Casimir force can be obtained from the flat one by replacing the plate distance d with the proper distance of the plates d_p and by taking into account (6.58). This is, however, precisely what the Klein-Gordon calculations have already shown [3, 39, 47]. Second, it is remarkable that this „substitution rule“ does not hold for the Casimir energy (6.59). If one applies this rule (6.58), the energy is slightly off by the term $\Delta E = -E_C^{\text{flat}}\frac{\lambda}{2}$. The Klein-Gordon calculations did not show this issue because they just looked at the Casimir force and energy densities, not the energy itself. A possible explanation for this result may be that forces are directly measurable, whereas this statement is not valid for energies; only differences in energies are measurable.
An analog calculation for the respective TM modes is necessary to grant no symmetry breaking of the results for the TE and TM modes because this is not unlikely [23]. At the end of all calculations, it will turn out that there is none, independent of which setup is chosen.

6.1.2. Transversal magnetic modes

The calculation is completely analogue to the one before in subsection 6.1.1. The unperturbed fields from (2.13) are

$$\mathbf{E}^{(0)} = -\mathrm{N}_{\mathrm{TM}} \begin{pmatrix} k_\perp^2 \cos(k_x x)\cos(\sigma) \\ k_x k_y \sin(k_x x)\sin(\sigma) \\ k_x k_z \sin(k_x x)\sin(\sigma) \end{pmatrix}\ , \tag{6.60}$$

$$\mathbf{B}^{(0)} = \mathrm{N_{TM}} \begin{pmatrix} 0 \\ -k_z \frac{\omega}{c^2} \cos(k_x x) \cos(\sigma) \\ k_y \frac{\omega}{c^2} \cos(k_x x) \cos(\sigma) \end{pmatrix} . \tag{6.61}$$

Gauss' law yields

$$\rho^{(1)} = \varepsilon_0 h^{11} \partial_1 E_1^{(0)} = \varepsilon_0 h^{11} \mathrm{N_{TM}} k_x k_\perp^2 \sin(k_x x) \cos(\sigma) \tag{6.62}$$

Ampère's law is represented by

$$\mathbf{j}^{(1)} = -\mathrm{N_{TM}} \frac{1}{\mu_0} \begin{pmatrix} \mathrm{N_{TM}} k_\perp^2 h^{11} \frac{\omega}{c^2} \cos(k_x x) \sin(\sigma) \\ -\mathrm{N_{TM}} k_x k_y \left(h^{00} \frac{\omega^2}{c^2} + h^{11} k_x^2 \right) \frac{\omega}{c^2} \sin(k_x x) \cos(\sigma) \\ -\mathrm{N_{TM}} k_x k_z \left(h^{00} \frac{\omega^2}{c^2} + h^{11} k_x^2 \right) \frac{\omega}{c^2} \sin(k_x x) \cos(\sigma) \end{pmatrix} . \tag{6.63}$$

The wave equations read

$$\Box \mathbf{B}^{(1)} = \mathrm{N_{TM}} \frac{\omega}{c^2} \left(h^{00} \frac{\omega^2}{c^2} + h^{11} k_x^2 \right) \begin{pmatrix} 0 \\ -k_z \\ k_y \end{pmatrix} \cos(k_x x) \cos(\sigma) , \tag{6.64}$$

$$\Box \mathbf{E}^{(1)} = -\mathrm{N_{TM}} \left(h^{00} \frac{\omega^2}{c^2} + h^{11} k_x^2 \right) \begin{pmatrix} k_\perp^2 \cos(k_x x) \cos(\sigma) \\ k_x k_y \sin(k_x x) \sin(\sigma) \\ k_x k_z \sin(k_x x) \sin(\sigma) \end{pmatrix} . \tag{6.65}$$

The corresponding solutions are given by

$$\mathbf{B}^{(1)} = \mathrm{N_{TM}} \frac{h^{00} \frac{\omega^2}{c^2} + h^{11} k_x^2}{2 k_x^2} \begin{pmatrix} 0 \\ -k_z \\ k_y \end{pmatrix} \cos(k_x x) \sigma \sin(\sigma) , \tag{6.66}$$

$$\mathbf{E}^{(1)} = \mathrm{N_{TM}} \frac{h^{00} \frac{\omega^2}{c^2} + h^{11} k_x^2}{2 k_x^2} \begin{pmatrix} k_\perp^2 \cos(k_x x) \sigma v \\ k_x k_y \sin(k_x x) \left[\sigma \cos(\sigma) - \sin(\sigma) \right] \\ k_x k_z \sin(k_x x) \left[\sigma \cos(\sigma) - \sin(\sigma) \right] \end{pmatrix} . \tag{6.67}$$

The perturbed electric field reads

$$E^{\text{curved}}_{\text{TM};x} \approx E^{(0)}_x + E^{(1)}_x \tag{6.68}$$
$$= \mathrm{N}_{\text{TM}} k_\perp^2 \cos(k_x x) \left\{ -\cos(\sigma) - \frac{h^{00}\frac{\omega^2}{c^2} + h^{11}k_x^2}{2k_x^2} \sigma \sin(\sigma) \right\} \tag{6.69}$$
$$\approx \mathrm{N}_{\text{TM}} k_\perp^2 \cos(k_x x) \left\{ -\cos(\sigma)\cos(\Delta\sigma) - \sin(\sigma)\sin(\Delta\sigma) \right\} \tag{6.70}$$
$$= -\mathrm{N}_{\text{TM}} k_\perp^2 \cos(k_x x) \cos\left(\sigma - \Delta\sigma\right) \ . \tag{6.71}$$

$$E^{\text{curved}}_{\text{TM};y,z} \approx E^{(0)}_{y,z} + E^{(1)}_{y,z} \tag{6.72}$$
$$= \mathrm{N}_{\text{TM}} k_x k_{y,z} \sin(k_x x) \left\{ -\sin(\sigma) + \frac{h^{00}\frac{\omega^2}{c^2} + h^{11}k_x^2}{2k_x^2} \left[\sigma\cos(\sigma) - \sin(\sigma)\right] \right\} \tag{6.73}$$
$$\approx \mathrm{N}_{\text{TM}} k_x k_{y,z} \sin(k_x x) \Bigg\{ -\sin(\sigma)\cos(\Delta\sigma) + \cos(\sigma)\sin(\Delta\sigma) \tag{6.74}$$
$$- \frac{h^{00}\frac{\omega^2}{c^2} + h^{11}k_x^2}{2k_x^2} \left[\sin(\sigma)\cos(\Delta\sigma) - \cos(\sigma)\sin(\Delta\sigma)\right] \Bigg\} \tag{6.75}$$
$$= -\mathrm{N}_{\text{TM}} k_x k_{y,z} \sin(k_x x) \left(1 + \frac{h^{00}\frac{\omega^2}{c^2} + h^{11}k_x^2}{2k_x^2} \right) \sin(\sigma - \Delta\sigma) \ . \tag{6.76}$$

The perturbed magnetic induction field is represented by

$$\mathbf{B}^{\text{curved}}_{\text{TM}} \approx \mathbf{B}^{(0)} + \mathbf{B}^{(1)} \tag{6.77}$$
$$= \mathrm{N}_{\text{TM}} \frac{\omega}{c^2} \begin{pmatrix} 0 \\ -k_z \\ k_y \end{pmatrix} \cos(k_x x) \left\{ \cos(\sigma) + \frac{h^{00}\frac{\omega^2}{c^2} + h^{11}k_x^2}{2k_x^2} \sigma \sin(\sigma) \right\} \tag{6.78}$$
$$\approx \mathrm{N}_{\text{TM}} \frac{\omega}{c^2} \begin{pmatrix} 0 \\ -k_z \\ k_y \end{pmatrix} \cos(k_x x) \left\{ \cos(\sigma)\cos(\Delta\sigma) + \sin(\Delta\sigma)\sin(\sigma) \right\} \tag{6.79}$$
$$= \mathrm{N}_{\text{TM}} \frac{\omega}{c^2} \begin{pmatrix} 0 \\ -k_z \\ k_y \end{pmatrix} \cos(k_x x) \cos(\sigma - \Delta\sigma) \ . \tag{6.80}$$

Again $\sin(\sigma - \Delta\sigma)$ and $\cos(\sigma - \Delta\sigma)$ terms appear. Therefore, the dispersion relation in (6.35) holds for the TM modes, too.

6.2. Setup II

This chapter investigates the Casimir effect of setup II in figure 1.5 under the condition that it is located at (6.4) and not moving at all. As already mentioned, the surface normal is perpendicular to the gravitational force.

The wave vector components are

$$\begin{aligned} \mathbf{k}_\perp \cdot \mathbf{r}_\perp &= k_x x + k_z z \ , \\ k_\parallel &= k_y \ . \end{aligned} \tag{6.81}$$

Inserting these in (6.7) leads to the familiar notation from section 6.1.

6.2.1. Transversal electric modes

In the following way, the unperturbed electromagnetic fields are given by an antisymmetric permutation of the vector components in (6.9) and (6.10):

$$\mathbf{E}^{(0)} = \mathrm{N_{TE}}\omega \begin{pmatrix} -k_z \\ 0 \\ k_x \end{pmatrix} \sin(k_y y)\sin(\sigma) \ , \tag{6.82}$$

$$\mathbf{B}^{(0)} = -\mathrm{N_{TE}} \begin{pmatrix} k_x k_y \cos(k_y y)\cos(\sigma) \\ k_\perp^2 \sin(k_y y)\sin(\sigma) \\ k_y k_z \cos(k_y y)\cos(\sigma) \end{pmatrix} \ . \tag{6.83}$$

Gauss' law reads

$$\rho^{(1)} = -\varepsilon_0 h^{11} \mathrm{N_{TE}}\omega k_x k_z \sin(k_y y)\cos(\sigma) \ . \tag{6.84}$$

Ampère's law is given by

$$\mathbf{j}^{(1)} = -\frac{1}{\mu_0} \begin{pmatrix} -h^{00}\mathrm{N_{TE}}\frac{\omega^2}{c^2} k_z \sin(k_y y)\cos(\sigma) \\ h^{11}\mathrm{N_{TE}} k_x k_y k_z \cos(k_y y)\sin(\sigma) \\ \mathrm{N_{TE}} k_x \sin(k_y y)\cos(\sigma)\left(h^{00}\frac{\omega^2}{c^2} + h^{11}k_x^2\right) \end{pmatrix} \ . \tag{6.85}$$

The according wave equations are represented by

$$\Box \mathbf{E}^{(1)} = \begin{pmatrix} -\mathrm{N}_{\mathrm{TE}}\omega k_z \sin(k_y y)\sin(\sigma)\left(h^{00}\frac{\omega^2}{c^2} + h^{11}k_x^2\right) \\ 0 \\ \mathrm{N}_{\mathrm{TE}}\omega k_x \sin(k_y y)\sin(\sigma)\left(h^{00}\frac{\omega^2}{c^2} + h^{11}k_x^2\right) \end{pmatrix}, \tag{6.86}$$

$$\Box \mathbf{B}^{(1)} = \begin{pmatrix} -\mathrm{N}_{\mathrm{TE}} k_x k_y \cos(k_y y)\cos(\sigma)\left(h^{00}\frac{\omega^2}{c^2} + h^{11}k_x^2\right) \\ -\mathrm{N}_{\mathrm{TE}} k_\perp^2 \sin(k_y y)\sin(\sigma)\left(h^{00}\frac{\omega^2}{c^2} + h^{11}k_x^2\right) \\ -\mathrm{N}_{\mathrm{TE}} k_y k_z \cos(k_y y)\cos(\sigma)\left(h^{00}\frac{\omega^2}{c^2} + h^{11}k_x^2\right) \end{pmatrix}. \tag{6.87}$$

The solutions are given by

$$\mathbf{E}^{(1)} = \mathrm{N}_{\mathrm{TE}}\omega \frac{h^{00}\frac{\omega^2}{c^2} + h^{11}k_x^2}{2k_y^2} \begin{pmatrix} k_z \\ 0 \\ -k_x \end{pmatrix} \sin(k_y y)\sigma\cos(\sigma)\ , \tag{6.88}$$

$$\mathbf{B}^{(1)} = \mathrm{N}_{\mathrm{TE}} \frac{h^{00}\frac{\omega^2}{c^2} + h^{11}k_x^2}{2k_y^2} \begin{pmatrix} -k_x k_y\left[\sigma\sin(\sigma) + \cos(\sigma)\right]\cos(k_y y) \\ k_\perp^2 \sigma\cos(\sigma)\sin(k_y y) \\ -k_y k_z\left[\sigma\sin(\sigma) + \cos(\sigma)\right]\cos(k_y y) \end{pmatrix}. \tag{6.89}$$

The new electric field reads

$$\begin{aligned} \mathbf{E}_{\mathrm{TE}}^{\mathrm{curved}} &\approx \mathbf{E}^{(0)} + \mathbf{E}^{(1)} && (6.90) \\ &= \mathrm{N}_{\mathrm{TE}}\omega\sin(k_y y)\begin{pmatrix} -k_z \\ 0 \\ k_x \end{pmatrix}\left\{\sin(\sigma) - \frac{h^{00}\frac{\omega^2}{c^2} + h^{11}k_x^2}{2k_y^2}\sigma\cos(\sigma)\right\} && (6.91) \\ &\approx \mathrm{N}_{\mathrm{TE}}\omega\sin(k_y y)\begin{pmatrix} -k_z \\ 0 \\ k_x \end{pmatrix}\left\{\sin(\sigma)\cos(\Delta\sigma) - \cos(\sigma)\sin(\Delta\sigma)\right\} && (6.92) \\ &= \mathrm{N}_{\mathrm{TE}}\omega\sin(k_y y)\begin{pmatrix} -k_z \\ 0 \\ k_x \end{pmatrix}\sin(\sigma - \Delta\sigma)\ . && (6.93) \end{aligned}$$

For the new magnetic induction field it is necessary to split up the components

$$
\begin{aligned}
B^{\text{curved}}_{\text{TE};y} &\approx B^{(0)}_y + B^{(1)}_y && (6.94)\\
&= -\mathrm{N}_{\text{TE}} k_\perp^2 \sin(k_y y)\left\{\sin(\sigma) + \frac{h^{00}\frac{\omega^2}{c^2} + h^{11}k_x^2}{2k_y^2}\sigma\cos(\sigma)\right\} && (6.95)\\
&\approx -\mathrm{N}_{\text{TE}} k_\perp^2 \sin(k_y y)\left\{\sin(\sigma)\cos(\Delta\sigma) - \cos(\sigma)\sin(\Delta\sigma)\right\} && (6.96)\\
&= -\mathrm{N}_{\text{TE}} k_\perp^2 \sin(k_y y)\sin(\sigma - \Delta\sigma)\ , && (6.97)
\end{aligned}
$$

$$
\begin{aligned}
B^{\text{curved}}_{\text{TE};x,z} &\approx B^{(0)}_{x,z} + B^{(1)}_{x,z} && (6.98)\\
&= -\mathrm{N}_{\text{TE}} k_y k_{x,z}\cos(k_y y)\left\{\cos(\sigma) + \frac{h^{00}\frac{\omega^2}{c^2} + h^{11}k_x^2}{2k_y^2}\left[\sigma\sin(\sigma) + \cos(\sigma)\right]\right\} && (6.99)\\
&\approx -\mathrm{N}_{\text{TE}} k_y k_{x,z}\cos(k_y y)\left(1 + \frac{h^{00}\frac{\omega^2}{c^2} + h^{11}k_x^2}{2k_y^2}\right)\left\{\cos(\sigma)\cos(\Delta\sigma) + \sin(\sigma)\sin(\Delta\sigma)\right\} && (6.100)\\
&= -\mathrm{N}_{\text{TE}} k_y k_{x,z}\cos(k_y y)\left(1 + \frac{h^{00}\frac{\omega^2}{c^2} + h^{11}k_x^2}{2k_y^2}\right)\cos(\sigma - \Delta\sigma)\ . && (6.101)
\end{aligned}
$$

In the end, this leads to the same dispersion relation as in (6.35). However, this time the transversal wave vectors that are integrated have different directions compared to the case in section 6.1. Therefore, it is necessary to evaluate the new integral:

$$
\begin{aligned}
E_C^{h^{11}} &= \hbar c A\left(\sum_{n=0}^{\infty}{}' - \int_0^\infty \mathrm{d}n\right)\int \frac{\mathrm{d}^2\mathbf{k}_\perp}{(2\pi)^2}\left(-\frac{h^{11}}{2}\right)\frac{k_x^2}{\sqrt{k_y^2 + k_\perp^2}} && (6.102)\\
&= -\frac{h^{11}}{2}\hbar c A\left(\sum_{n=0}^{\infty}{}' - \int_0^\infty \mathrm{d}n\right) 4\int_0^\infty\int_0^\infty \frac{\mathrm{d}k_x\,\mathrm{d}k_z}{(2\pi)^2}\frac{k_x^2}{\sqrt{k_x^2 + k_y^2 + k_z^2}}\ . && (6.103)
\end{aligned}
$$

With a transformation to polar coordinates follows:

$$
\begin{aligned}
E_C^{h^{11}} &= -\frac{h^{11}}{2}\hbar c A\left(\sum_{n=0}^{\infty}{}' - \int_0^\infty \mathrm{d}n\right) 4\int_0^\infty\int_0^{\frac{\pi}{2}} \frac{1}{(2\pi)^2}\frac{k^2\sin^2(\varphi)}{\sqrt{k^2 + k_y^2}}k\,\mathrm{d}k\,\mathrm{d}\varphi && (6.104)\\
&= -\frac{h^{11}}{2}\hbar c A\left(\sum_{n=0}^{\infty}{}' - \int_0^\infty \mathrm{d}n\right)\frac{1}{4\pi}\int_0^\infty \frac{k^3\,\mathrm{d}k}{\sqrt{k^2 + k_y^2}}\ . && (6.105)
\end{aligned}
$$

Substitute $u = \frac{d}{\pi}\sqrt{k_x^2 + k^2} = \frac{d}{\pi}\sqrt{\frac{\pi^2 n^2}{d^2} + k^2}$ with $\mathrm{d}u = \frac{d^2}{\pi^2}\frac{k}{u}\,\mathrm{d}k$:

$$
E_C^{h^{11}} = -\frac{h^{11}}{2}\hbar c A\left(\sum_{n=0}^{\infty}{}' - \int_0^\infty \mathrm{d}n\right)\frac{\pi^2}{4d^3}\int_{|n|}^\infty u^2 - n^2\,\mathrm{d}u\ . \qquad (6.106)
$$

The first term is equal to (2.39), the second one corresponds to (2.39). Taking into account the proper signs, this leads to

$$E_C^{h^{11}} = -\frac{h^{11}}{2}\hbar c A \frac{\pi^2}{4d^3}\left(-\frac{1}{360}+\frac{1}{120}\right) \tag{6.107}$$

$$= -\frac{h^{11}}{2}\hbar c A \frac{\pi^2}{720d^3} \tag{6.108}$$

$$= \frac{h^{11}}{2} E_C^{\text{flat}} \, . \tag{6.109}$$

Including the constant energy shift due to the h^{00} element that can be calculated without solving an integral, the whole first-order correction reads

$$E_C^{\text{curved}} = E_C^{\text{flat}}\left[1 - \frac{1}{2}\left(h^{00} - h^{11}\right)\right] \, . \tag{6.110}$$

As already discussed in section 6.1, the surface area of the plates must be adjusted because one edge length is parallel to the direction of the gravitational force. Assuming that the plate area combines in the flat case by $A = L_x L_z$ where L_x denotes the edge length parallel to the gravitational force without loss of generality. According to (3.4), (5.20), and (6.3), this yields

$$L_{1,p} = \sqrt{-g_{11}}L_x = \sqrt{-\left(\eta_{11} + h_{11}\right)}L_x \tag{6.111}$$

$$= \left(1 - \frac{h_{11}}{2}\right) L_x + \mathcal{O}\left(h_{11}^2\right) \, . \tag{6.112}$$

Thus, the proper surface area of setup II results in

$$A_p = \left(1 - \frac{h_{11}}{2}\right) L_x L_z + \mathcal{O}\left(h_{11}^2\right) \, . \tag{6.113}$$

Hence, the complete first-order corrected Casimir energy reads

$$E_C^{\text{curved}} = \left(1 - \frac{h_{11}}{2}\right) E_C^{\text{flat}}\left[1 - \frac{1}{2}\left(h^{00} - h^{11}\right)\right] \, . \tag{6.114}$$

In the special case $h^{00} = h^{11} = \lambda$ and $h_{11} = -\lambda$, valid for a gravitation source in Schwarzschild spacetime at a distance (6.4) to the Casimir setup, the second correction term vanishes and

$$E_C^{\text{curved}} = \left(1 + \frac{\lambda}{2}\right) E_C^{\text{flat}} = E_C^{\text{flat}}(d_p, A_p) \, , \tag{6.115}$$

hereby (5.20) and (5.21) were applied.
For the corresponding Casimir force this means

$$F_C^{\text{curved}} = \left(1 + \frac{\lambda}{2}\right) F_C^{\text{flat}} = F_C^{\text{flat}}(d_p, A_p) \tag{6.116}$$

the replacement rule valid for setup I is satisfied for the energy and the force in the case of setup II. As a remarkable result the Casimir force for setup II is slightly more attractive than in the flat case.

6.2.2. Transversal magnetic modes

The unperturbed fields for the TM modes read

$$\mathbf{E}^{(0)} = -\mathrm{N}_{\mathrm{TM}} \begin{pmatrix} k_x k_y \sin(k_y y)\sin(\sigma) \\ k_\perp^2 \cos(k_y y)\cos(\sigma) \\ k_y k_z \sin(k_y y)\sin(\sigma) \end{pmatrix} , \tag{6.117}$$

$$\mathbf{B}^{(0)} = \mathrm{N}_{\mathrm{TM}} \begin{pmatrix} k_z \frac{\omega}{c^2} \cos(k_y y)\cos(\sigma) \\ 0 \\ -k_x \frac{\omega}{c^2} \cos(k_y y)\cos(\sigma) \end{pmatrix} . \tag{6.118}$$

Gauss' law is given by

$$\rho^{(1)} = -\varepsilon_0 h^{11} \mathrm{N}_{\mathrm{TM}} k_x^2 k_y \sin(k_y y)\cos(\sigma) . \tag{6.119}$$

Ampère's law simplifies to

$$\mathbf{j}^{(1)} = -\frac{1}{\mu_0} \begin{pmatrix} -\mathrm{N}_{\mathrm{TM}} h^{00} \frac{\omega}{c^2} k_x k_y \sin(k_y y)\cos(\sigma) \\ +\mathrm{N}_{\mathrm{TM}} \frac{\omega}{c^2} \cos(k_y y)\sin(\sigma) \left(h^{00} k_\perp^2 + h^{11} k_x^2\right) \\ -\mathrm{N}_{\mathrm{TM}} h^{00} \frac{\omega}{c^2} k_y k_z \sin(k_y y)\cos(\sigma) \end{pmatrix} . \tag{6.120}$$

The corresponding wave equations are represented by

$$\Box \mathbf{E}^{(1)} = \begin{pmatrix} -\mathrm{N}_{\mathrm{TM}} k_x k_y \sin(k_y y)\sin(\sigma) \left(h^{00} \frac{\omega^2}{c^2} + h^{11} k_x^2\right) \\ -\mathrm{N}_{\mathrm{TM}} k_\perp^2 \cos(k_y y)\cos(\sigma) \left(h^{00} \frac{\omega^2}{c^2} + h^{11} k_x^2\right) \\ -\mathrm{N}_{\mathrm{TM}} k_y k_z \sin(k_y y)\sin(\sigma) \left(h^{00} \frac{\omega^2}{c^2} + h^{11} k_x^2\right) \end{pmatrix} , \tag{6.121}$$

$$\Box \mathbf{B}^{(1)} = \begin{pmatrix} \mathrm{N}_{\mathrm{TM}} \frac{\omega}{c^2} k_z \cos(k_y y)\cos(\sigma) \left(h^{00} \frac{\omega^2}{c^2} + h^{11} k_x^2\right) \\ 0 \\ -\mathrm{N}_{\mathrm{TM}} \frac{\omega}{c^2} k_x \cos(k_y y)\cos(\sigma) \left(h^{00} \frac{\omega^2}{c^2} + h^{11} k_x^2\right) \end{pmatrix} . \tag{6.122}$$

These equations are solved by

$$\mathbf{E}^{(1)} = \mathrm{N}_{\mathrm{TM}} \frac{h^{00}\frac{\omega^2}{c^2} + h^{11}k_x^2}{2k_y^2} \begin{pmatrix} k_x k_y \sin(k_y y)\left[\sigma\cos(\sigma) - \sin(\sigma)\right] \\ -k_\perp^2 \cos(k_y y)\sigma\sin(\sigma) \\ k_y k_z \sin(k_y y)\left[\sigma\cos(\sigma) - \sin(\sigma)\right] \end{pmatrix} , \tag{6.123}$$

$$\mathbf{B}^{(1)} = \mathrm{N}_{\mathrm{TM}} \frac{\omega}{c^2} \frac{h^{00}\frac{\omega^2}{c^2} + h^{11}k_x^2}{2k_y^2} \begin{pmatrix} k_z \\ 0 \\ -k_x \end{pmatrix} \cos(k_y y)\sigma\sin(\sigma) \; . \tag{6.124}$$

The new magnetic induction field calculates to

$$\begin{aligned}
\mathbf{B}_{\mathrm{TM}}^{\mathrm{curved}} &\approx \mathbf{B}^{(0)} + \mathbf{B}^{(1)} && (6.125)\\
&= \mathrm{N}_{\mathrm{TM}} \frac{\omega}{c^2} \cos(k_y y) \begin{pmatrix} k_z \\ 0 \\ -k_x \end{pmatrix} \left\{ \cos(\sigma) + \frac{h^{00}\frac{\omega^2}{c^2} + h^{11}k_x^2}{2k_y^2} \sigma \sin(\sigma) \right\} && (6.126)\\
&\approx \mathrm{N}_{\mathrm{TM}} \frac{\omega}{c^2} \cos(k_y y) \begin{pmatrix} k_z \\ 0 \\ -k_x \end{pmatrix} \left\{ \cos(\sigma)\cos(\Delta\sigma) + \sin(\sigma)\sin(\Delta\sigma) \right\} && (6.127)\\
&= \mathrm{N}_{\mathrm{TM}} \frac{\omega}{c^2} \cos(k_y y) \begin{pmatrix} k_z \\ 0 \\ -k_x \end{pmatrix} \cos(\sigma - \Delta\sigma) \; . && (6.128)
\end{aligned}$$

For the new electric field a split up of the components is necessary via

$$\begin{aligned}
E_{\mathrm{TM};y}^{\mathrm{curved}} &\approx E_y^{(0)} + E_y^{(1)} && (6.129)\\
&= -\mathrm{N}_{\mathrm{TM}} k_\perp^2 \cos(k_y y) \left\{ \cos(\sigma) + \frac{h^{00}\frac{\omega^2}{c^2} + h^{11}k_x^2}{2k_y^2} \sigma \sin(\sigma) \right\} && (6.130)\\
&\approx -\mathrm{N}_{\mathrm{TM}} k_\perp^2 \cos(k_y y) \left\{ \cos(\sigma)\cos(\Delta\sigma) + \sin(\sigma)\sin(\Delta\sigma) \right\} && (6.131)\\
&= -\mathrm{N}_{\mathrm{TM}} k_\perp^2 \cos(k_y y) \cos(\sigma - \Delta\sigma) \; , && (6.132)
\end{aligned}$$

$$
\begin{aligned}
E^{\text{curved}}_{\text{TM};x,z} &\approx E^{(0)}_{x,z} + E^{(1)}_{x,z} && (6.133)\\
&= \mathrm{N}_{\text{TM}} k_{x,z} k_y \sin(k_y y) \left\{ -\sin(\sigma) + \frac{h^{00}\frac{\omega^2}{c^2} + h^{11}k_x^2}{2k_y^2} \left[\sigma\cos(\sigma) - \sin(\sigma)\right] \right\} && (6.134)\\
&\approx \mathrm{N}_{\text{TM}} k_{x,z} k_y \sin(k_y y) \Bigg\{ -\sin(\sigma)\cos(\Delta\sigma) + \cos(\sigma)\sin(\Delta\sigma) && (6.135)\\
&- \frac{h^{00}\frac{\omega^2}{c^2} + h^{11}k_x^2}{2k_y^2} \sin(\sigma)\cos(\Delta\sigma) + \frac{h^{00}\frac{\omega^2}{c^2} + h^{11}k_x^2}{2k_y^2} \cos(\sigma)\sin(\Delta\sigma) \Bigg\} && (6.136)\\
&= -\mathrm{N}_{\text{TM}} k_{x,z} k_y \sin(k_y y) \left(1 + \frac{h^{00}\frac{\omega^2}{c^2} + h^{11}k_x^2}{2k_y^2}\right) \sin(\sigma - \Delta\sigma)\ . && (6.137)
\end{aligned}
$$

This leads again to the same dispersion relation as in (6.35), because of the $\cos(\sigma - \Delta\sigma)$ and $\sin(\sigma - \Delta\sigma)$ terms. Hence, the results valid for the TM modes coincide with them for the TE modes.

6.3. Setup *III*

This chapter investigates the Casimir effect of setup *III* in figure 1.5 under the condition that it is located at (6.4) and not moving at all. As already mentioned, the surface normal is perpendicular to the gravitational force.

The wave vector components are given by

$$
\begin{aligned}
\mathbf{k}_\perp \cdot \mathbf{r}_\perp &= k_x x + k_y y\ ,\\
k_\parallel &= k_z\ .
\end{aligned}
\tag{6.138}
$$

Inserting these in (6.7) leads to the familiar notation from section 6.1.

6.3.1. Transversal electric modes

In the following way, the unperturbed electromagnetic fields are given by an antisymmetric permutation of the vector components in (6.9) and (6.10):

$$
\mathbf{E}^{(0)} = \mathrm{N}_{\text{TE}}\,\omega \begin{pmatrix} k_y \\ -k_x \\ 0 \end{pmatrix} \sin(k_z z)\sin(\sigma)\ , \tag{6.139}
$$

$$
\mathbf{B}^{(0)} = -\mathrm{N}_{\text{TE}} \begin{pmatrix} k_x k_z \cos(k_z z)\cos(\sigma) \\ k_y k_z \cos(k_z z)\sin(\sigma) \\ k_\perp^2 \sin(k_z z)\cos(\sigma) \end{pmatrix}\ . \tag{6.140}
$$

Gauss' law reads

$$\rho^{(1)} = \varepsilon_0 h^{11} \mathrm{N_{TE}} \omega k_x k_y \sin(k_z z)\cos(\sigma)\ . \tag{6.141}$$

Ampère's law is given by

$$\mathbf{j}^{(1)} = -\frac{1}{\mu_0}\begin{pmatrix} \mathrm{N_{TE}} h^{00} k_y \frac{\omega^2}{c^2}\sin(k_z z)\cos(\sigma) \\ -\mathrm{N_{TE}} k_x \sin(k_z z)\cos(\sigma)\left(h^{00}\frac{\omega^2}{c^2} + h^{11}k_\perp^2\right) \\ -\mathrm{N_{TE}} h^{11} k_x k_y k_z \cos(k_z z)\sin(\sigma) \end{pmatrix}\ . \tag{6.142}$$

The according wave equations are represented by

$$\Box\mathbf{E}^{(1)} = \mathrm{N_{TE}}\omega\left(h^{00}\frac{\omega^2}{c^2} + h^{11}k_x^2\right)\begin{pmatrix} k_y \\ -k_x \\ 0 \end{pmatrix}\sin(k_z z)\sin(\sigma)\ , \tag{6.143}$$

$$\Box\mathbf{B}^{(1)} = \mathrm{N_{TE}}\left(h^{00}\frac{\omega^2}{c^2} + h^{11}k_x^2\right)\begin{pmatrix} -k_x k_z \cos(k_z z)\cos(\sigma) \\ -k_y k_z \cos(k_z z)\cos(\sigma) \\ -k_\perp^2 \sin(k_z z)\sin(\sigma) \end{pmatrix} \tag{6.144}$$

The solutions are given by

$$\mathbf{E}^{(1)} = \mathrm{N_{TE}}\omega\frac{h^{00}\frac{\omega^2}{c^2} + h^{11}k_x^2}{2k_z^2}\begin{pmatrix} -k_y \\ k_x \\ 0 \end{pmatrix}\sin(k_z z)\sigma\cos(\sigma)\ , \tag{6.145}$$

$$\mathbf{B}^{(1)} = \mathrm{N_{TE}}\frac{h^{00}\frac{\omega^2}{c^2} + h^{11}k_x^2}{2k_z^2}\begin{pmatrix} -k_x k_z \cos(k_z z)\left[\sigma\sin(\sigma) + \cos(\sigma)\right] \\ -k_y k_z \cos(k_z z)\left[\sigma\sin(\sigma) + \cos(\sigma)\right] \\ k_\perp^2 \sin(k_z z)\sigma\cos(\sigma) \end{pmatrix} \tag{6.146}$$

The new electric field reads

$$\begin{aligned}
\mathbf{E}_{\mathrm{TE}}^{\mathrm{curved}} &\approx \mathbf{E}^{(0)} + \mathbf{E}^{(1)} && (6.147)\\
&= \mathrm{N}_{\mathrm{TE}}\omega \sin(k_z z) \begin{pmatrix} k_y \\ -k_x \\ 0 \end{pmatrix} \left\{ \sin(\sigma) - \frac{h^{00}\frac{\omega^2}{c^2} + h^{11}k_x^2}{2k_z^2} \sigma \cos(\sigma) \right\} && (6.148)\\
&\approx \mathrm{N}_{\mathrm{TE}}\omega \sin(k_z z) \begin{pmatrix} k_y \\ -k_x \\ 0 \end{pmatrix} \left\{ \sin(\sigma)\cos(\Delta\sigma) - \cos(\sigma)\sin(\Delta\sigma) \right\} && (6.149)\\
&= \mathrm{N}_{\mathrm{TE}}\omega \sin(k_z z) \begin{pmatrix} k_y \\ -k_x \\ 0 \end{pmatrix} \sin(\sigma - \Delta\sigma) \, . && (6.150)
\end{aligned}$$

For the new magnetic induction it is necessary to split up the components

$$\begin{aligned}
B_{\mathrm{TE};z}^{\mathrm{curved}} &\approx B_z^{(0)} + B_z^{(1)} && (6.151)\\
&= \mathrm{N}_{\mathrm{TE}} k_\perp^2 \sin(k_z z) \left\{ -\sin(\sigma) + \frac{h^{00}\frac{\omega^2}{c^2} + h^{11}k_x^2}{2k_z^2} \cos(\sigma) \right\} && (6.152)\\
&\approx \mathrm{N}_{\mathrm{TE}} k_\perp^2 \sin(k_z z) \left\{ -\sin(\sigma)\cos(\Delta\sigma) + \cos(\sigma)\sin(\Delta\sigma) \right\} && (6.153)\\
&= -\mathrm{N}_{\mathrm{TE}} k_\perp^2 \sin(k_z z) \sin(\sigma - \Delta\sigma) \, , && (6.154)
\end{aligned}$$

$$\begin{aligned}
B_{\mathrm{TE};x,y}^{\mathrm{curved}} &\approx B_{x,y}^{(0)} + B_{x,y}^{(1)} && (6.155)\\
&= -\mathrm{N}_{\mathrm{TE}} k_{x,y} k_z \cos(k_z z) \left\{ \cos(\sigma) + \frac{h^{00}\frac{\omega^2}{c^2} + h^{11}k_x^2}{2k_z^2} \sigma \sin(\sigma) + \frac{h^{00}\frac{\omega^2}{c^2} + h^{11}k_x^2}{2k_z^2} \cos(\sigma) \right\} && (6.156)\\
&\approx -\mathrm{N}_{\mathrm{TE}} k_{x,y} k_z \cos(k_z z) \Big\{ \cos(\sigma)\cos(\Delta\sigma) + \sin(\sigma)\sin(\Delta\sigma) && (6.157)\\
&+ \frac{h^{00}\frac{\omega^2}{c^2} + h^{11}k_x^2}{2k_z^2} \cos(\sigma)\cos(\Delta\sigma) + \frac{h^{00}\frac{\omega^2}{c^2} + h^{11}k_x^2}{2k_z^2} \sin(\sigma)\sin(\Delta\sigma) \Big\} && (6.158)\\
&= -\mathrm{N}_{\mathrm{TE}} k_{x,y} k_z \cos(k_z z) \left(1 + \frac{h^{00}\frac{\omega^2}{c^2} + h^{11}k_x^2}{2k_z^2} \right) \cos(\sigma - \Delta\sigma) \, . && (6.159)
\end{aligned}$$

Altogether, the same dispersion relation as in (6.35) appears. Thus, the Casimir energy of setup II in section 6.2 coincides with the one of setup III. Note that in this case, even the surface area adjustment is taken into account. Strictly spoken for the area $A = L_x L_z$, where L_x must be changed to the proper length $L_{1,x}$, for setup II, the edge length L_x needs to be changed to $L_{x,p}$, whereas L_z stays unaffected, which yields the same result.

6.3.2. Transversal magnetic modes

The unperturbed fields for the TM modes read

$$\mathbf{E}^{(0)} = -\mathrm{N}_{\mathrm{TM}} \begin{pmatrix} k_x k_z \sin(k_z z)\sin(\sigma) \\ k_y k_z \sin(k_z z)\sin(\sigma) \\ k_\perp^2 \cos(k_z z)\cos(\sigma) \end{pmatrix} , \tag{6.160}$$

$$\mathbf{B}^{(0)} = \mathrm{N}_{\mathrm{TM}} \begin{pmatrix} -k_y \frac{\omega}{c^2} \cos(k_z z)\cos(\sigma) \\ k_x \frac{\omega}{c^2} \cos(k_z z)\cos(\sigma) \\ 0 \end{pmatrix} . \tag{6.161}$$

Gauss' law is given by

$$\rho^{(1)} = -\varepsilon_0 \mathrm{N}_{\mathrm{TM}} h^{11} k_x^2 k_z \sin(k_z z)\cos(\sigma) . \tag{6.162}$$

Ampère's law simplifies to

$$\mathbf{j}^{(1)} = -\frac{1}{\mu_0} \begin{pmatrix} -\mathrm{N}_{\mathrm{TM}} h^{00} k_x k_z \frac{\omega}{c^2} \sin(k_z z)\cos(\sigma) \\ -\mathrm{N}_{\mathrm{TM}} h^{00} k_y k_z \frac{\omega}{c^2} \sin(k_z z)\cos(\sigma) \\ \mathrm{N}_{\mathrm{TM}} \frac{\omega}{c^2} \cos(k_z z)\sin(\sigma) \left(h^{00} \frac{\omega^2}{c^2} + h^{11} k_x^2 \right) \end{pmatrix} . \tag{6.163}$$

The according wave equations are represented by

$$\Box \mathbf{E}^{(1)} = -\mathrm{N}_{\mathrm{TM}} \left(h^{00} \frac{\omega^2}{c^2} + h^{11} k_x^2 \right) \begin{pmatrix} k_x k_z \sin(k_z z)\sin(\sigma) \\ k_y k_z \sin(k_z z)\sin(\sigma) \\ k_\perp^2 \cos(k_z z)\cos(\sigma) \end{pmatrix} , \tag{6.164}$$

$$\Box \mathbf{B}^{(1)} = \mathrm{N}_{\mathrm{TM}} \frac{\omega}{c^2} \left(h^{00} \frac{\omega^2}{c^2} + h^{11} k_x^2 \right) \begin{pmatrix} -k_y \\ k_x \\ 0 \end{pmatrix} \cos(k_z z)\cos(\sigma) . \tag{6.165}$$

These equations are solved by

$$\mathbf{E}^{(1)} = \mathrm{N}_{\mathrm{TM}} \frac{h^{00}\frac{\omega^2}{c^2} + h^{11}k_x^2}{2k_z^2} \begin{pmatrix} k_x k_z \sin(k_z z)\left[\sigma\cos(\sigma) - \sin(\sigma)\right] \\ k_y k_z \sin(k_z z)\left[\sigma\cos(\sigma) - \sin(\sigma)\right] \\ -k_\perp^2 \cos(k_z z)\sigma\sin(\sigma) \end{pmatrix} , \tag{6.166}$$

$$\mathbf{B}^{(1)} = \mathrm{N}_{\mathrm{TM}} \frac{\omega}{c^2} \frac{h^{00}\frac{\omega^2}{c^2} + h^{11}k_x^2}{2k_z^2} \begin{pmatrix} -k_y \\ k_x \\ 0 \end{pmatrix} \cos(k_z z)\sigma\sin(\sigma) . \tag{6.167}$$

The new magnetic induction field calculates to

$$\begin{aligned} \mathbf{B}_{\mathrm{TM}}^{\mathrm{curved}} &\approx \mathbf{B}^{(0)} + \mathbf{B}^{(1)} && (6.168) \\ &= \mathrm{N}_{\mathrm{TM}} \frac{\omega}{c^2} \cos(k_z z) \begin{pmatrix} -k_y \\ k_x \\ 0 \end{pmatrix} \left\{ \cos(\sigma) + \frac{h^{00}\frac{\omega^2}{c^2} + h^{11}k_x^2}{2k_z^2} \sin(\sigma) \right\} && (6.169) \\ &\approx \mathrm{N}_{\mathrm{TM}} \frac{\omega}{c^2} \cos(k_z z) \begin{pmatrix} -k_y \\ k_x \\ 0 \end{pmatrix} \left\{ \cos(\sigma)\cos(\Delta\sigma) + \sin(\sigma)\sin(\Delta\sigma) \right\} && (6.170) \\ &= \mathrm{N}_{\mathrm{TM}} \frac{\omega}{c^2} \cos(k_z z) \begin{pmatrix} -k_y \\ k_x \\ 0 \end{pmatrix} \cos(\sigma - \Delta\sigma) . && (6.171) \end{aligned}$$

For the new electric field it is necessary to split up the components

$$\begin{aligned} E_{\mathrm{TM};z}^{\mathrm{curved}} &\approx E_z^{(0)} + E_z^{(1)} && (6.172) \\ &= -\mathrm{N}_{\mathrm{TM}} k_\perp^2 \cos(k_z z) \left\{ \cos(\sigma) + \frac{h^{00}\frac{\omega^2}{c^2} + h^{11}k_x^2}{2k_z^2} \sigma\sin(\sigma) \right\} && (6.173) \\ &\approx -\mathrm{N}_{\mathrm{TM}} k_\perp^2 \cos(k_z z) \left\{ \cos(\sigma)\cos(\Delta\sigma) + \sin(\sigma)\sin(\Delta\sigma) \right\} && (6.174) \\ &= -\mathrm{N}_{\mathrm{TM}} \cos(k_z z) k_\perp^2 \cos(\sigma - \Delta\sigma) , && (6.175) \end{aligned}$$

$$E^{\text{curved}}_{\text{TM};x,y} \approx E^{(0)}_{x,y} + E^{(1)}_{x,y} \tag{6.176}$$

$$= \mathrm{N}_{\text{TM}} k_z k_{x,y} \sin(k_z z) \left\{ -\sin(\sigma) + \frac{h^{00}\frac{\omega^2}{c^2} + h^{11}k_x^2}{2k_z^2} \sigma \cos(\sigma) - \frac{h^{00}\frac{\omega^2}{c^2} + h^{11}k_x^2}{2k_z^2} \sin(\sigma) \right\} \tag{6.177}$$

$$\approx \mathrm{N}_{\text{TM}} k_z k_{x,y} \sin(k_z z) \Bigg\{ -\sin(\sigma)\cos(\Delta\sigma) + \cos(\sigma)\sin(\Delta\sigma) \tag{6.178}$$

$$- \frac{h^{00}\frac{\omega^2}{c^2} + h^{11}k_x^2}{2k_z^2} \sin(\sigma)\cos(\Delta\sigma) + \frac{h^{00}\frac{\omega^2}{c^2} + h^{11}k_x^2}{2k_z^2} \cos(\sigma)\sin(\Delta\sigma) \Bigg\} \tag{6.179}$$

$$= \mathrm{N}_{\text{TM}} k_z k_{x,y} \sin(k_z z) \left(1 + \frac{h^{00}\frac{\omega^2}{c^2} + h^{11}k_x^2}{2k_z^2} \right) \sin(\sigma - \Delta\sigma) \; . \tag{6.180}$$

This leads again to the same dispersion relation as in (6.35) because of the $\cos(\sigma - \Delta\sigma)$ and $\sin(\sigma - \Delta\sigma)$ terms. Hence, the results for the TM modes coincide with those for the TE modes.

6.4. Anisotropy of the dispersion relation

Note that the original dispersion relation (6.30) is isotropic, whereas the renormalized dispersion (6.35) is anisotropic. The isotropy of (6.30) is based on the absolute value of the wave vector $|\mathbf{k}|$. Hence, the surfaces of equal frequency ω are spherical. The correction related to the h^{00} element does not break the isotropy because it is also proportional to the absolute value of the wave vector. Comparing two surfaces of equal frequency, would reveal that these would occur at larger values of $|\mathbf{k}|$, which is called that the radius of the sphere increases equally in all directions. The anisotropy of (6.35) is due to the fraction related to the h^{11} element, namely $k_x^2 \big/ |k|^2$. Since the dispersion relation is the same for all three setups but the longitudinal and transversal wave vector directions change a separate analyze of each case is necessary. Do not overestimate this anisotropy, it is just an effective model to investigate the presence of weak gravity in Minkowski spacetime. The properties of the vacuum do not change whether in Minkowski or curved spacetime. This could be seen in section 5.2, where the original charge density and the original current density are set zo zero since these are the fundamental properties of the vacuum. However, there occur first order densities, which are interpreted as effective ones to reproduce the effect of weak gravity in Minkowski spacetime. That fact that these fulfill charge conservation, see section 5.3, justifies this. The calculations revealed an additional factor that must be taken into account:
We conclude that if in the flat case the vacuum between the plates is replaced by a medium with an anisotropic behavior (6.35) and the corresponding effective charge- and current densities are present, this reproduces the effect of weak gravity.

6.4.1. Setup *I*

For setup I the longitudinal wave vector component is k_x as it appears in the dispersion relation (6.35). Thus, the surface of constant frequency, is deformed from a sphere to an ellipsoid, where the $\mathbf{k}_x$-axis is stronger stretched than the perpendicular direction. The deformation can be clearly seen comparing an arbitrary surface of equal frequency in flat spacetime in figure 6.1a and in curved spacetime in figure 6.1b. Considering $\mathbf{k}_x$ represents the major axis of the ellipsoid, it is prolate because for large k_x the correction of the dispersion relation tends to minus infinity, which requires a larger $|\mathbf{k}|$ component for the same surface of equal frequency as in the flat, spherical case. In general there occurs a superposition of a slightly oblate and a strongly prolate ellipsoid. The oblate contribution is referred to the $1/|k|$ term, which is only sufficient for small $|\mathbf{k}|$ and tends to zero for large ones. The other term is quadratic in k_x and is more relevant for larger $|\mathbf{k}|$. Both effects are demonstrated in figures 6.1 and 6.2.

6.4.2. Setups II and III

The simultaneous analysis of setups II and III is based on the assumption that both transversal wave vector components appear in the same way, namely

$$\text{setup} \quad II: \quad k_x = k_z \; , \tag{6.181}$$

$$\text{setup} \; III: \quad k_x = k_y \; . \tag{6.182}$$

Consequently, the component k_x in the dispersion relation can be replaced by

$$k_x^2 = \frac{k_\perp^2}{2} \; , \tag{6.183}$$

in both cases. Therefore, the anisotropy of setup II and III coincide. Without loss of generality the plots are made for setup II.

The first difference to setup I is that the monotonically increasing part is now proportional to the transverse wave vector component. The monotonically nonincreasing part does not really change. As a result the ellipsoid is more an oblate one if $\mathbf{k}_x$ denotes the major axis. The corresponding plots are shown in figures 6.3 and 6.4.

To clarify the results of the difference between the perturbed dispersion relation (6.35) and the Minkowskian one (6.30)

$$\Delta\omega = \frac{1}{2} c|\mathbf{k}| \left(h^{00} + h^{11} \frac{k_x^2}{|\mathbf{k}|} \right) \tag{6.184}$$

is shown in figures 6.5 and 6.6 using two different scales.

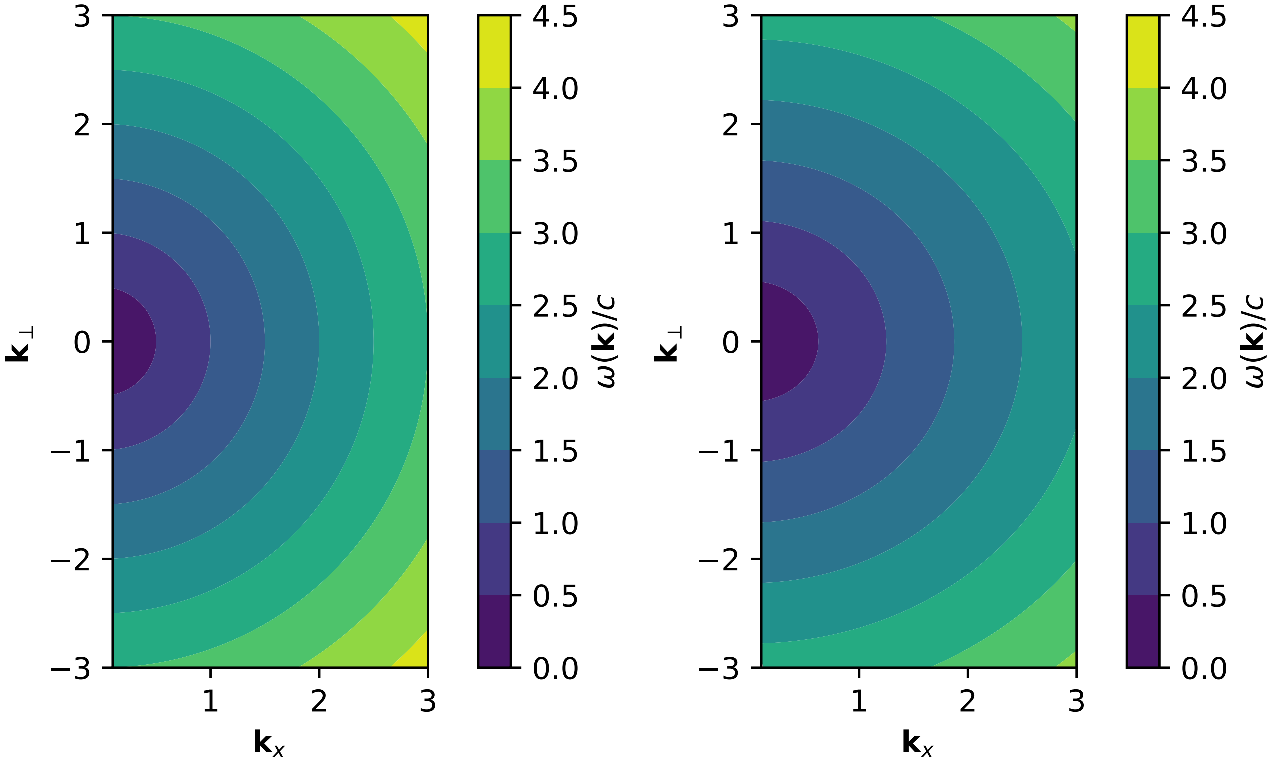

(a) *Contour plot of the dispersion relation* (6.30) *of the Casimir effect in Minkowski spacetime.*

(b) *Contour plot of the dispersion relation* (6.35) *of the Casimir effect in weak gravity for* $h^{00} = h^{11} = 0.2$.

Figure 6.1.: *Comparison of the dispersion relations of the Casimir effect in a flat and a slightly curved spacetime using contour plots. The color scheme of the angular frequency* ω *was chosen identical for both cases for better comparability. In addition, the values of the smallness parameters* h^{00}, h^{11} *are exaggerated for better visibility of the associated effects.*
The dispersion shown in 6.1a is equivalent to the cross section of a (half) sphere. This is due to the fact that the dispersion (6.30) *depends exclusively on the absolute value of the wave vector. The dispersion relation in 6.1b shows the cross section of an (half) ellipsoid. This fact is revealed by comparing 6.1a and 6.1b for the values* $2.0 < \omega < 2.5$ *of the angular frequency for instance. A strong stretching along the* $\mathbf{k}_x$ *axis occurs since the corresponding surface of equal frequency is located at higher values of* $\mathbf{k}_x$ *in 6.1b as in 6.1a. For the same reason a stretching along the* $\mathbf{k}_\perp$ *axis is also a recognizable. This one is not as strong as it appears in* $\mathbf{k}_x$ *direction.*

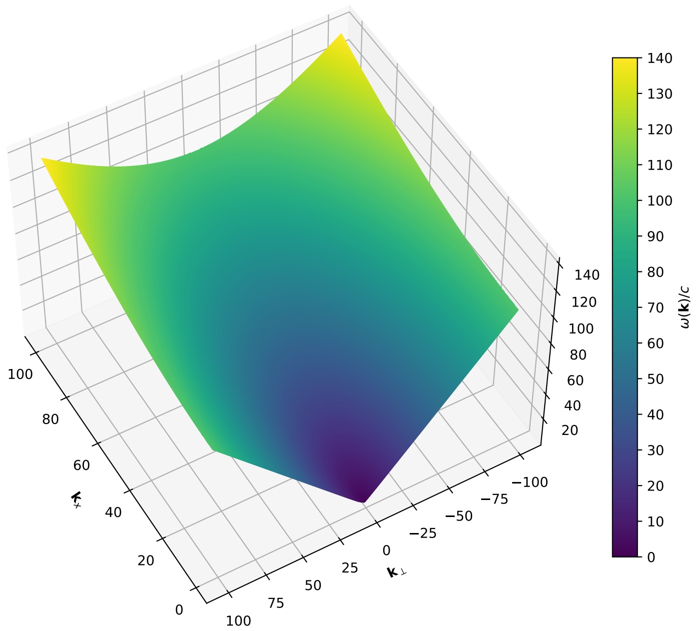

(a) *3D contour plot of the dispersion relation* (6.30) *of the Casimir effect in Minkowski spacetime. This one is valid for all three setups shown in figure 1.5.*

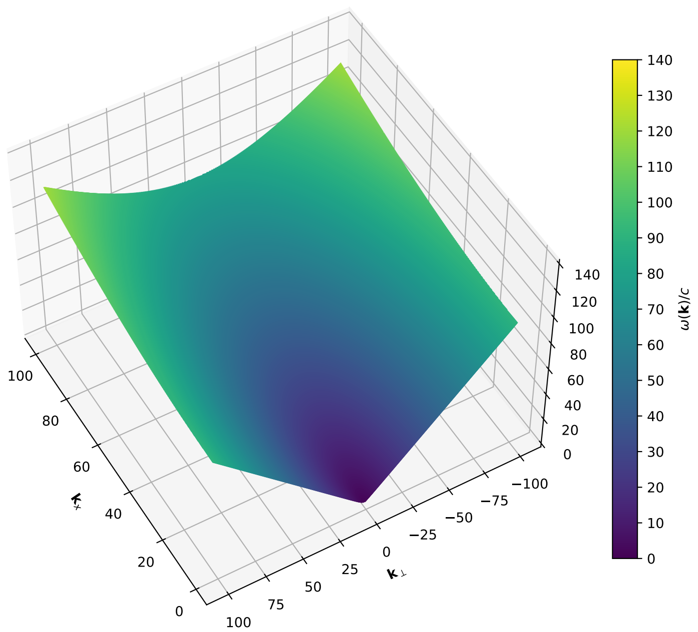

(b) *3D contour plot of the dispersion relation* (6.35) *of the Casimir effect for setup I in weak gravity for* $h^{00} = h^{11} = 0.2$.

Figure 6.2.: *Comparison of the dispersion relations of the Casimir effect in a flat and a slightly curved spacetime using three-dimensional contour plots. Note that a decrease of* ω *from 6.2a to 6.2b coincides with a stretching of the isotropic, spherical dispersion to an ellipsoid.*

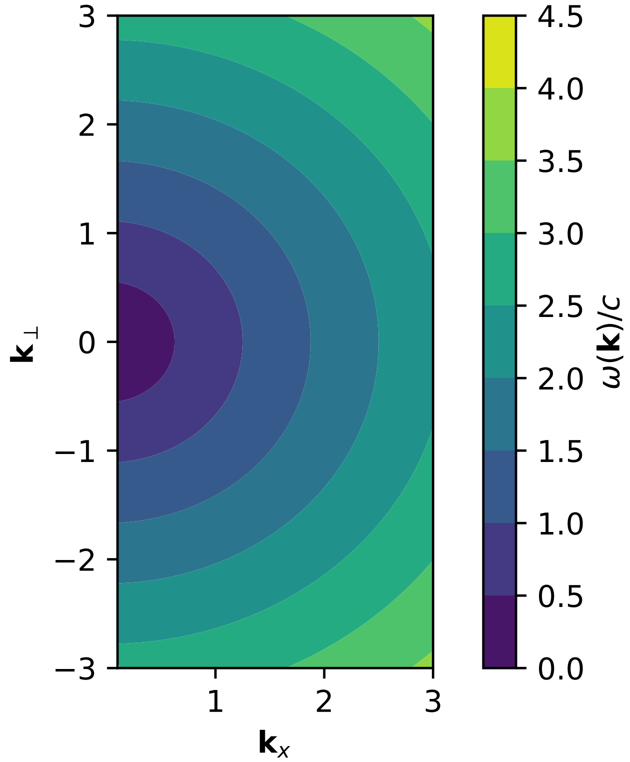

(a) *Contour plot of the dispersion relation* (6.35) *of the Casimir effect for setup I in weak gravity for* $h^{00} = h^{11} = 0.2$.

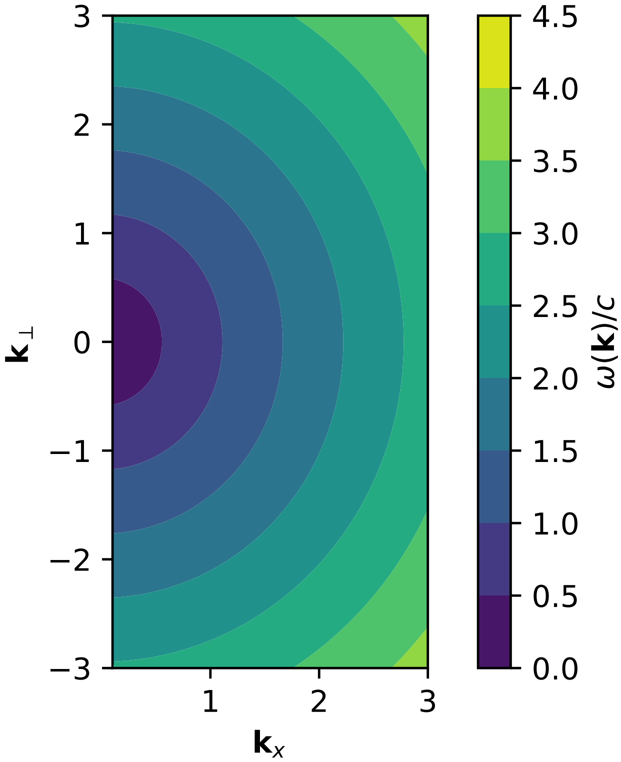

(b) *Contour plot of the dispersion relation* (6.35) *of the Casimir effect for setup II in weak gravity for* $h^{00} = h^{11} = 0.2$ *and* $k_x = k_z$.

Figure 6.3.: *Comparison of the dispersion relations of the Casimir effect for setups II and III in a regime of weak gravity using three-dimensional contour plots. Having a closer look to the surface of equal frequency* $2.0 < \omega < 2.5$ *reveals that setup II behaves more like a sphere along the* $\mathbf{k}_x$, *see figure 6.1a, than setup I does because this area is located at smaller values of* k_x. *Along the* $\mathbf{k}_\perp$*-axis the opposite behavior occurs, the regarded area nearly ends at* $k_\perp \approx 3.0$ *for setup II but already ends at* $k_\perp \approx 2.8$ *for setup I, which are both higher than in the flat case, see figure 6.1a, where it already ends at* $k_\perp \approx 2.5$. *Fixing* $\mathbf{k}_x$ *as the major axis setup II behaves oblate, is the resulting statement.*

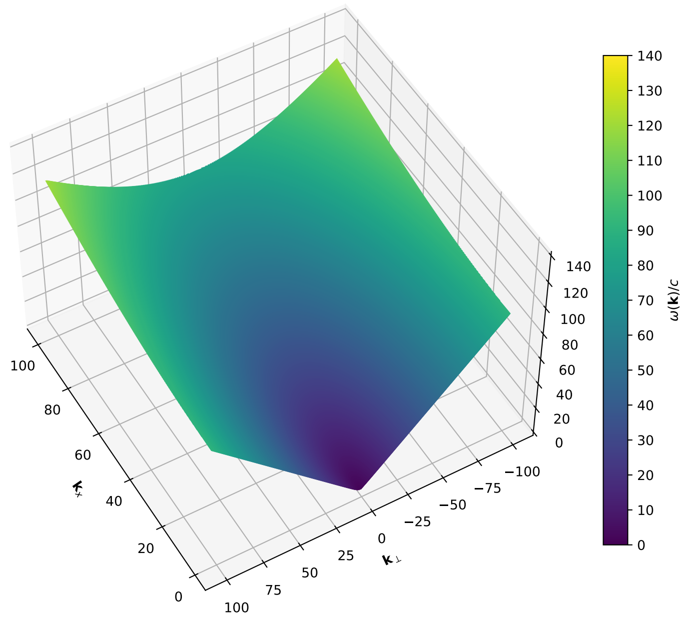

(a) *3D contour plot of the dispersion relation* (6.35) *of the Casimir for setup I effect in weak gravity for* $h^{00} = h^{11} = 0.2$.

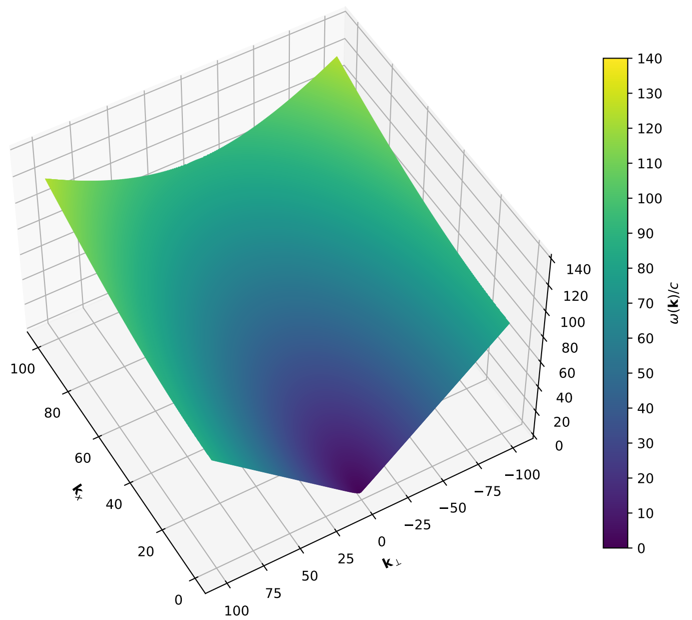

(b) *3D contour plot of the dispersion relation* (6.35) *of the Casimir for setup II effect in weak gravity for* $h^{00} = h^{11} = 0.2$ *and* $k_x = k_z$.

Figure 6.4.: *Comparison of the dispersion relations of the Casimir effect for setups I and II in a regime of weak gravity using three-dimensional contour plots. On the one hand it can be seen that at $k_\perp = 0$ and $k_x = 100$ has larger values ω for setup II than for setup I, only slightly lower than in figure 6.2a. This means that setup II behaves more like a sphere along the $\mathbf{k}_x$ axis than setup I. On the other hand at $k_x = 0$ and $k_\perp = -100$ setup II is smaller than setup I is. Note that setup I in weak gravity 6.2b is already lower than in the flat case 6.1a. Thus, setup II is along the $\mathbf{k}_\perp$-axis more off from a sphere than setup I is. Setting $\mathbf{k}_x$ as the major axis in both cases, the ellipsoid for setup I is mostly prolate, for setup II mostly oblate, in the regime of weak gravity.*

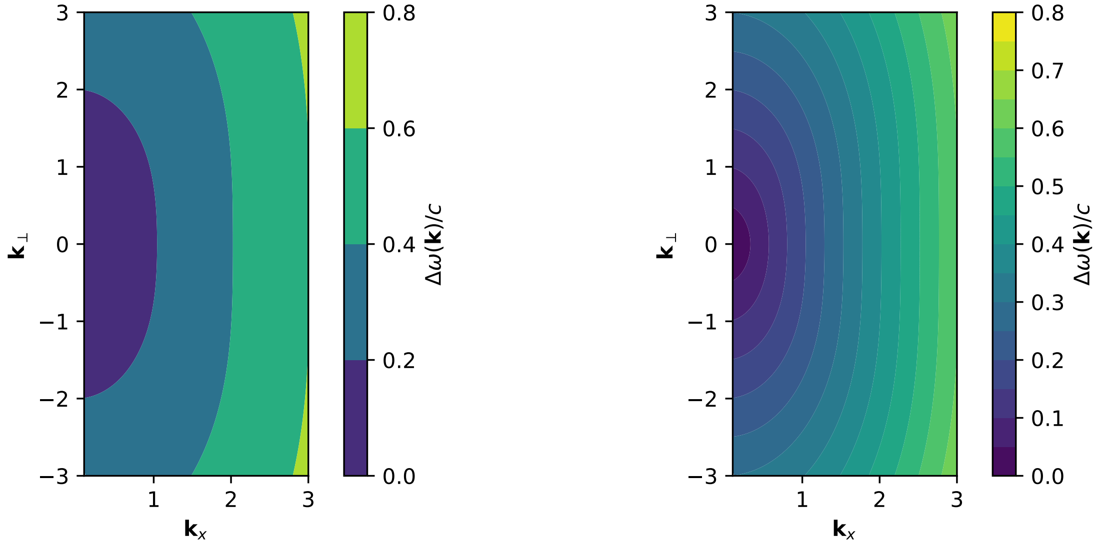

(a) *3D contour plot of (6.184) for $h^{00} = h^{11} = 0.2$. The scale width is 0.20.*

(b) *3D contour plot of (6.184) for $h^{00} = h^{11} = 0.2$. The scale width is 0.05.*

Figure 6.5.: *Contour plot of (6.184) for setup I using two different scales. Because $\Delta\omega$ increases more rapidly along the $\mathbf{k}_x$ than in $\mathbf{k}_\perp$ direction the deviation from a sphere is greater along the $\mathbf{k}_x$-axis. This agrees with the statement that the resulting ellipsoid is more prolate than oblate if $\mathbf{k}_x$ is chosen as the major axis.*

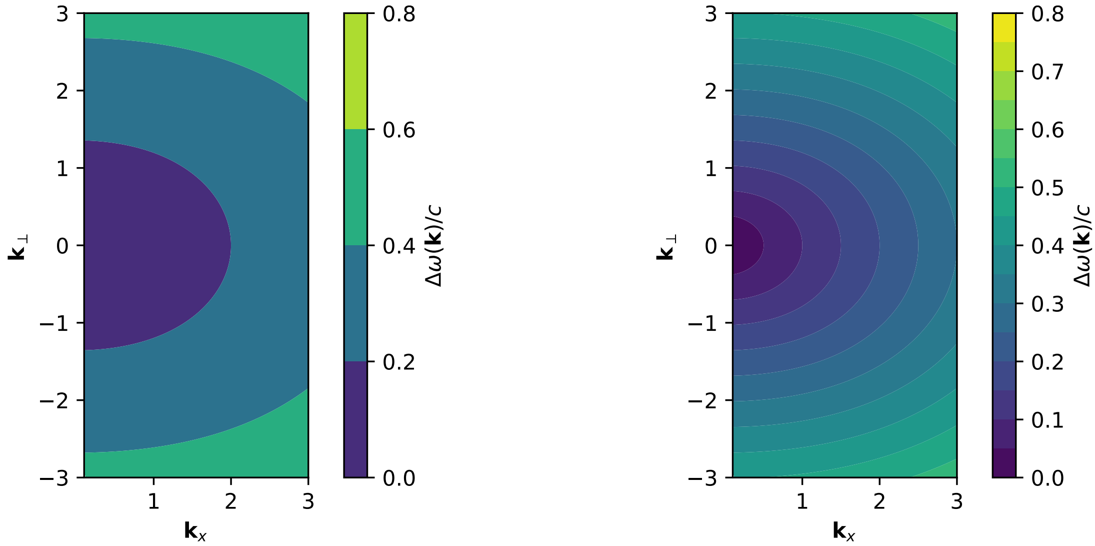

(a) *3D contour plot of (6.184) for $h^{00} = h^{11} = 0.2$ and $k_x = k_z$. The scale width is 0.20.*

(b) *3D contour plot of (6.184) for $h^{00} = h^{11} = 0.2$ and $k_x = k_z$. The scale width is 0.05.*

Figure 6.6.: *Contour plot of (6.184) for setup II using two different scales. Because $\Delta\omega$ increases more rapidly along the $\mathbf{k}_\perp$ than in $\mathbf{k}_x$ direction the deviation from a sphere is greater along the $\mathbf{k}_\perp$-axis. This agrees with the statement that the resulting ellipsoid is more oblate than prolate if $\mathbf{k}_x$ is chosen as the major axis.*

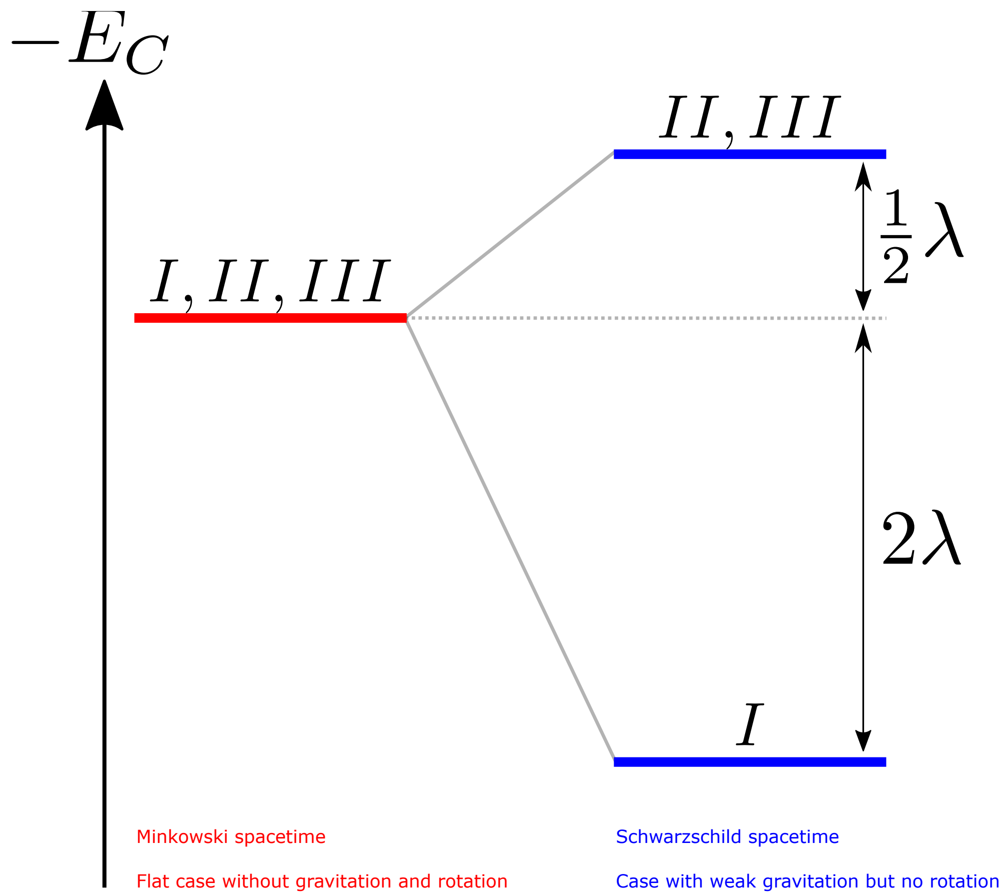

Figure 6.7.: *Energy splitting for the three Casimir settings introduced in figure 1.5 next to a source of weak gravity in Schwarzschild spacetime. The dotted line denotes the Casimir energy in Minkowski spacetime. Setup II and III increase their energies only to the change of the surface area by an amount of $-\lambda/2$. For setup I the surface area does not change, but its plate distance, yielding an energy decrease of 2λ compared to the flat case. Hereby, $\lambda = h^{11} = h^{00}$ is related via equations (6.3) and (5.21) to the Schwarzschild metric at position (6.4). The figure is not to scale.*

6.5. Overview

This chapter summarizes the results of sections 6.1 – 6.4.

First, the vectorial Maxwell equations are combined with a Poincaré-Lindstedt method in the framework of time-independent first-order perturbation theory to calculate the Casimir energies and force for the three different setups, see figure 1.5, for arbitrary constant perturbed metrics (6.3). It turned out that the results for setup I coincide with those of a Klein-Gordon theory approach [39, 47]. It appears that the gravitational influenced Casimir force F_C^{curved} can be obtained by replacing the plate distance d and the surface area A by its general relativistic counterparts, namely the proper plate distance d_p and the proper surface area A_p. However, for the perturbed Casimir energy E_C^{curved} such an replacement rule does not always lead to appropriate results.

Second, analog calculations reveal that Casimir energies and forces of setups II and III are identi-

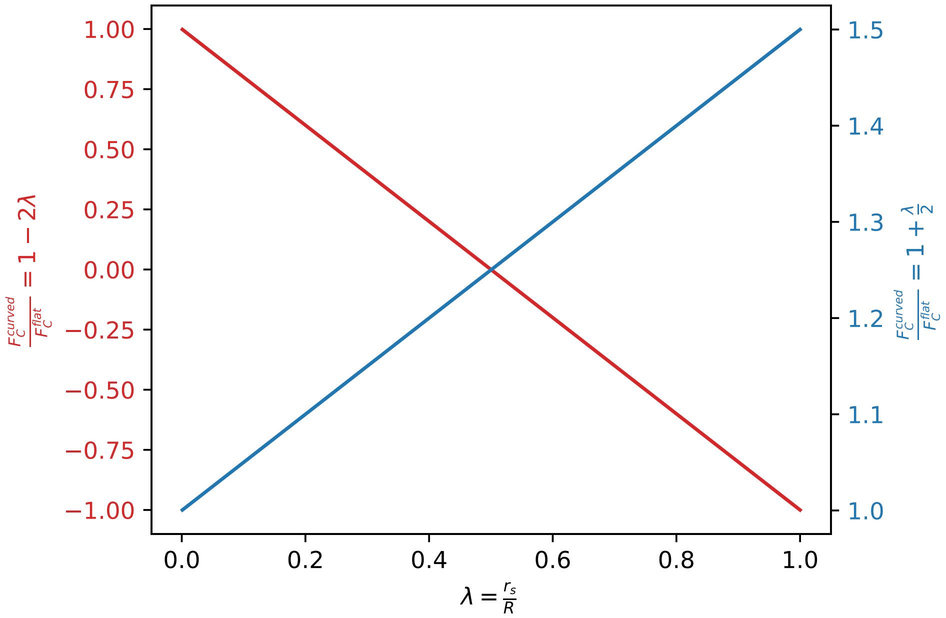

Figure 6.8.: *Ratio of the perturbed Casimir force in the presence of weak gravity to the Casimir force in a Minkowskian spacetime for setup I (red) and setups II and III (blue). Values taken from table 6.3 in the case of $h^{00} = h^{11} = \lambda$, valid in Schwarzschild spacetime.*

cal. Furthermore, both quantities satisfy the replacement rule. That the replacement rule, claimed by Klein-Gordon theory, is valid even for the other setups is insightful because it can be assumed that a more general idea is behind that. The validity of the replacement rule even for the Casimir energies of setups II and III is a fascinating result.

Third, comparing the Casimir energies of the three setups in Schwarzschild spacetime to the flat case, provided in figure 6.7, shows that for setup I it decreases by a factor 2λ, whereas it increases for setups II and III. Due to the presence of a source of gravity a symmetry breaking occurs, which lifts the degeneracy of the three setups in Minkowski spacetime. Since the smallness parameter $\lambda = r_s/R$ is constant for a fixed location, these shifts transfer to the Casimir force. The ratio of the Casimir force in weak gravity and the Casimir force in Minkowski spacetime is compared in figure 6.8. Note that the ratio is monotonically increasing in λ for setups II and III. Phenomenologically, where differences in the mode density inside the plates and the surrounding vacuum are responsible for the Casimir force this means: The mode density inside the plates decreases for setups II and III the closer they get to the event horizon r_s.
For setup I a completely different interpretation occurs: The closer the setup gets to the point $R = 2r_s$ the more the mode density between the plates increases. At the mentioned point, the mode densities between the plates and the surrounding vacuum coincide and the resulting Casimir force vanishes; the plates do not attract each other. If the setup gets even closer to the event horizon the Casimir force begins to be repulsive since the mode density between the plates is larger than the one outside. Keeping in mind that the condition for weak gravity (6.4) equal to $\lambda \ll 1$ is not satisfied close to the event horizon, so a breakdown of the perturbative approach is expected. Nevertheless, the statement itself is remarkable.

Fourth, the dispersion relation, which is identical for all three setups and for both the TE (2.11) and TM modes (2.13), is investigated more closely in section 6.4. The main result is that there occurs an effective anisotropy. This means that the effect of weak gravity is primarily equivalent to replacing the vacuum between the plates by an anisotropic medium in Minkowski spacetime. Although the dispersion relation (6.35) itself is the same for all three setups, the orientation of the plates with respect to the source of gravity yields different results. Identifying the vacuum with an isotropic, spherical dispersion, the dispersion relation of setup I is mainly prolate, whereas setups II and III occur mostly oblate if $\mathbf{k}_x$ defines the major axis.

Fifth, for any constant perturbed metric $h^{\mu\nu}$ the first-order continuity equation is satisfied, see section 5.3. Thus, the first-order charge density $\rho^{(1)}$ and current density $\mathbf{j}^{(1)}$ can be identified with physical meaningful quantities. An interesting behavior is that they do not necessarily disappear on the plate surfaces or in between, whereas in the flat case, they vanish between the plates. Furthermore, they are proportional to the inhomogeneities of the wave equations (5.44); explicitly for every setup see (6.11), (6.62), (6.84), (6.119), (6.141), (6.162) for the charge densities and (6.13), (6.63), (6.85), (6.120), (6.142), (6.163) for the current densities. The analytically correct description of the Casimir effect in a curved spacetime with vanishing charge- and current densities is perturbatively analogue to a description in Minkowski spacetime but with an effective charge density ρ_{eff} and an effective current density $\mathbf{j}_{\text{eff}}$. Considering only terms proportional to the first order leads to the identification $\rho_{\text{eff}} = \rho^{(1)}$ and $\mathbf{j}_{\text{eff}} = \mathbf{j}^{(1)}$. From a physical point of view, the anisotropic dispersion relation and the effective charge and current densities are mutually dependent for a correct description in Minkowski spacetime. Nethertheless, at the moment, it is not clear how an experimental realization for this purpose would look like.

Sixth, the basic results provided by Klein-Gordon theory coincide with those of Maxwell's equations except a factor of two, denoting the two polarization directions of light [39, 47]. This agrees with the argumentation stated in chapter 1.

Seventh, measuring this effect is an unsolved problem so far and seems impossible nowadays [47]. The comparison of the forces of different setups opens up a possibility with today's technical capabilities. A precise consideration is based on table 6.3, which summarizes the results in Schwarzschild spacetime and is discussed next.

Table 6.1.: *Results for the Casimir setup I of figure 1.5 in the presence of weak gravity (6.3) using first-order perturbation theory, contributions of the particular solutions of the wave equations (5.44) and the conditions (6.3), (6.4).*

Quantities	I 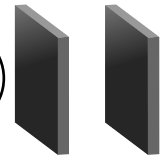
Dispersion relation: $\omega(\mathbf{k})$	$c\lvert\mathbf{k}\rvert\left[1-\frac{1}{2}\left(h^{00}+h^{11}\frac{k_x^2}{\lvert\mathbf{k}\rvert^2}\right)\right]$
Casimir Energy: E_C^{curved}	$E_C^{\text{flat}}\left[1-\frac{1}{2}\left(h^{00}+3h^{11}\right)\right]$
Electric field (TE): $\mathbf{E}_{\text{TE}}^{\text{curved}}$	$\mathrm{N}_{\text{TE}}\omega\sin(k_x x)\begin{pmatrix}0\\k_z\\-k_y\end{pmatrix}\sin(\sigma-\Delta\sigma)$
Magnetic induction field (TE): $\mathbf{B}_{\text{TE}}^{\text{curved}}$	$-\mathrm{N}_{\text{TE}}\begin{pmatrix}k_\perp^2\sin(k_x x)\sin(\sigma-\Delta\sigma)\\ k_x k_y\left(1+\frac{h^{00}\frac{\omega^2}{c^2}+h^{11}k_x^2}{2k_x^2}\right)\cos(k_x x)\cos(\sigma-\Delta\sigma)\\ k_x k_z\left(1+\frac{h^{00}\frac{\omega^2}{c^2}+h^{11}k_x^2}{2k_x^2}\right)\cos(k_x x)\cos(\sigma-\Delta\sigma)\end{pmatrix}$
Electric field (TM): $\mathbf{E}_{\text{TM}}^{\text{curved}}$	$-\mathrm{N}_{\text{TM}}\begin{pmatrix}k_\perp^2\cos(k_x x)\cos(\sigma-\Delta\sigma)\\ k_x k_y\left(1+\frac{h^{00}\frac{\omega^2}{c^2}+h^{11}k_x^2}{2k_x^2}\right)\sin(k_x x)\sin(\sigma-\Delta\sigma)\\ k_x k_z\left(1+\frac{h^{00}\frac{\omega^2}{c^2}+h^{11}k_x^2}{2k_x^2}\right)\sin(k_x x)\sin(\sigma-\Delta\sigma)\end{pmatrix}$
Magnetic induction field (TM): $\mathbf{B}_{\text{TM}}^{\text{curved}}$	$\mathrm{N}_{\text{TM}}\frac{\omega}{c^2}\begin{pmatrix}0\\-k_z\\k_y\end{pmatrix}\cos(k_x x)\cos(\sigma-\Delta\sigma)$

Table 6.2.: *Results for the Casimir setups II and III of figure 1.5 in the presence of weak gravity (6.3) using first-order perturbation theory, contributions of the particular solutions of the wave equations (5.44) and the conditions (6.3), (6.4).*

Quantities	II 	III 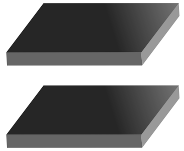
$\omega(\mathbf{k})$	$c\lvert\mathbf{k}\rvert\left[1-\frac{1}{2}\left(h^{00}+h^{11}\frac{k_x^2}{\lvert\mathbf{k}\rvert^2}\right)\right]$	$c\lvert\mathbf{k}\rvert\left[1-\frac{1}{2}\left(h^{00}+h^{11}\frac{k_x^2}{\lvert\mathbf{k}\rvert^2}\right)\right]$
E_C^{curved}	$E_C^{\text{flat}}\left(1-\frac{h_{11}}{2}\right)\left[1-\frac{1}{2}\left(h^{00}-h^{11}\right)\right]$	$E_C^{\text{flat}}\left(1-\frac{h_{11}}{2}\right)\left[1-\frac{1}{2}\left(h^{00}-h^{11}\right)\right]$
$\mathbf{E}_{\text{TE}}^{\text{curved}}$	$\mathrm{N}_{\text{TE}}\omega\sin(k_y y)\begin{pmatrix}-k_z\\0\\k_x\end{pmatrix}\sin(\sigma-\Delta\sigma)$	$\mathrm{N}_{\text{TE}}\omega\sin(k_z z)\begin{pmatrix}k_y\\-k_x\\0\end{pmatrix}\sin(\sigma-\Delta\sigma)$
$\mathbf{B}_{\text{TE}}^{\text{curved}}$	$-\mathrm{N}_{\text{TE}}\begin{pmatrix}k_x k_y\cos(k_y y)\left(1+\frac{h^{00}\frac{\omega^2}{c^2}+h^{11}k_x^2}{2k_y^2}\right)\cos(\sigma-\Delta\sigma)\\k_\perp^2\sin(k_y y)\sin(\sigma-\Delta\sigma)\\k_y k_z\cos(k_y y)\left(1+\frac{h^{00}\frac{\omega^2}{c^2}+h^{11}k_x^2}{2k_y^2}\right)\cos(\sigma-\Delta\sigma)\end{pmatrix}$	$-\mathrm{N}_{\text{TE}}\begin{pmatrix}k_x k_z\cos(k_z z)\left(1+\frac{h^{00}\frac{\omega^2}{c^2}+h^{11}k_x^2}{2k_z^2}\right)\cos(\sigma-\Delta\sigma)\\k_y k_z\cos(k_z z)\left(1+\frac{h^{00}\frac{\omega^2}{c^2}+h^{11}k_x^2}{2k_z^2}\right)\cos(\sigma-\Delta\sigma)\\k_\perp^2\sin(k_z z)\sin(\sigma-\Delta\sigma)\end{pmatrix}$
$\mathbf{E}_{\text{TM}}^{\text{curved}}$	$-\mathrm{N}_{\text{TM}}\begin{pmatrix}k_x k_y\sin(k_y y)\left(1+\frac{h^{00}\frac{\omega^2}{c^2}+h^{11}k_x^2}{2k_y^2}\right)\sin(\sigma-\Delta\sigma)\\k_\perp^2\cos(k_y y)\cos(\sigma-\Delta\sigma)\\k_y k_z\sin(k_y y)\left(1+\frac{h^{00}\frac{\omega^2}{c^2}+h^{11}k_x^2}{2k_y^2}\right)\sin(\sigma-\Delta\sigma)\end{pmatrix}$	$-\mathrm{N}_{\text{TM}}\begin{pmatrix}k_x k_z\sin(k_z z)\left(1+\frac{h^{00}\frac{\omega^2}{c^2}+h^{11}k_x^2}{2k_z^2}\right)\sin(\sigma-\Delta\sigma)\\k_y k_z\sin(k_z z)\left(1+\frac{h^{00}\frac{\omega^2}{c^2}+h^{11}k_x^2}{2k_z^2}\right)\sin(\sigma-\Delta\sigma)\\k_\perp^2\cos(k_z z)\cos(\sigma-\Delta\sigma)\end{pmatrix}$
$\mathbf{B}_{\text{TM}}^{\text{curved}}$	$\mathrm{N}_{\text{TM}}\frac{\omega}{c^2}\cos(k_y y)\begin{pmatrix}k_z\\0\\-k_x\end{pmatrix}\cos(\sigma-\Delta\sigma)$	$\mathrm{N}_{\text{TM}}\frac{\omega}{c^2}\cos(k_z z)\begin{pmatrix}-k_y\\k_x\\0\end{pmatrix}\cos(\sigma-\Delta\sigma)$

Table 6.3.: *Casimir energies and forces for three setups in the presence of weak gravity* (6.3) *with respect to the provided conditions* (6.3) *and* (6.4).

Quantities	*I* 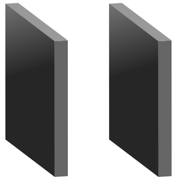	*II* 	*III* 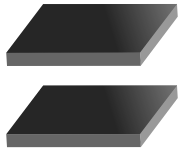
E_C^{flat}	$-\frac{\pi^2\hbar cA}{720d^3}$	$-\frac{\pi^2\hbar cA}{720d^3}$	$-\frac{\pi^2\hbar cA}{720d^3}$
$E_C^{h^{00}}$	$E_C^{\text{flat}}\left(1-\frac{h^{00}}{2}\right)$	$E_C^{\text{flat}}\left(1-\frac{h_{11}}{2}\right)\left(1-\frac{h^{00}}{2}\right)$	$E_C^{\text{flat}}\left(1-\frac{h_{11}}{2}\right)\left(1-\frac{h^{00}}{2}\right)$
$E_C^{h^{11}}$	$E_C^{\text{flat}}\left(1-\frac{3h^{11}}{2}\right)$	$E_C^{\text{flat}}\left(1-\frac{h_{11}}{2}\right)\left(1+\frac{h^{11}}{2}\right)$	$E_C^{\text{flat}}\left(1-\frac{h_{11}}{2}\right)\left(1+\frac{h^{11}}{2}\right)$
$E_C^{\text{curved}}=E_C^{h^{00}}+E_C^{h^{11}}$	$E_C^{\text{flat}}\left[1-\frac{1}{2}\left(h^{00}+3h^{11}\right)\right]$	$E_C^{\text{flat}}\left(1-\frac{h_{11}}{2}\right)\left[1-\frac{1}{2}\left(h^{00}-h^{11}\right)\right]$	$E_C^{\text{flat}}\left(1-\frac{h_{11}}{2}\right)\left[1-\frac{1}{2}\left(h^{00}-h^{11}\right)\right]$
$F_C^{\text{curved}}=-\frac{\partial E_C^{\text{curved}}}{\partial d}$	$F_C^{\text{flat}}\left[1-\frac{1}{2}\left(h^{00}+3h^{11}\right)\right]$	$F_C^{\text{flat}}\left(1-\frac{h_{11}}{2}\right)\left[1-\frac{1}{2}\left(h^{00}-h^{11}\right)\right]$	$F_C^{\text{flat}}\left(1-\frac{h_{11}}{2}\right)\left[1-\frac{1}{2}\left(h^{00}-h^{11}\right)\right]$
$E_C^{\text{curved}}\left(h^{00}=h^{11}=\lambda\right)$	$E_C^{\text{flat}}\left(1-2\lambda\right)\neq E_C^{\text{flat}}(d_p,A_p)$	$E_C^{\text{flat}}\left(1+\frac{\lambda}{2}\right)=E_C^{\text{flat}}(d_p,A_p)$	$E_C^{\text{flat}}\left(1+\frac{\lambda}{2}\right)=E_C^{\text{flat}}(d_p,A_p)$
$F_C^{\text{curved}}\left(h^{00}=h^{11}=\lambda\right)$	$F_C^{\text{flat}}\left(1-2\lambda\right)=F_C^{\text{flat}}(d_p,A_p)$	$F_C^{\text{flat}}\left(1+\frac{\lambda}{2}\right)=F_C^{\text{flat}}(d_p,A_p)$	$F_C^{\text{flat}}\left(1+\frac{\lambda}{2}\right)=F_C^{\text{flat}}(d_p,A_p)$

6.6. Measurements

Following up on the idea of measuring different Casimir orientations, already outlined in chapter 1, this chapter does just that, based on the previous results from chapters 6.1 – 6.3, which are summarized in section 6.5. Especially the concrete values from table 6.3 are essential in this section. Note that only forces and energy differences can be measured. For the sake of an easier comparability of different experimental setups the focus lies on measuring force differences in Schwarzschild spacetime $h^{00} = h^{11} = \lambda = r_s/R$.

6.6.1. Comparison of setup II and III

Due to the symmetry of setups II and III the Casimir force F_C^{curved} in the presence of weak gravity is identical, see table 6.3. The corresponding difference is zero and it can be stated

$$F_C^{II} - F_C^{III} = 0 \,, \tag{6.185}$$

with the corresponding dimensionless parameter

$$\frac{F_C^{II}}{F_C^{III}} - 1 = 0 \,. \tag{6.186}$$

For an experimental realization it is recommended to use the difference of these two setups as a test measurement. If there occur additional effects like finite velocities of the Casimir setup or the source of gravity, or further corrections, this can be read off from the values (6.185) and (6.186) being non-zero.

6.6.2. Comparison of setup I and III

Due to the equality of setup II and III in their corresponding Casimir energies and forces, see figure 6.7 and table 6.3, the comparison of setup I with setup II or setup III yields the same result. Therefore, without loss of generality setup III is chosen for the following formulae. The corresponding difference reads

$$F_C^{I} - F_C^{III} = -\frac{5}{2}\lambda F_C^{\text{flat}} \,, \tag{6.187}$$

with the corresponding dimensionless parameter

$$\frac{F_C^{I}}{F_C^{III}} - 1 = -\frac{5}{2}\lambda \,. \tag{6.188}$$

This corresponds to the case of a Schwarzschild metric, see (5.21) with $a = 0$, and the additional restriction that the Casimir setups are exactly at the fixed position given by (6.4).
In order to check whether the effects of gravity on the Casimir effect can be verified by measurement on Earth, within the gravity field of the sun, one now sets $r_s = r_{s\ \text{sun}}$ and $R = R_{\text{mean sun}}$, which appear in table 5.1 in the fourth row, second column, yielding

$$\lambda_{\text{mean Earth-Sun}} = 1.97 \cdot 10^{-5} \,. \tag{6.189}$$

Note that the mean distance is assumed meaning the elliptical orbit of the Earth is approximated by a circle. Due to the small eccentricity of the Earth orbit $\epsilon_{\text{Earth}} \approx 0.016$ this assumption is reasonable [21, p. 625]. Remember that an atomic force microscope (AFM) can resolve forces up to 10^{-13} N nowadays, see chapter 1. Thus, a small deviation in the Casimir force, proportional to (6.189) is measurable, if the Casimir force in the Minkowski case is not larger than 10^{-8} N. Thus, a relation between the plate distance d and the plate area A can be derived

$$d \lessapprox 1.9 \cdot 10^{-5} \sqrt{m} \cdot \sqrt[4]{A} \,. \tag{6.190}$$

According to chapter 1 distances between 0.1 and 0.9 μm are achievable using a plane-sphere geometry. For the plane-plane geometry, mainly investigated in this thesis, values of the breakthrough experiment by Lamoreaux are used [29]. He used two circular plates with a diameter of 2.54 cm and distances $d \in [0.6; 6]$ μm. Using Lamoreaux's plate area of around 5.1 cm^2 and inserting this into (6.190) leads to a distance of approximately $d \lessapprox 2.86$ μm, which is exactly in the range between $d \in [0.6; 6]$ μm. However, there are several delicate issues compared to the original experimental setup.
Getting relevant experimental data provides a good understanding of additional physical effects like temperature, finite conductivity, roughness of the plates and much more. These effects are generically taken into account in precision measurements to provide a high agreement between experiment and theory in the range of a few percent. Exactly there occurs the problem: If the standard corrections are included, an accuracy of a few percent is obtained. However, the effect to be measured is in the range of $\lambda \propto 0.001$ %. Obviously, this is a challenge for the experiment, but also for the theory to provide a description of the (classical) effects involved as accurate as possible. From a technical point of view, it would be possible to prove the gravitational influences on the Casimir energy today, but from a metrological point of view, this is rather challenging. If one artificially negates effects such as a finite temperature by cooling the experiment, sets up the experiment in a vacuum, and additionally pays attention to plates that have an extremely high conductivity, it might be possible; but this would have to be looked at more closely. In addition, it must be considered that the experiment must be pivoted and the orientation with respect to the sun must be constantly checked; but this should not be a problem to implement. It cannot be conclusively determined whether the effect considered here is measurable today. It is certainly conceivable, but the effort required for such an experiment would be enormous. Note that the effect of the gravitational impact of the Earth itself is four orders of magnitude smaller than that of the Sun; therefore it is negligible, see fourth row table 5.1.

Another method to measure this small effect would be to eliminate statistical errors. Since these always occur in the same way for all three setups, measuring the differences between the three setups leads to the fact that only gravity causes a measurable difference. For the plates themselves, it would be advisable to use the same ones, as then influences of roughness and finite conductivity are identical for all three setups. Furthermore, the temperature must be controlled so that there are no differences between the different setups, i.e., it is best to keep it constant. A constant temperature will become attainable if one uses a satellite in the Earth's shadow or even in the moon's shadow.

6.6.3. Comparing flat and curved spacetime results

Another way to determine the influence of gravity is to take advantage of the incontrovertible fact that all Casimir experiments conducted on Earth are influenced by gravity. Because these measurements are quite accurate and a lot of effort is put into them, measuring the flat Casimir energy and comparing it with the ones with gravity could reveal the energy difference. Where in our astronomical neighborhood are points where spacetime is locally flat? The answer is given by the five Lagrange points of the three-body system formed by Sun, Earth and an orbiter of negligible mass. At these points the gravitational influence of Sun and Earth cancel out each other and as provided by figure 6.9 the spacetime is locally flat. For a short-term mission the radially unstable Lagrange points L_1 to L_3 can be used [12, 46]. But for a long-term investigation and the circumstance that the orbiter will not stand still at the Lagrange point, the asymptotically stable points L_4 and L_5 are preferred. For these two points, the probe remains in their vicinity even without a correction maneuver [46]. One fact that must not be ignored is that the gravitational forces of the remaining bodies in the solar system have not been considered here since the Lagrange points are only solutions of the reduced three-body problem. The difference of the Casimir force measured for setup II in Schwarzschild spacetime and any other setup in Minkowski spacetime reads

$$F_C^{II,\mathrm{curved}} - F_C^{\mathrm{flat}} = \frac{\lambda}{2} F_C^{\mathrm{flat}} \,, \tag{6.191}$$

with the corresponding dimensionless parameter

$$\frac{F_C^{II,\mathrm{curved}}}{F_C^{\mathrm{flat}}} - 1 = \frac{\lambda}{2} \,. \tag{6.192}$$

So, compared to the measurements provided in subsection 6.6.2 only the prefactor of the measured force changes. This does not influence the measurability at all. Therefore, this measurement should be also valid to verify the influence of weak gravity.

Based on the idea to look for points where the Minkowskian case is fulfilled, the idea of using a reduced-gravity aircraft occurs. In the system of the moving aircraft a measurement without the influence of Earth's gravity is available. However, this will be less suitable than the Lagrange points, since the main gravitational influence for all objects in our solar system is provided by the Sun, see table 5.1.

.

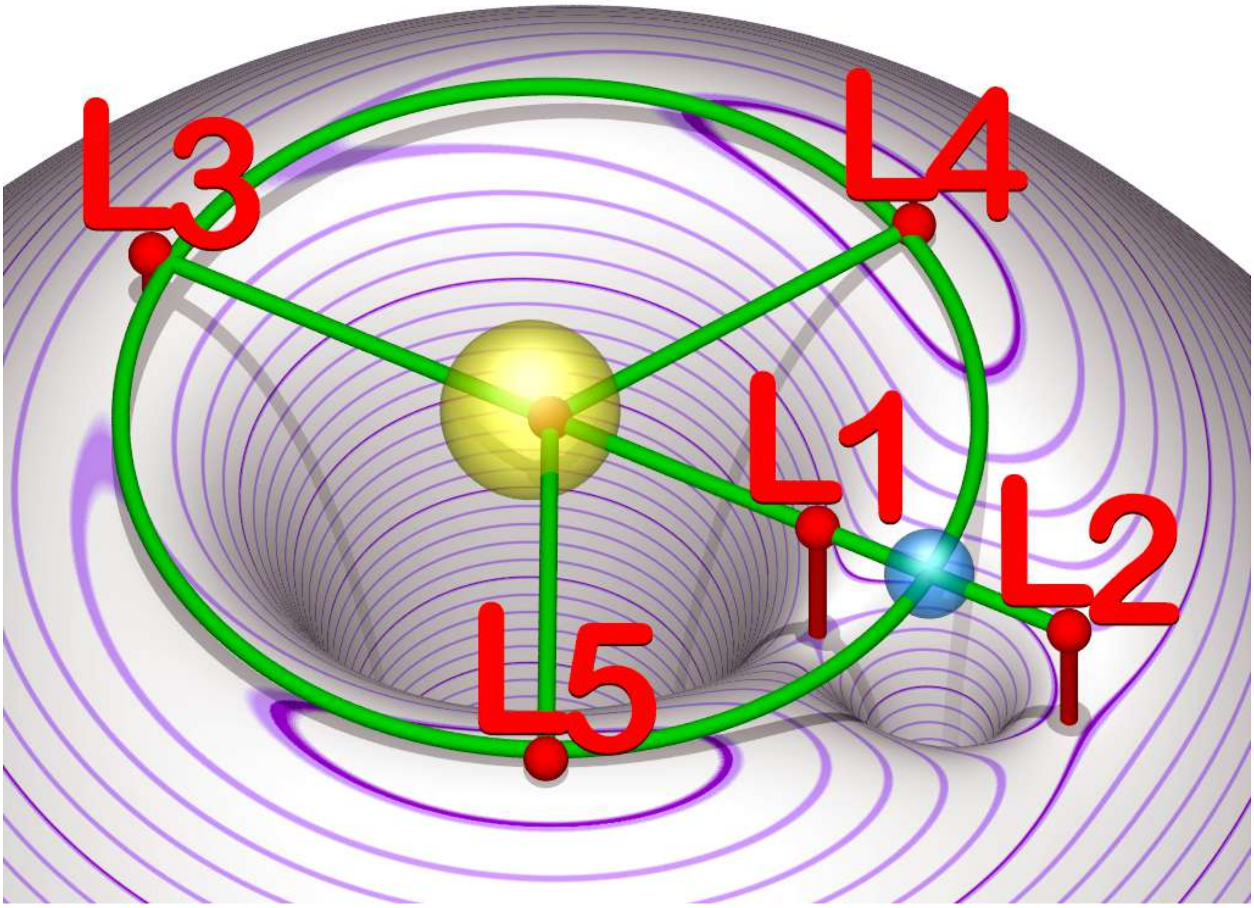

Figure 6.9.: *„Image showing the relationship between the five Lagrangian points (red) of a planet (blue) orbiting a star (yellow), and the effective potential (gravitational + rotational) in the plane containing the orbit (grey surface with purple contours of equal potential)". Equipotential lines of the gravity field in the co-rotating reference frame as rubber mat model drawn in purple. The mass ratio is 1:10, so L1 and L2 stand out clearly in the section in the orbital plane. At the Lagrange points L_1 – L_5 the spacetime is locally flat [57, quote & figure].*

7. Casimir effect for fixed setups close to a slowly rotating source of weak gravity

The most effortless extension of the Casimir effect near a non-rotating, non-charged source of gravity described by the Schwarzschild metric is taking into account a small angular momentum. An extension of the corresponding Kerr metric in the dimensionless spin parameter χ was already done in section 3.5. The corresponding metric of this Slow-Rotation Approximation (SRA) is shown in (3.49) and approximated in Cartesian coordinates in (5.21). The generalized form for a fixed Casimir setup around the slowly rotating source of weak gravity (6.4) reads

$$h^{\mu\nu} = \begin{pmatrix} h^{00} & 0 & h^{02} & 0 \\ 0 & h^{11} & 0 & 0 \\ h^{20} & 0 & 0 & 0 \\ 0 & 0 & 0 & 0 \end{pmatrix} . \tag{7.1}$$

Compared to (6.3), the h^{20} and h^{02} entries are new. Because Maxwell's equations are linear, different solutions can be combined with another one by adding them up. It is sufficient to solve only Gauss' (5.40) and Ampère's law (5.42) for these new elements and add them to the solutions known from chapter 6. The renormalization is performed using the pattern from subsection 6.1.1. The calculations are only performed using the TE modes because no other result is expected for the TM modes, as shown in section 6.5.

7.1. Setup I

In this section, setup I from figure 1.5 is calculated using the metric (7.1). Because the results related to the h^{00} and h^{11} elements are already known from section 6.1, the focus here lies on the corrections related to the $h^{20} = h^{02}$ element. It will show up that the previous assumption from chapter 6 that only the real part of the zeroth-order solutions, mainly focused on the TE modes (2.11), leads to an incomplete first-order solution considering slow rotations.

7.1.1. Transversal electric modes - Real part

Applying the real part of (2.11) as already used in subsection 6.1.1 and concretizing Gauss' law (5.40) for only the $h^{20} = h^{02}$ elements yields

$$\rho^{(1)} = \varepsilon_0 c \sum_m \epsilon_{kmn} h^{n0} \partial_m B^{k(0)} = \varepsilon_0 h^{20} c \left(\partial_3 B^{1(0)} - \partial_1 B^{3(0)} \right) . \tag{7.2}$$

Analogously, the Ampère's law (5.42) simplifies as follows

$$\mathbf{j}^{(1)} = \frac{1}{\mu_0}\left(\frac{1}{c}h^{0l}\partial_l E_p^{(0)} + \epsilon_{kmp}h^{m\mu}\partial_\mu B^{k(0)}\right) \tag{7.3}$$

$$= \frac{1}{\mu_0}\begin{pmatrix} \frac{1}{c}h^{20}\partial_2 E_1^{(0)} + h^{20}\partial_0 B^{3(0)} \\ \frac{1}{c}h^{20}\partial_2 E_2^{(0)} \\ \frac{1}{c}h^{20}\partial_2 E_3^{(0)} - h^{20}\partial_0 B^{1(0)} \end{pmatrix} . \tag{7.4}$$

Inserting the real part of the TE modes (2.11) into (7.2) and (7.4) leads to

$$\rho^{(1)} = -\varepsilon_0 \mathrm{N}_{\mathrm{TE}} k_z \sin(k_x x)\cos(\sigma) h^{20}\frac{\omega^2}{c} , \tag{7.5}$$

$$\mathbf{j}^{(1)} = -\frac{1}{\mu_0}\mathrm{N}_{\mathrm{TE}}\frac{\omega}{c}h^{20}\begin{pmatrix} k_x k_z \cos(k_x x)\sin(\sigma) \\ -k_y k_z \sin(k_x x)\cos(\sigma) \\ \left(k_y^2 + k_\perp^2\right)\sin(k_x x)\cos(\sigma) \end{pmatrix} . \tag{7.6}$$

The corresponding wave equations using (5.44) are

$$\Box\mathbf{E}^{(1)} = \mathrm{N}_{\mathrm{TE}}\frac{\omega^2}{c}2h^{20}\begin{pmatrix} 0 \\ -k_y k_z \sin(k_x x)\sin(\sigma) \\ k_y^2 \sin(k_x x)\sin(\sigma) \end{pmatrix} , \tag{7.7}$$

$$\Box\mathbf{B}^{(1)} = -\mathrm{N}_{\mathrm{TE}}\frac{\omega}{c}2h^{20}k_\perp^2\begin{pmatrix} k_y \sin(k_x x)\sin(\sigma) \\ k_x \cos(k_x x)\cos(\sigma) \\ 0 \end{pmatrix} . \tag{7.8}$$

The solutions are given by

$$\mathbf{E}^{(1)} = -\mathrm{N}_{\mathrm{TE}}\omega\frac{h^{20}k_y\frac{\omega}{c}}{k_x^2}\begin{pmatrix} 0 \\ -k_z \\ k_y \end{pmatrix}\sin(k_x x)\sigma\cos(\sigma) , \tag{7.9}$$

$$\mathbf{B}^{(1)} = -\mathrm{N}_{\mathrm{TE}}\frac{h^{20}k_y\frac{\omega}{c}}{k_x^2}\begin{pmatrix} k_\perp^2 \sin(k_x x)\sigma\cos(\sigma) \\ -k_x k_y \cos(k_x x)\left[\sigma\sin(\sigma) + \cos(\sigma)\right] \\ -k_x k_z \cos(k_x x)\left[\sigma\sin(\sigma) + \cos(\sigma)\right] \end{pmatrix} . \tag{7.10}$$

Together with the unperturbed solutions (6.9) and the solutions for the h^{00} and h^{11} entries (6.16), the result for the SRA is given by

$$\mathbf{E}_{\mathrm{tot}}^{\mathrm{curved}} = \mathrm{N}_{\mathrm{TE}}\omega\sin(k_x x)\begin{pmatrix}0\\-k_z\\k_y\end{pmatrix}\left\{-\sin(\sigma)+\frac{h^{00}\frac{\omega^2}{c^2}+h^{11}k_x^2}{2k_x^2}\sigma\cos(\sigma)-\frac{h^{20}k_y\frac{\omega}{c}}{k_x^2}\sigma\cos(\sigma)\right\} \tag{7.11}$$

$$= \mathrm{N}_{\mathrm{TE}}\omega\sin(k_x x)\begin{pmatrix}0\\-k_z\\k_y\end{pmatrix}\left\{-\sin(\sigma)+\left[\frac{h^{00}\frac{\omega^2}{c^2}+h^{11}k_x^2}{2k_x^2}-\frac{h^{20}k_y\frac{\omega}{c}}{k_x^2}\right]\sigma\cos(\sigma)\right\} \tag{7.12}$$

$$\approx \mathrm{N}_{\mathrm{TE}}\omega\sin(k_x x)\begin{pmatrix}0\\-k_z\\k_y\end{pmatrix}\{-\sin(\sigma)\cos(\Delta\sigma)+\sin(\Delta\sigma)\cos(\sigma)\} \tag{7.13}$$

$$= \mathrm{N}_{\mathrm{TE}}\omega\sin(k_x x)\begin{pmatrix}0\\k_z\\-k_y\end{pmatrix}\sin(\sigma-\Delta\sigma)\ . \tag{7.14}$$

In this case a redefinition of the parameter $\Delta\sigma = \left[\frac{h^{00}\frac{\omega^2}{c^2}+h^{11}k_x^2}{2k_x^2}-\frac{h^{20}k_y\frac{\omega}{c}}{k_x^2}\right]\sigma$ from (6.7) is necessary. Analogously, the renormalization parameter $\tilde{\lambda} = \left[\frac{h^{00}\frac{\omega^2}{c^2}+h^{11}k_x^2}{2k_x^2}-\frac{h^{20}k_y\frac{\omega}{c}}{k_x^2}\right]$ must be redefined. The renormalization process then stays unchanged compared to subsection 6.1.1. The dispersion relation reads

$$\omega(\mathbf{k}) = c|\mathbf{k}|\left(1-\frac{h^{00}}{2}-\frac{h^{11}}{2}\frac{k_x^2}{|\mathbf{k}|^2}+h^{20}\frac{k_y}{|\mathbf{k}|}\right)\ , \tag{7.15}$$

where $\frac{\omega}{c} = |\mathbf{k}|$ was used to cancel one $|\mathbf{k}|$ factor in the denominator related to the h^{20} element. Due to the „+“ sign in (7.15), it is suggestive to think that superluminal speed might appear. With respect to the „−“ sign of h^{20} itself, compared to (5.21), this is not the case as long as the Kerr Spin parameter a is positive. This corresponds to a counterclockwise rotation of the source of gravity, which transforms approximately into a clockwise rotation of the Casimir setup around a fixed source of weak gravity. However, there is an issue if the source of weak gravity would rotate clockwise because it is expected that the two rotation directions are energetically degenerate.

Analogously for the magnetic induction field, where again a case analysis is necessary, yields

$$\mathbf{B}_{\mathrm{tot},x} = -\mathrm{N}_{\mathrm{TE}}k_\perp^2\sin(k_x x)\{\sin(\sigma)\cos(\Delta\sigma)-\sin(\Delta\sigma)\cos(\sigma)\} \tag{7.16}$$

$$= -\mathrm{N}_{\mathrm{TE}}k_\perp^2\sin(k_x x)\sin(\sigma-\Delta\sigma)\ , \tag{7.17}$$

$$\mathbf{B}_{\text{tot},y,z} = -\mathrm{N}_{\mathrm{TE}} k_x k_{y,z} \cos(k_x x) \left\{ \cos(\sigma)\cos(\Delta\sigma) + \left[\frac{h^{00}\frac{\omega^2}{c^2} + h^{11}k_x^2}{2k_x^2} - \frac{h^{20}k_y\frac{\omega}{c}}{k_x^2} \right] [\sigma\sin(\sigma) + \cos(\sigma)] \right\} \tag{7.18}$$

$$\approx -\mathrm{N}_{\mathrm{TE}} k_x k_{y,z} \cos(k_x x) \Bigg\{ \cos(\sigma)\cos(\Delta\sigma) + \sin(\Delta\sigma)\sin(\sigma) \tag{7.19}$$

$$+ \left[\frac{h^{00}\frac{\omega^2}{c^2} + h^{11}k_x^2}{2k_x^2} - \frac{h^{20}k_y\frac{\omega}{c}}{k_x^2} \right] \cos(\sigma)\cos(\Delta\sigma) + \left[\frac{h^{00}\frac{\omega^2}{c^2} + h^{11}k_x^2}{2k_x^2} - \frac{h^{20}k_y\frac{\omega}{c}}{k_x^2} \right] \sin(\Delta\sigma)\sin(\sigma) \Bigg\} \tag{7.20}$$

$$= -\mathrm{N}_{\mathrm{TE}} k_x k_{y,z} \cos(k_x x) \left(1 + \frac{h^{00}\frac{\omega^2}{c^2} + h^{11}k_x^2}{2k_x^2} - \frac{h^{20}k_y\frac{\omega}{c}}{k_x^2} \right) \cos(\sigma - \Delta\sigma) \; . \tag{7.21}$$

Let us evaluate the Casimir energy for setup I, according to its dispersion relation in (7.15). The relevant term, which is new, reads

$$\omega^\star = h^{20} k_y \; . \tag{7.22}$$

The energy shift, according to (2.25), where the dispersion relation is replaced by the expression above, is given by

$$E_C^{h^{20}} = \hbar c A \left(\sum_{n=0}^{\infty}{}' - \int_0^\infty \mathrm{d}n \right) \int \frac{\mathrm{d}^2\mathbf{k}_\perp}{(2\pi)^2} \omega^\star \tag{7.23}$$

$$= \hbar c A \left(\sum_{n=0}^{\infty}{}' - \int_0^\infty \mathrm{d}n \right) \int \frac{\mathrm{d}k_y\,\mathrm{d}k_z}{(2\pi)^2} \left(h^{20} k_y \right) \; . \tag{7.24}$$

Recognize that the integrand is proportional to k_y, i.e., independent from y and z. Further, remember that $\left(\sum_{n=0}^{\infty}{}' - \int_0^\infty \mathrm{d}n\right)$ depends on the parameter n, that is connected to the longitudinal $\mathbf{k}$-vector component, in this case k_x. So, in (7.24) the difference of a series and an integral of a function, that is independent of exactly its parameter n, must be calculated. Using the APSF (2.27) and putting in $f(n) = 1$ leads to the result $C \in \mathbb{R}$ that can be freely choosen, due to the theorem of integral calculus and, consequently, the derivative of any real number vanishes. At exactly this point the APSF is not the best regularization method, although it was until now beyond doubt. It should be noted, that $0 \in \mathbb{R}$ is also allowed in the case of the APSF, what is the most obvious solution. To verify this assumption and knowing the result must stay unaffected by the concrete regularization method, also EMSF and PSF, mentioned in the appendix B are used. In the case of the EMSF (B.3) the derivatives of the integrand in (7.24) with respect to the parameter n must be calculated. And due to its independency the result is zero. Investigating the same issue with PSF (B.15), note that the function $f(n) = 1$ is even, in the corresponding calculation only a series starting from $n = 1$ over a delta function $\delta(n)$ appears. The result is $\sum_{n=1}\delta(n) = 0$, due to (B.19). Summarizing these three results the Casimir energy shift due to the slow rotation of the source of gravity is

$$E_C^{h^{20}} = 0 \; . \tag{7.25}$$

The rotation does not change the Casimir energy valid in Schwarzschild metric for setup I at all. The issue that this solution seems only being valid in the case the gravitating object rotates counterclockwise is not solved yet.

7.1.2. Transversal electric modes - Imaginary part

The TE modes are given by (2.11). Let us now assume the imaginary part instead of the real part to be the unperturbed solution. It is expected that this will coincide with the case where $h^{20} < 0$ and, due to the minus sign in the corresponding metric element (5.21), fits the case, where the gravitating object rotates counterclockwise $a > 0$.

The imaginary part of the zeroth-order of the magnetic field $\mathrm{Im}\{\mathbf{E}^{(0)}\}$, shortly denoted as $\mathbf{E}^{(0)}$ is given by

$$\mathbf{E}^{(0)} = -\mathrm{N}_{\mathrm{TE}} \begin{pmatrix} 0 \\ k_z \\ k_y \end{pmatrix} \omega \sin(k_x x) \cos(\sigma) \; . \tag{7.26}$$

The imaginary part of the zeroth-order magnetic induction field $\mathrm{Im}\{\mathbf{B}^{(0)}\}$, only called $\mathbf{B}^{(0)}$, reads

$$\mathbf{B}^{(0)} = \mathrm{N}_{\mathrm{TE}} \begin{pmatrix} k_\perp^2 \sin(k_x x) \cos(\sigma) \\ -k_x k_y \cos(k_x x) \sin(\sigma) \\ -k_x k_z \cos(k_x x) \sin(\sigma) \end{pmatrix} \; . \tag{7.27}$$

The Gauss' law is then represented by

$$\rho^{(1)} = -\varepsilon_0 \mathrm{N}_{\mathrm{TE}} h^{20} k_z \frac{\omega^2}{c} \sin(k_x x) \sin(\sigma) \; , \tag{7.28}$$

and Ampère's law via

$$\mathbf{j}^{(1)} = \frac{1}{\mu_0} \mathrm{N}_{\mathrm{TE}} \frac{\omega}{c} \begin{pmatrix} k_x k_z \cos(k_x x) \cos(\sigma) \\ k_y k_z \sin(k_x x) \sin(\sigma) \\ -\left(k_y^2 + k_\perp^2\right) \sin(k_x x) \sin(\sigma) \end{pmatrix} \; . \tag{7.29}$$

The corresponding wave equations are given by

$$\Box\mathbf{E}^{(1)} = 2\mathrm{N}_{\mathrm{TE}} h^{20} \frac{\omega^2}{c} k_y \begin{pmatrix} 0 \\ k_z \\ k_y \end{pmatrix} \sin(k_x x)\cos(\sigma) \;, \tag{7.30}$$

$$\Box\mathbf{B}^{(1)} = 2\mathrm{N}_{\mathrm{TE}} \frac{\omega}{c} h^{20} k_y \begin{pmatrix} k_\perp^2 \sin(k_x x)\cos(\sigma) \\ k_x k_y \cos(k_x x)\sin(\sigma) \\ k_x k_z \cos(k_x x)\sin(\sigma) \end{pmatrix} \;. \tag{7.31}$$

The corresponding solutions read

$$\mathbf{E}^{(1)} = \mathrm{N}_{\mathrm{TE}} h^{20} \frac{\omega^2}{c} \frac{k_y}{k_x^2} \begin{pmatrix} 0 \\ k_z \\ -k_y \end{pmatrix} \sin(k_x x)\sigma\sin(\sigma) \;, \tag{7.32}$$

$$\mathbf{B}^{(1)} = -\mathrm{N}_{\mathrm{TE}} \frac{\omega}{c} h^{20} \frac{k_y}{k_x^2} \begin{pmatrix} k_\perp^2 \sin(k_x x)\sigma\sin(\sigma) \\ k_y k_x \cos(k_x x)\sigma\cos(\sigma) \\ k_z k_x \cos(k_x x)\sigma\cos(\sigma) \end{pmatrix} \;. \tag{7.33}$$

Because of the consideration of only terms proportional to the metric entry $h^{20} = h^{02}$, the renormalization parameter must be changed to $\tilde{\lambda} = k_y \frac{\omega}{c} h^{20}$ and $\Delta\sigma = k_y \frac{\omega}{c} h^{20}\sigma$ accordingly.
The new perturbed electric field yields

$$\mathbf{E}_{\mathrm{TE}}^{\mathrm{curved}} = \mathrm{N}_{\mathrm{TE}} \begin{pmatrix} 0 \\ k_z \\ -k_y \end{pmatrix} \omega \sin(k_x x)\cos(\sigma + \Delta\sigma) \;. \tag{7.34}$$

The new perturbed magnetic induction field is represented by

$$\mathbf{B}_{\mathrm{TE}}^{\mathrm{curved}} = \mathrm{N}_{\mathrm{TE}} \begin{pmatrix} k_\perp^2 \sin(k_x x)\cos(\sigma + \Delta\sigma) \\ -k_x k_y \cos(k_x x)\sin(\sigma + \Delta\sigma) \\ -k_x k_z \cos(k_x x)\sin(\sigma + \Delta\sigma) \end{pmatrix} \;. \tag{7.35}$$

The big difference between these calculations and the ones before are the terms $\cos(\sigma + \Delta\sigma)$ and $\sin(\sigma + \Delta\sigma)$. These yield a dispersion relation related to the h^{20} metric entry, via

$$\omega(\mathbf{k}) = c|\mathbf{k}| \left(1 - h^{20}\frac{k_y}{|\mathbf{k}|}\right) . \tag{7.36}$$

Assuming that the dispersion relation associated with the h^{00} and h^{11} will not change, however, the real or the imaginary part will be taken into account, and the complete dispersion relation considering the metric entries as shown in (7.1), reads

$$\omega(\mathbf{k}) = c|\mathbf{k}| \left(1 - \frac{h^{00}}{2} - \frac{h^{11}}{2}\frac{k_x^2}{|\mathbf{k}|^2} - h^{20}\frac{k_y}{|\mathbf{k}|}\right) . \tag{7.37}$$

Comparing (7.15) and (7.37) shows that only the term proportional to the h^{20} shows different signs. Assuming that spacetime perturbed by weak gravity does not violate the maximum speed of electromagnetic waves in vacuum c leads to the condition

$$\omega(\mathbf{k}) = c|\mathbf{k}|X \leq c|\mathbf{k}| \Longrightarrow X \leq 1 , \tag{7.38}$$

where X denotes an arbitrary correction factor of the dispersion relation caused by weak gravity. Identify the terms in round brackets in (7.15) and (7.37) with the parameter X and consider (7.38) leads to two conditions:

1. For (7.15), calculated using the real part of the TE modes (2.11), where the h^{20} element has a plus sign, the element itself must be negative not to violate condition (7.38). According to the exact shape of the perturbed metric, given in (5.21), where a minus sign occurs in the metric element, the Kerr spin parameter a must be positive $a > 0$. Remind that this is true for all positive positions $x > 0$, especially the position (6.4), which is always assumed for the exact evaluation of the Casimir energy.

2. Analogously, the dispersion relation (7.37), which is generated using the imaginary part of the TE modes (2.11), leads to the condition that at position (6.4), the Kerr spin parameter a must be negative $a < 0$.

Note that such a more profound investigation was unnecessary for the h^{00} and h^{11} metric elements because these parameters are always positive according to (5.21) and occur with minus signs in the dispersion relation (6.35). Therefore condition (7.38) is always satisfied.

Summarizing the results of this and the previous subsection 7.1.1 yields the following statement in the framework of the SRA (3.49) for only assuming first-order terms in λ and a:
The rotational direction of the gravitational source does not change the Casimir energies of setup I shown in 1.5. However, the two directions are related to different components of the flat case solutions via the inhomogeneous wave equations (5.44). Namely, the clockwise rotation $a > 0$ is related to the real part, and the counterclockwise rotation $a < 0$ to the imaginary part.

7.2. Setup II

Setup II is unique because it is the setup whose surface normal of the plates is parallel to the rotation vector. The symmetry breaking the calculation without rotation showed that this is the setup where a change of the Casimir energy is expected.

Let us assume the dispersion relation for all three setups will coincide as it was in chapter 6. Then (7.15) would also describe the dispersion of setup II around a counterclockwise rotating source of weak gravity. The energy shift would be given by

$$E_C^{h^{20}} = \hbar c A \left(\sum_{n=0}^{\infty}{}' - \int_0^\infty \mathrm{d}n \right) \int \frac{\mathrm{d}^2\mathbf{k}_\perp}{(2\pi)^2} \left(h^{20} k_y\right) \tag{7.39}$$

$$= \hbar c A \left(\sum_{n=0}^{\infty}{}' - \int_0^\infty \mathrm{d}n \right) \int \frac{\mathrm{d}k_x\,\mathrm{d}k_z}{(2\pi)^2} \left(h^{20} k_y\right) \ . \tag{7.40}$$

This time, the $k_y = n\pi/d$ is the longitudinal component, and the integrand depends on the parameter n. Therefore, the regularization would not vanish in general, justifying a closer investigation. Putting together (6.82), (7.2) and (7.4) leads to

$$\rho^{(1)} = 0 \ , \tag{7.41}$$

$$\mathbf{j}^{(1)} = -\frac{1}{\mu_0} \mathrm{N_{TE}} 2h^{20} \frac{\omega}{c} k_y \begin{pmatrix} k_z \\ 0 \\ -k_x \end{pmatrix} \cos(k_y y)\sin(\sigma) \ , \tag{7.42}$$

and the wave equations

$$\Box \mathbf{E}^{(1)} = \mathrm{N_{TE}} 2h^{20} \frac{\omega^2}{c} k_y \begin{pmatrix} -k_z \\ 0 \\ k_x \end{pmatrix} \cos(k_y y)\cos(\sigma) \ , \tag{7.43}$$

$$\Box \mathbf{B}^{(1)} = -\mathrm{N_{TE}} 2h^{20} \frac{\omega}{c} k_y \begin{pmatrix} k_y k_x \sin(k_y y)\sin(\sigma) \\ k_\perp^2 \cos(k_y y)\cos(\sigma) \\ k_y k_z \sin(k_y y)\sin(\sigma) \end{pmatrix} \ . \tag{7.44}$$

The solutions are given by

$$\mathbf{E}^{(1)} = \mathrm{N}_{\mathrm{TE}}\omega \frac{h^{20} k_y \frac{\omega}{c}}{k_y^2} \begin{pmatrix} -k_z \\ 0 \\ k_x \end{pmatrix} \cos(k_y y)\sigma \sin(\sigma) \,, \tag{7.45}$$

$$\mathbf{B}^{(1)} = \mathrm{N}_{\mathrm{TE}} \frac{h^{20} k_y \frac{\omega}{c}}{k_y^2} \begin{pmatrix} \sin(k_y y)\sigma \cos(\sigma) \\ -\cos(k_y y)\left[\sigma \sin(\sigma) + \cos(\sigma)\right] \\ \sin(k_y y)\sigma \cos(\sigma) \end{pmatrix} . \tag{7.46}$$

Adding up the zeroth-order solution and the components related to the h^{00} and h^{11} elements (6.88) denoted as $\mathbf{E}^{(1)}_{h^{00},h^{11}}$ and the new solution (7.45) called $\mathbf{E}^{(1)}_{h^{20}}$ yields

$$\mathbf{E}^{\mathrm{curved}}_{\mathrm{tot}} \approx \mathbf{E}^{(0)} + \mathbf{E}^{(1)}_{h^{00},h^{11}} + \mathbf{E}^{(1)}_{h^{20}} \tag{7.47}$$

$$= \begin{pmatrix} -k_z \\ 0 \\ k_x \end{pmatrix} \mathrm{N}_{\mathrm{TE}}\omega \sin(k_y y)\sin(\sigma) \tag{7.48}$$

$$- \mathrm{N}_{\mathrm{TE}}\omega \begin{pmatrix} -k_z \\ 0 \\ k_x \end{pmatrix} \frac{h^{00}\frac{\omega^2}{c^2} + h^{11}k_x^2}{2k_y^2} \sin(k_y y)\sigma\cos(\sigma) + \mathrm{N}_{\mathrm{TE}}\omega \begin{pmatrix} -k_z \\ 0 \\ k_x \end{pmatrix} \frac{h^{20}k_y\frac{\omega}{c}}{k_y^2} \cos(k_y y)\sigma\sin(\sigma) \tag{7.49}$$

$$= \mathrm{N}_{\mathrm{TE}}\omega \begin{pmatrix} -k_z \\ 0 \\ k_x \end{pmatrix} \left\{ \sin(k_y y)\sin(\sigma) - \frac{h^{00}\frac{\omega^2}{c^2} + h^{11}k_x^2}{2k_y^2} \sin(k_y y)\sigma\cos(\sigma) + \frac{h^{20}k_y\frac{\omega}{c}}{k_y^2}\cos(k_y y)\sigma\sin(\sigma) \right\} . \tag{7.50}$$

Introducing the new parameters $\Delta\sigma_{h^{00},h^{11}}$, and $\Delta\sigma_{h^{20}}$ to respect the different smallness parameters and applying several Taylor series leads to

$$\begin{aligned} \mathbf{E}^{\mathrm{curved}}_{\mathrm{tot}} = \mathrm{N}_{\mathrm{TE}}\omega \begin{pmatrix} -k_z \\ 0 \\ k_x \end{pmatrix} \Big\{ &\sin(k_y y)\left[\sin(\sigma)\cos\left(\Delta\sigma_{h^{00},h^{11}}\right)\cos(\Delta\sigma_{h^{20}}) - \sin\left(\Delta\sigma_{h^{00},h^{11}}\right)\cos(\sigma)\cos(\Delta\sigma_{h^{20}})\right] \\ &+ \cos(k_y y)\sin(\Delta\sigma_{h^{20}})\sin(\sigma)\cos\left(\Delta\sigma_{h^{00},h^{11}}\right) \Big\} . \end{aligned} \tag{7.51}$$

The idea now is to combine half of the zeroth-order electric field with (6.88) and the other half with (7.45):

$$\mathbf{E}_{\text{tot}}^{\text{curved}} = \left(\frac{1}{2}\mathbf{E}^{(0)} + \mathbf{E}^{(1)}_{h^{00},h^{11}}\right) + \left(\frac{1}{2}\mathbf{E}^{(0)} + \mathbf{E}^{(1)}_{h^{20}}\right) \tag{7.52}$$

$$\begin{aligned} &= \frac{1}{4}\left[\cos\left(\sigma - \Delta\sigma_{h^{00},h^{11}} - k_y y\right) - \cos\left(\sigma - \Delta\sigma_{h^{00},h^{11}} + k_y y\right)\right] \\ &+ \frac{1}{4}\left[\cos(\sigma - \Delta\sigma_{h^{20}} - k_y y) - \cos(\sigma + \Delta\sigma_{h^{20}} + k_y y)\right] \ . \end{aligned} \tag{7.53}$$

For the renormalization process the variables $\tilde{\lambda}_{h^{00},h^{11}} = 2\frac{h^{00}\frac{\omega^2}{c^2}+h^{11}k_x^2}{2k_y^2}$ and $\tilde{\lambda}_{h^{20}} = 2\frac{h^{20}k_y\frac{\omega}{c}}{k_y^2}$ are sufficient to distinguish the four cases where $\sigma = k_x x + k_z z - \omega t$ is equal for all of them:

1. $\sigma - k_y y - \Delta\sigma_{h^{00},h^{11}} = \sigma\left(1 + \tilde{\lambda}_{h^{00},h^{11}}\right) - k_y y \stackrel{!}{=} k_x' x + k_y' y + k_z' - \omega' t$
   $\Longrightarrow k_x' = k_x\left(1 - \tilde{\lambda}_{h^{00},h^{11}}\right),\ k_y' = -k_y,\ k_z' = k_z\left(1 - \tilde{\lambda}_{h^{00},h^{11}}\right),\ \omega' = \omega\left(1 - \tilde{\lambda}_{h^{00},h^{11}}\right)$
   $\Longrightarrow \omega^{(1)} = -\frac{ck_y^2\tilde{\lambda}_{h^{00},h^{11}}}{\left|\mathbf{k}^{(0)}\right|}$

2. $\sigma + k_y y - \Delta\sigma_{h^{00},h^{11}} \stackrel{\text{analog}}{\Longrightarrow} \omega^{(1)} = -\frac{ck_y^2\tilde{\lambda}_{h^{00},h^{11}}}{\left|\mathbf{k}^{(0)}\right|}$
   The dispersion relation related to the h^{00} and h^{11} elements is two times the same because the dispersion relation is proportional to ${k_y'}^2$ and the difference in the minus sign for k_y' does not change anything. This would not lead to the same dispersion relation as predicted in (6.35). Considering the prefactor 1/4 and that two independent cos terms yield the same dispersion relation, a combined prefactor of 1/2 must be added to the current $\omega^{(1)}$, which agrees with (6.35).

3. $\sigma - \Delta\sigma_{h^{20}} - k_y y = \sigma\left(1 - \tilde{\lambda}_{h^{20}}\right) - k_y y \stackrel{!}{=} k_x' x + k_y' y + k_z' - \omega' t$
   $\Longrightarrow k_x' = k_x\left(1 - \tilde{\lambda}_{h^{20}}\right),\ k_y' = -k_y,\ k_z' = k_z\left(1 - \tilde{\lambda}_{h^{20}}\right),\ \omega' = \omega\left(1 - \tilde{\lambda}_{h^{20}}\right)$
   $\Longrightarrow \omega^{(1)} = -\frac{ck_y^2\tilde{\lambda}_{h^{20}}}{\left|\mathbf{k}^{(0)}\right|}$
   Considering the weighting factor 1/4 results in $\omega(\mathbf{k}) = c\left|\mathbf{k}^{(0)}\right|\left(1 - \frac{h^{20}k_y}{2\left|\mathbf{k}^{(0)}\right|}\right)$.

4. $\sigma - \Delta\sigma_{h^{20}} + k_y y = \sigma\left(1 + \tilde{\lambda}_{h^{20}}\right) - k_y y \stackrel{!}{=} k_x' x + k_y' y + k_z' - \omega' t$
   $\Longrightarrow k_x' = k_x\left(1 + \tilde{\lambda}_{h^{20}}\right),\ k_y' = -k_y,\ k_z' = k_z\left(1 + \tilde{\lambda}_{h^{20}}\right),\ \omega' = \omega\left(1 + \tilde{\lambda}_{h^{20}}\right)$
   $\Longrightarrow \omega^{(1)} = +\frac{ck_y^2\tilde{\lambda}_{h^{20}}}{\left|\mathbf{k}^{(0)}\right|}$
   Considering the weighting factor 1/4 results in $\omega(\mathbf{k}) = c\left|\mathbf{k}^{(0)}\right|\left(1 + \frac{h^{20}k_y}{2\left|\mathbf{k}^{(0)}\right|}\right)$.
   This time the dispersion relations related to the h^{20} metric entry are not identical. Hence, condition (7.38) must not be violated both solutions must be identified with different $h^{20} \propto a$ Kerr spin parameters, namely different rotation directions of the source of gravity. The Casimir energy does not change due to the rotation direction since the correction's absolute value is the same.

Due to the different dispersion relations under points 3 and 4, there is no unique renormalized dispersion relation for both rotation directions simultaneously. This reveals the question of what happens in this case and why the tools, which worked well in other cases, fail here? Following the idea that considering the imaginary part could solve this problem reveals the next issue because the part related to the h^{20} element in (7.53) yields instead

$$\frac{1}{4}\left[\sin(\sigma+\Delta\sigma+k_y y)+\sin(-\sigma+\Delta\sigma+k_y y)\right] \ . \tag{7.54}$$

Therefore, the same issue that different renormalized angular frequencies occur arises. Thus, we conclude that setup II is not solved yet, and due to the lack of time, a detailed investigation is not possible. Either there is an issue in the perturbation theory approach itself. Maybe applying the Poincaré–Lindstedt method to a partial differential equation is not allowed any time. Alternatively, something is not considered that makes setup II fundamentally different from the other setups.

7.3. Setup III

In this section setup III from figure 1.5 is calculated using the metric (7.1). The calculation is completely analogous to the one in section 7.1.

Putting (6.139) into (7.2) and (7.4) leads to

$$\rho^{(1)} = \varepsilon_0 \mathrm{N}_{\mathrm{TE}} \frac{\omega^2}{c} h^{20} k_x \sin(k_z z)\cos(\sigma) \ , \tag{7.55}$$

$$\mathbf{j}^{(1)} = -\frac{1}{\mu_0}\mathrm{N}_{\mathrm{TE}}\frac{\omega^2}{c}h^{20}\begin{pmatrix} -\frac{\omega^2}{c^2}\sin(k_z z)\cos(\sigma) \\ k_x k_y \sin(k_z z)\cos(\sigma) \\ -k_x k_z \cos(k_z z)\sin(\sigma)\end{pmatrix} \ . \tag{7.56}$$

The wave equations read

$$\Box\mathbf{E}^{(1)} = \mathrm{N}_{\mathrm{TE}}\omega\left(-2k_y h^{20}\frac{\omega}{c}\right)\begin{pmatrix} k_y \\ -k_x \\ 0\end{pmatrix}\sin(k_z z)\sin(\sigma) \ , \tag{7.57}$$

$$\Box\mathbf{B}^{(1)} = \mathrm{N}_{\mathrm{TE}}\left(2k_y h^{20}\frac{\omega}{c}\right)\begin{pmatrix} k_x k_z\cos(k_z z)\cos(\sigma) \\ k_y k_z \cos(k_z z)\cos(\sigma) \\ k_\perp^2 \sin(k_z z)\sin(\sigma)\end{pmatrix} \tag{7.58}$$

with the solutions

$$\mathbf{E}^{(1)} = \mathrm{N}_{\mathrm{TE}}\omega \frac{h^{20} k_y \frac{\omega}{c}}{k_z^2} \begin{pmatrix} k_y \\ -k_x \\ 0 \end{pmatrix} \sin(k_z z)\sin(\sigma) \ , \tag{7.59}$$

$$\mathbf{B}^{(1)} = -\mathrm{N}_{\mathrm{TE}} \frac{h^{20} k_y \frac{\omega}{c}}{k_z^2} \begin{pmatrix} -k_x k_z \cos(k_z z)\left[\sigma\sin(\sigma) + \cos(\sigma)\right] \\ -k_y k_z \cos(k_z z)\left[\sigma\sin(\sigma) + \cos(\sigma)\right] \\ k_\perp^2 \sin(k_z z)\sigma\cos(\sigma) \end{pmatrix} . \tag{7.60}$$

Adding up all solutions for the zeroth-order (6.139) and those related to the h^{00} and h^{11} elements (6.145) and the new result according to the h^{20} element (7.59) yields

$$\mathbf{E}_{\mathrm{tot}}^{\mathrm{curved}} = \mathrm{N}_{\mathrm{TE}}\omega\sin(k_z z) \begin{pmatrix} k_y \\ -k_x \\ 0 \end{pmatrix} \left\{ \sin(\sigma) - \frac{h^{00}\frac{\omega^2}{c^2} + h^{11}k_x^2}{2k_z^2}\sigma\cos(\sigma) + \frac{h^{20}k_y\frac{\omega}{c}}{k_z^2}\sigma\cos(\sigma) \right\} \tag{7.61}$$

$$= \mathrm{N}_{\mathrm{TE}}\omega\sin(k_z z) \begin{pmatrix} k_y \\ -k_x \\ 0 \end{pmatrix} \left\{ \sin(\sigma)\cos(\sigma) - \sin(\Delta\sigma)\cos(\sigma) \right\} \tag{7.62}$$

$$= \mathrm{N}_{\mathrm{TE}}\omega\sin(k_z z) \begin{pmatrix} k_y \\ -k_x \\ 0 \end{pmatrix} \sin(\sigma - \Delta\sigma) \ . \tag{7.63}$$

Similar for the magnetic induction field using (6.139), (6.145) and (7.59) leads to

$$\mathbf{B}_{\mathrm{tot},z}^{\mathrm{curved}} = \mathrm{N}_{\mathrm{TE}}k_\perp^2\sin(k_z z) \left\{ -\sin(\sigma) + \frac{h^{00}\frac{\omega^2}{c^2} + h^{11}k_x^2}{2k_z^2}\sigma\cos(\sigma) - \frac{h^{20}k_y\frac{\omega}{c}}{k_z^2}\sigma\cos(\sigma) \right\} \tag{7.64}$$

$$\approx \mathrm{N}_{\mathrm{TE}}k_\perp^2\sin(k_z z)\left\{ -\sin(\sigma)\cos(\Delta\sigma) + \sin(\Delta\sigma)\cos(\sigma) \right\} \tag{7.65}$$

$$= -\mathrm{N}_{\mathrm{TE}}k_\perp^2\sin(k_z z)\sin(\sigma - \Delta\sigma) \ , \tag{7.66}$$

$$\mathbf{B}^{\text{curved}}_{\text{tot},x,y} = -\mathrm{N}_{\mathrm{TE}} k_{x,y} k_z \cos(k_z z) \left\{ \cos(\sigma) + \left(\frac{h^{00}\frac{\omega^2}{c^2} + h^{11}k_x^2}{2k_z^2} - \frac{h^{20}k_y\frac{\omega}{c}}{k_z^2} \right) [\sigma \sin(\sigma) + \cos(\sigma)] \right\} \tag{7.67}$$

$$\approx -\mathrm{N}_{\mathrm{TE}} k_{x,y} k_z \cos(k_z z) \Bigg\{ \cos(\sigma)\cos(\Delta\sigma) + \sin(\sigma)\sin(\Delta\sigma) \tag{7.68}$$

$$+ \left(\frac{h^{00}\frac{\omega^2}{c^2} + h^{11}k_x^2}{2k_z^2} - \frac{h^{20}k_y\frac{\omega}{c}}{k_z^2} \right) \cos(\sigma)\cos(\Delta\sigma) + \left(\frac{h^{00}\frac{\omega^2}{c^2} + h^{11}k_x^2}{2k_z^2} - \frac{h^{20}k_y\frac{\omega}{c}}{k_z^2} \right) \sin(\sigma)\sin(\Delta\sigma) \Bigg\} \tag{7.69}$$

$$= -\mathrm{N}_{\mathrm{TE}} k_{x,y} k_x \cos(k_z z) \left(1 + \frac{h^{00}\frac{\omega^2}{c^2} + h^{11}k_x^2}{2k_z^2} - \frac{h^{20}k_y\frac{\omega}{c}}{k_z^2} \right) \cos(\sigma - \Delta\sigma) \; . \tag{7.70}$$

This produces the same dispersion relation as for the electric field and, in particular, coincides with the dispersion relation (7.15) for setup I.
The Casimir energy shift is calculated by

$$E_C^{h^{20}} = \hbar c A \left(\sum_{n=0}^{\infty}{}' - \int_0^{\infty} \mathrm{d}n \right) \int \frac{\mathrm{d}^2\mathbf{k}_\perp}{(2\pi)^2} \left(h^{20} k_y \right) \tag{7.71}$$

$$= \hbar c A \left(\sum_{n=0}^{\infty}{}' - \int_0^{\infty} \mathrm{d}n \right) \int \frac{\mathrm{d}k_x\,\mathrm{d}k_y}{(2\pi)^2} \left(h^{20} k_y \right) \tag{7.72}$$

$$= 0 \; . \tag{7.73}$$

As already seen in section 7.1, the integrand is independent of the parameter $n \propto k_z$, and with the same arguments as given for setup I, the result is zero. So, even setup III stays utterly unaffected by slow rotations.

Finally, there should be something said about the other rotation direction. As already provided for setup I in subsection 7.1.2, the imaginary part should lead to a correct solution for the other rotation direction. By constructing the unperturbed electric field and the unperturbed magnetic induction field via a shift of indices, clear evidence is given. Moreover, the property that the k_y wave vector component is not related to the parameter $n \propto k_z$, which yields a zero for the distribution $E_C^{h^{20}}$ of the Casimir energy, verifies this assumption. A straightforward calculation can also check it. Thus, setup III has the same dispersion relations in the SRA as setup I (7.15) and (7.37), which can be summarized to

$$\omega(\mathbf{k}) = \begin{cases} c|\mathbf{k}| \left(1 - \frac{h^{00}}{2} - \frac{h^{11}}{2}\frac{k_x^2}{|\mathbf{k}|^2} - h^{20}\frac{k_y}{|\mathbf{k}|} \right) & \text{for } a < 0 \; , \\ c|\mathbf{k}| \left(1 - \frac{h^{00}}{2} - \frac{h^{11}}{2}\frac{k_x^2}{|\mathbf{k}|^2} + h^{20}\frac{k_y}{|\mathbf{k}|} \right) & \text{for } a > 0 \; . \end{cases} \tag{7.74}$$

7.4. Overview

This chapter summarizes the results of sections 7.1 – 7.3 and completes the results obtained in sections 6.1 – 6.3 for a slowly rotating source of weak gravity.

First, the perturbative approach already used in chapter 6 is successfully applied to setup I for small angular momentum. As a result, the Casimir energy of setup I close to a slowly rotating source of weak gravity does not differ from the one next to a non-rotating source of weak gravity, see figure 7.1. This coincides with the result obtained by a Klein-Gordon theory approach [3].

Second, it appears that the two rotation directions of the source of weak gravity are related to different parts of the complex solution in the flat case, namely the real and imaginary parts of the TE modes (2.11) and TM modes (2.13). This fact did not appear in the case of a non-rotating source of weak gravity, see chapter 6. However, it is assumed that real and imaginary solutions lead to the same results in these cases. Subsequently, calculations using the whole complex form of the TE and TM modes would have made more sense. Since there were initially major problems in solving the corresponding inhomogeneous wave equations (5.44), the split-up into real and imaginary parts was applied. In the end, the dispersion relation valid for setup I is given by (7.74), which means that the Casimir energy does not depend on the rotation direction and superluminal speed does not occur.

Third, an analog calculation yields the new result that setup III behaves identically to setup I. There is no energy shift due to small angular momentum, see figure 7.1. Heuristically, this can be explained via the directions of the azimuthal rotation of the source of weak gravity and the perpendicular surface normal of setups I and III, see figure 1.5.

Fourth, the same method is applied to setup II impressively demonstrates the limitations of this approach. Whether using the real or imaginary part does not lead to a unique dispersion relation. Nevertheless, because this setup's surface normal is parallel to the rotation direction, it is expected that there will occur an energy shift, see figure 7.1. At the moment, it is unclear how large this shift will be and how the technical issues to determine can be solved. Maybe a transformation into the rotating reference system provides a possible solution to this issue.

Table 7.1 shows the corresponding Casimir energies and forces term by term.

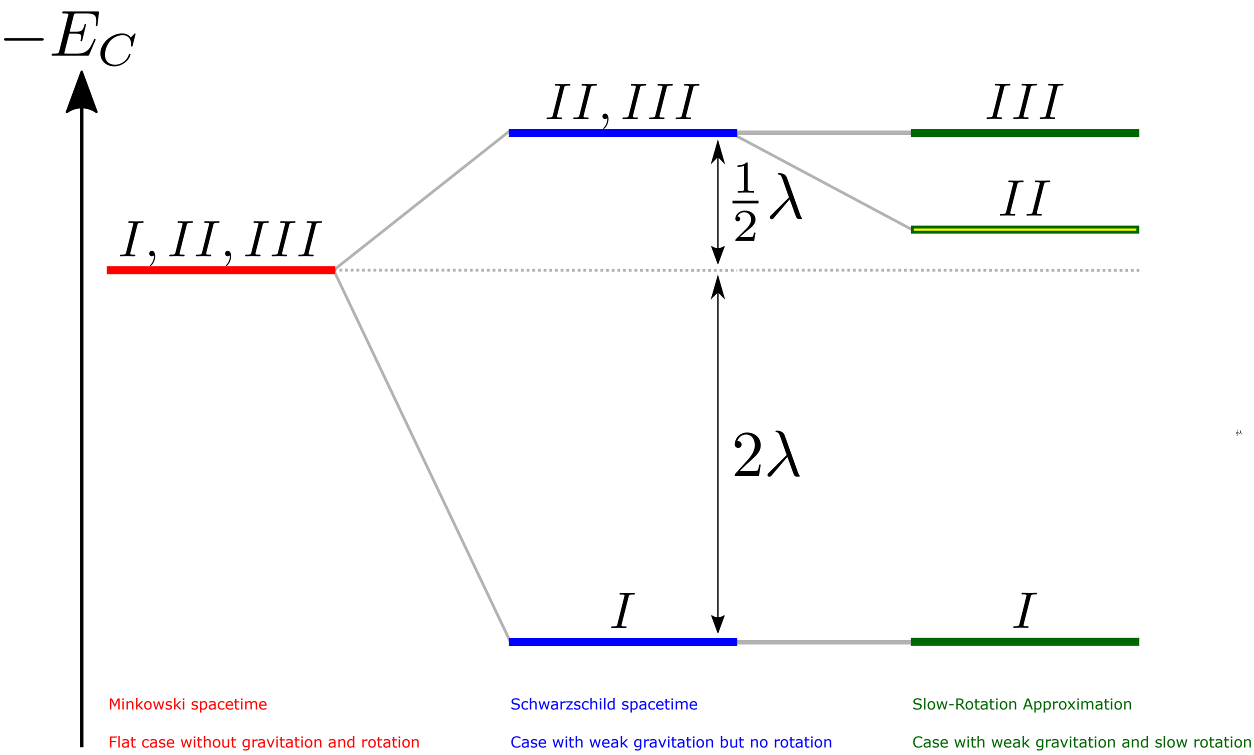

Figure 7.1.: *Energy splitting for the three Casimir settings introduced in figure 1.5 in the Slow-Rotation Approximation (3.49) with a small Kerr spin parameter a. The red line denotes the Casimir energy in Minkowski spacetime. Setups I and III do not change their Casimir energy compared to the case without a small angular momentum. The calculation for setup II failed why it has a yellow center, indicated by a yellow line, showing that a finite energy shift is expected but it is unclear what it looks like. The figure is not to scale.*

Table 7.1.: *Casimir energies and forces for three setups in the Slow-Rotation Approximation (SRA) with respect to the provided parameters. For setup II the calculation failed and the according, unknown correction are denoted by „?“ for the sake of completeness.*

Quantities	I 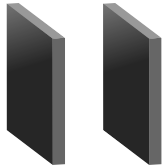	II 	III 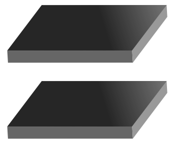
E_C^{flat}	$-\frac{\pi^2\hbar c A}{720d^3}$	$-\frac{\pi^2\hbar c A}{720d^3}$	$-\frac{\pi^2\hbar c A}{720d^3}$
$E_C^{h^{00}}$	$E_C^{\text{flat}}\left(1-\frac{h^{00}}{2}\right)$	$E_C^{\text{flat}}\left(1-\frac{h_{11}}{2}\right)\left(1-\frac{h^{00}}{2}\right)$	$E_C^{\text{flat}}\left(1-\frac{h_{11}}{2}\right)\left(1-\frac{h^{00}}{2}\right)$
$E_C^{h^{11}}$	$E_C^{\text{flat}}\left(1-\frac{3h^{11}}{2}\right)$	$E_C^{\text{flat}}\left(1-\frac{h_{11}}{2}\right)\left(1+\frac{h^{11}}{2}\right)$	$E_C^{\text{flat}}\left(1-\frac{h_{11}}{2}\right)\left(1+\frac{h^{11}}{2}\right)$
$E_C^{h^{20}}$	E_C^{flat}	**?**	$E_C^{\text{flat}}\left(1-\frac{h_{11}}{2}\right)$
$E_C^{\text{curved}} = E_C^{h^{00}} + E_C^{h^{11}} + E_C^{h^{20}}$	$E_C^{\text{flat}}\left[1-\frac{1}{2}\left(h^{00}+3h^{11}\right)\right]$	$E_C^{\text{flat}}\left(1-\frac{h_{11}}{2}\right)\left[1-\frac{1}{2}\left(h^{00}-h^{11}\right)\right]+\mathbf{?}$	$E_C^{\text{flat}}\left(1-\frac{h_{11}}{2}\right)\left[1-\frac{1}{2}\left(h^{00}-h^{11}\right)\right]$
$F_C^{\text{curved}} = -\frac{\partial E_C^{\text{curved}}}{\partial d}$	$F_C^{\text{flat}}\left[1-\frac{1}{2}\left(h^{00}+3h^{11}\right)\right]$	$F_C^{\text{flat}}\left(1-\frac{h_{11}}{2}\right)\left[1-\frac{1}{2}\left(h^{00}-h^{11}\right)\right]+\mathbf{?}$	$F_C^{\text{flat}}\left(1-\frac{h_{11}}{2}\right)\left[1-\frac{1}{2}\left(h^{00}-h^{11}\right)\right]$
$E_C^{\text{curved}}\left(h^{00}=h^{11}=\lambda, h^{20}\right)$	$E_C^{\text{flat}}\left(1-2\lambda\right) \neq E_C^{\text{flat}}(d_p, A_p)$	$E_C^{\text{flat}}\left(1+\frac{\lambda}{2}\right)+\mathbf{?}$	$E_C^{\text{flat}}\left(1+\frac{\lambda}{2}\right) = E_C^{\text{flat}}(d_p, A_p)$
$F_C^{\text{curved}}\left(h^{00}=h^{11}=\lambda\right)$	$F_C^{\text{flat}}\left(1-2\lambda\right) = F_C^{\text{flat}}(d_p, A_p)$	$F_C^{\text{flat}}\left(1+\frac{\lambda}{2}\right) = F_C^{\text{flat}}(d_p, A_p)+\mathbf{?}$	$F_C^{\text{flat}}\left(1+\frac{\lambda}{2}\right) = F_C^{\text{flat}}(d_p, A_p)$

8. Conclusion

The starting point of this thesis is investigating the Casimir effect in the regime of weak gravity to understand better how gravity influences a quantum-electrodynamical effect. The Casimir effect was chosen because it is already well understood in the absence of gravity and because precise measurement data are available. In addition, it is a multidisciplinary topic that already finds extensive technological application in the realm of microtechnology. Inspired by previous investigations using the scalar Klein-Gordon theory, this work's approach applies time-independent perturbation theory to solve the vectorial Maxwell equations in the presence of weak gravity. It is supplemented by a Poincaré-Lindstedt method for solving the corresponding partial differential equations without violating energy conservation.

Since such an approach has not yet been attempted, all relevant quantities and equations are decomposed into a flat part plus first-order perturbations. The metric used in this thesis is referred to as the Slow-Rotation Approximation (SRA) (3.49) because it reduces to the Schwarzschild metric if the Kerr spin parameter a vanishes. To utilize the weak gravity limit, the smallness parameter $\lambda = r_s/r$, describing the ratio of the event horizon to the distance to the center of mass, is introduced. If the Casimir setup is far from the center of mass, this parameter is small, and a perturbative approach yields meaningful results. For several objects in our solar system, the smallness parameter is shown in table 5.1. From this and the current measurement accuracy, the effects should be measurable within the solar system.

A mathematical peculiarity is the expansion of the determinant, which occurs in the corresponding equations, of the expanded metric $g_{\mu\nu} = \eta_{\mu\nu} + h_{\mu\nu}$, which is achieved by the use of elementary symmetric functions, see section 5.1 and appendix C. The corresponding expansion of Maxwell's equations in curved spacetime can be found in section 5.2 and reveals the structure typical for any perturbative approach: The first order correction of the electromagnetic field is determined by Gauss' and Ampère's law, with inhomogeneities given by the zeroth order. The corresponding particular solutions turn out to be relevant for a renormalization of the dispersion of electromagnetic waves. The physical meaningfulness of the first-order charge and current density are underpinned for any constant perturbation metric $h_{\mu\nu}$ in section 5.3. Thus, these quantities could be measured to verify this theoretical approach experimentally.

In order to ensure the broadest possible applicability, a generic metric (7.1) and three different setups, which are energetically degenerate in a Minkowski spacetime, see figure 1.5, are considered. Solving the upcoming partial differential equations and performing a renormalization of the dispersion as is detailed in section 6.1 yields tables 6.1 and 6.2, showing all results. It is noticeable that both zeroth-order solutions, namely the transversal electric modes (2.11) and the transversal magnetic modes, yield the same dispersion relation. Specializing the results for the Schwarzschild metric (3.43) yields the same replacement rule already shown by the Klein-Gordon theory [39, 47]: The Casimir force in curved spacetime is approximately given by using the formula of the flat case

(1.4) and by replacing all Minkowskian lengths by their general relativistic counterparts, namely the plate distance $d \to d_p$ and the surface area $A \to A_p$. Contrary to previous investigations, this rule applies not only to setup I but also to setups II and III, see table 6.3. The most significant difference to the results achieved by the Klein-Gordon theory is the appearance of a missing prefactor 2 in the Casimir energy and force, which corresponds to the two polarization directions of electromagnetic waves, as discussed in chapter 1.

Furthermore, comparing different orientations of the Casimir effect has not yet been performed in the literature. Consequently, also the associated dispersion relations have not yet been considered. But even more impressive is that one dispersion relation is valid for all three setups. The analysis provided in section 6.4 shows that the influence of weak gravity can effectively be implemented into the Minkowski metric by replacing the isotropic vacuum with an anisotropic medium, which satisfies (6.35), and considering the first-order charge and current densities, which generally do not vanish either on or between the plates. The fundamental difference between setup I and the other two can be seen by the corresponding anisotropies and, even more precisely, in their Casimir energies and forces.

The main achievement of this thesis is that gravity leads to symmetry breaking, which lifts the degeneracy of the three setups in Minkowski spacetime, see figure 6.7. The corresponding energy shifts differ essentially between setup I and the other two. Thus, the Casimir force in the first arrangement is weaker, while that of arrangements II and III is stronger than in the flat case. A phenomenological explanation for this circumstance is that for setup I, the surface normal and the gravitational force are parallel, whereas these quantities are perpendicular for setups II and III.

Thus, new possibilities for measuring the gravitational affected Casimir force are available. In section 6.6, two different types of measurements are suggested. The first is based on comparing two different setups, namely setup I and II, at the same position in spacetime. The second one focuses on comparing the same setup at different locations in spacetime, which corresponds to comparing the Casimir force with and without gravitational influence. Additionally, isolating energy shifts due to gravity from thermal noise and further perturbations, both methods are suitable to show experimental evidence of the gravitational effect with today's technical opportunities.

A first extension of the existing model is to allow the source of weak gravity to rotate slowly. An investigation via Klein-Gordon theory showed that setup I does not change its Casimir energy compared to the case without rotation [3]. This could be verified in section 7.1 and generalized to setup III in section 7.3. Heuristically, this can be understood by comparing the orientation of the rotation plane along the azimuthal unit vector and the surface normal of the Casimir setup, see figure 1.5. This time these quantities are parallel in setup II but perpendicular to the other two.

Since the results of the approach shown here agree widely with those of the Klein-Gordon theory, it can be claimed that within the framework of this thesis, a new approach for calculating the Casimir effect in the case of weak gravity has been successfully established.

9. Outlook

This thesis investigated the impact of weak gravity upon the Casimir effect using a perturbation theory approach. This is not an accurate description for obvious reasons, which is why the existing model can be easily extended. In particular, the dilemma that the calculated effect is so small makes it difficult to measure. Therefore, in the following, some extensions will present that aim to understand the Casimir effect more rigidly and simplify its measurability.

9.1. Second-order correction

From a theoretical point of view, it is interesting to calculate the second-order correction corresponding to stronger gravitational fields. The previous ansatz (5.1) must be expanded by

$$g^{\mu\nu} = \eta^{\mu\nu} + h^{(1)\mu\nu} + h^{(2)\mu\nu} \ , \tag{9.1}$$

$$h^{(1)\mu\nu} \propto \lambda \ , \ h^{(2)\mu\nu} \propto \lambda^2 \ , \tag{9.2}$$

$$\lambda = \frac{r_s}{r} \ll 1 \ . \tag{9.3}$$

This could lead to several new effects:

1. It would be possible that the degeneracy of the three setups will get completely broken, meaning that all three setups shown in figure 1.5 will have a different Casimir energy considering gravity. In the first order, setups II and III still showed degenerate Casimir energies, see figure 6.7

2. It may be possible that the dispersion relation 6.35, which is the same for all three setups next to a non-rotating gravitation source, might differ for each setup.

3. It is also feasible that the TE (2.11) and TM modes (2.13) will contribute differently to the Casimir energy.

What will happen is hard to predict because of the complex structure of Gauss' law (5.40) and Ampère's law (5.42), even in the vacuum case. In principle, it would be worth investigating which additional effects will occur. However, one must remember that the results of a perturbation theory are not analytically exact, and these effects might not be measurable today due to the smallness of λ, see table 5.1.

9.2. Dispersion relation

Unfortunately, the dispersion relation was not investigated by Klein-Gordon calculations [3, 39, 47]. It would be insightful to have a more general expression for particles with mass at hand. That

should lead to the flat case Casimir energy in the non-relativistic limit and the results provided by this thesis in the limiting case of vanishing rest mass.
Does this dispersion relation for the Klein-Gordon theory also show the anisotropy discussed in section 6.4? Do they also have an issue calculating the Casimir force for setup II in the case of a Slow-Rotation Approximation?
At the moment, even the investigations with the Klein-Gordon theory are incomplete. This thesis should be a thought-provoking impulse to first get an overview of the probably occurring phenomena with more common, scalar methods before one uses vectorial ones in the form of Maxwell's equations. This would also simplify the search for the possible error or inconsistency in the case of setup II in Slow-Rotation Approximation dealt with in section 7.2.

Based on the idea of comparing the results gained by Klein-Gordon theory and Maxwell's theory, there occurs the fascinating question, whether the gravitational correction term of the Casimir energy depends on the spin in general.
The Proca theory belongs to the standard model and generalizes Maxwell's theory for massive spin one particles, i.g. the photons, to massive spin one particles, i.e. the Z^0 and the $W^{\pm}$ bosons [19]. Thus, it is closely related to Maxwell's equations and contains, in addition, a mass term. Calculating the dispersion relation for the massive theories of both Klein-Gordon and Proca, it could either occur that they coincide and there is no dependency on the spin, or they differ from each other, and the gravitational correction is spin-dependent. However, this would be a fundamental finding, which could potentially explain the issue in section 7.2.

9.3. Lifshitz theory

The Lifschitz theory generalizes the simple Casimir effect to the force of two opposing dielectric matter blocks with plane-parallel surfaces [32]. Hence, the modeling of real materials is possible too. Repulsive forces can occur if the permittivities of the plates ε_1, ε_2, and of the fluid between the plates ε_3 fulfill $\varepsilon_1 > \varepsilon_3 > \varepsilon_2$ [48]; see figure 9.1. For experimental data to have a sufficiently high agreement with the theoretically predicted Casimir energy, including these corrections, is mandatory [32], which also requires complete knowledge of the optical properties of the chosen plate materials. Some experimental breakthroughs based on the Lifshitz theory are shown in figure 9.2, denoted as effects of dielectric response. Furthermore, Lifshitz was already aware that such experiments often happen at room temperature $T \approx 300$ K, so the influence of temperature on the Casimir energy would have to be included. However, the formula he derived was only an approximation, as it turned out later [5, 32].

9.4. Finite temperature

Until now, there was always the assumption that the temperature is set to $T = 0$, but this is not true for most experiments since they occur at room temperature [17, 30, 48]. Using a temperature-dependent Green's function, it is at least possible for the generic Casimir effect to give a general expression for arbitrary temperatures [5, eq. (2.10b)]. Two relevant special cases can be derived from this: One for low temperatures $k_B T \ll \hbar c/4\pi d$

$$F_C(T) = -\frac{\pi^2 A\hbar c}{240 d^4}\left[1 + \frac{16}{3}\left(\frac{k_B T d}{\hbar c}\right)^4 - \frac{240 k_B T d}{\pi\hbar c}\exp\left(-\frac{\pi\hbar c}{k_B T d}\right)\right] \tag{9.4}$$

and another one for high temperatures, which is irrelevant in the sense of astrophysical temperatures around $T \approx 2.7$ K [14]. Indeed, the estimate

$$T \approx 2.7 \text{ K} \ll \left.\frac{\hbar c}{4\pi k_B d}\right|_{d=1\mu\text{m}} \approx 182.3\text{K} \tag{9.5}$$

is satisfied assuming a Casimir setup in the interstellar medium with a plate distance $d = 1$ μm. For $T = 2.7$ K, the temperature correction (9.4) is of the order $10^{-11} \cdot F_C(T = 0)$ for plates distanced by $d = 1\mu$m. This correction is much smaller than the gravitational one related to objects in our solar system, see table 5.1. This is excellent news because „all present experiments agree well with the zero-temperature Casimir theory when surface roughness and finite conductivity corrections are included“ [5]. Remember, for all three setups provided in figure 1.5, the main result is that the gravitational effect can be considered by replacing the distance d with the proper distance d_p. Carrying out measurements at different temperatures in a gravitational field and comparing the qualitative course of the measurements with the theoretical curve given by (9.4), it would be possible to give first evidence that this substitution rule is generally valid even at finite temperatures.

9.5. Other geometries

Today the proximity force approximation is widely used to generalize the simple Casimir effect of two plane-parallel plates to other smooth geometries [16]. One example is the derivation of the Casimir energy of the plane-sphere geometry (1.5) already mentioned in chapter 1 because it is the setup best suited for experiments or technological applications; see figures 1.2 and 1.3. So it would be obvious to calculate the corrections of gravitation for different geometries of the Casimir plates. For a spherical geometry, the zeroth-order solutions will probably already be more complicated than for two plane-parallel plates. Since this thesis showed that the gravitational corrections only become noticeable along the x-axis, it would be exciting to see what proportion of these corrections would become noticeable with tilted plates. This would be a straightforward extension of the existing theory but could have many applications, especially since tilted plates, as shown in figure 9.1, provide an additional degree of freedom that experimenters can tweak.
Another interesting hypothesis would be: Is the substitution rule in first-order perturbation theory, that all Minkowskian lengths must be replaced by proper lengths, valid for other geometries? If so, what is the general idea behind that fact?
Some experimental breakthroughs based on the Casimir geometry are shown in figure 9.2.

9.6. More complex orbits

The previous calculations do not consider realizable experimental setups. The Casimir energy was calculated for the case of non-moving or only slow-rotating setups. The second case can be identified as being in a circular orbit around the source of gravity, but this is only an approximation even

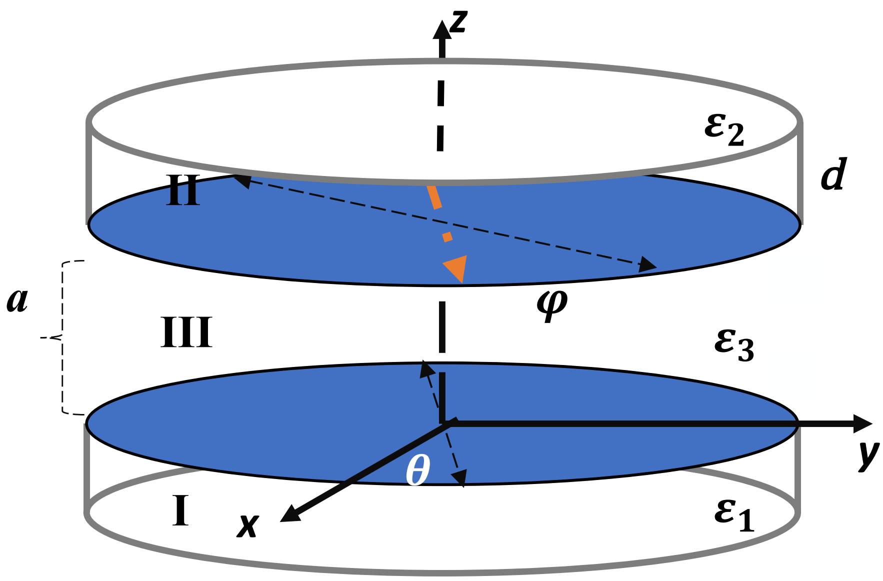

Figure 9.1.: *Casimir effect using two opposing disks of thickness d. The lower plate is pivoted and can be tilted relative to the upper plate. The distance between the disks a is much smaller than all other lengths. Additionally, three different permittivities, ε_1 describing the material at the bottom disk, ε_2 characterizing the material at the upper disk, and ε_3 for the medium between the plates, are considered. The thickness of the plates (grey) is also mentioned. The figure is not to scale [34].*

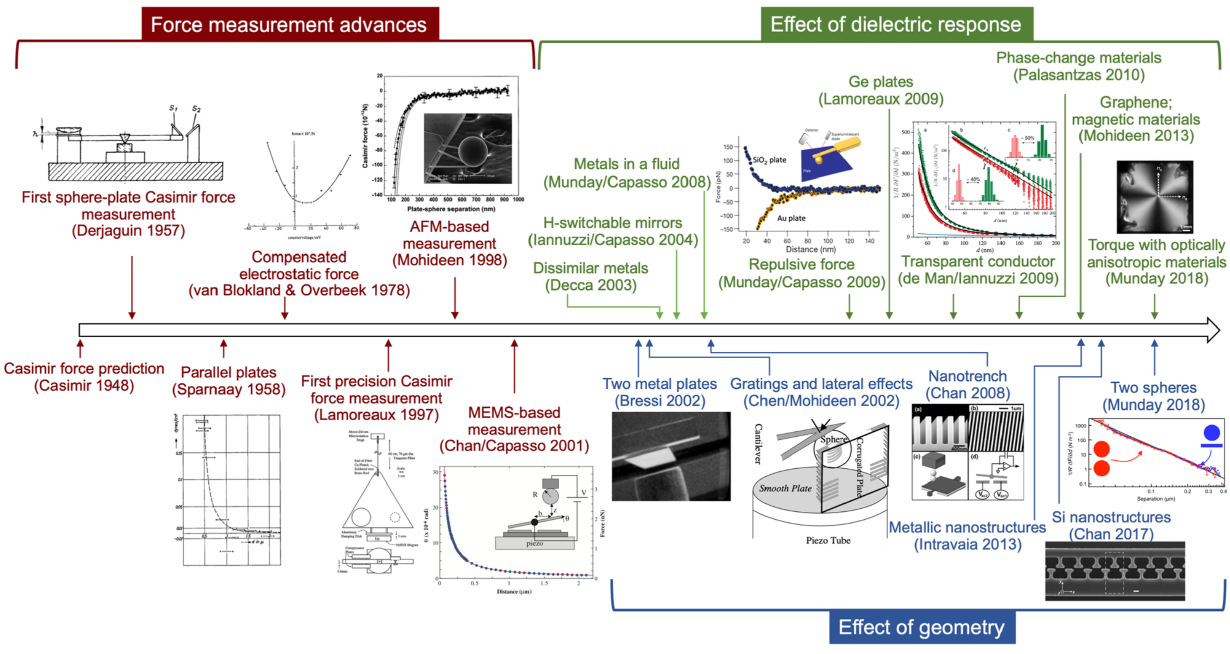

Figure 9.2.: *Some breakthroughs in measuring the Casimir effect in history, taking into account dielectric response and geometry that modify the interaction behavior [17].*

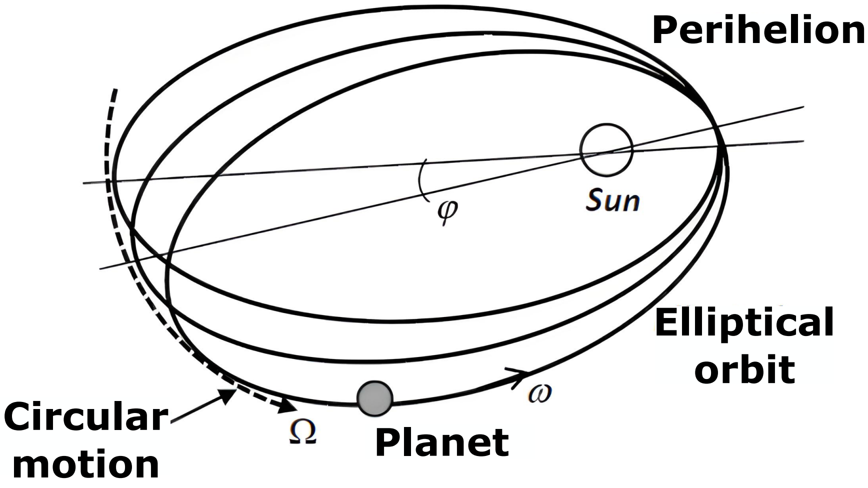

Figure 9.3.: *Mercury's perihelion shift is schematically illustrated in a rotating reference frame with angular velocity Ω [11, Resolution subsequently improved].*

for measurements on the Earth since the Earth's orbit is elliptical. For small eccentricities ε, it is reasonable to approximate the orbit by a circular one. That is why the statements made for measurements on Earth in section 6.6 are mostly correct. Considering objects closer to the sun, such as Mercury, which shows a perihelion shift, a description of the trajectory, see figure 9.3, is complex, and the corresponding Casimir energies are presumably more complicated. A more precise description would be possible by

1. First, generalize the calculations to the arbitrary metric

$$h^{\mu\nu} = \begin{pmatrix} h^{00} & 0 & 0 & 0 \\ 0 & h^{11} & h^{12} & 0 \\ 0 & h^{21} & h^{22} & 0 \\ 0 & 0 & 0 & 0 \end{pmatrix} , \tag{9.6}$$

   where the Casimir setup is assumed not to move. The dispersion relation related to the h^{00} and h^{11} elements can be found in (6.35). There can be made an educated guess how the dispersion relation of all three setups might change with respect to the h^{22} element, namely

$$\omega(\mathbf{k}) \approx c|\mathbf{k}| \left[1 - \frac{1}{2}\left(h^{00} + h^{11}\frac{k_x^2}{|\mathbf{k}|^2} + h^{22}\frac{k_y^2}{|\mathbf{k}|^2}\right)\right] . \tag{9.7}$$

   The contributions of the $h^{12} = h^{21}$ elements are expected to be more difficult due to the strong coupling in Gauss' law (5.40) and Ampère's law (5.42). Fixing the perturbed metric to a bunch of positions, as done to a single one in (6.4), the Casimir energies of the three setups could be calculated for any trajectory. However, the special relativistic influence will not be considered in this strategy.

2. The other option, which is much more accurate and challenging, is solving Maxwell's equations for a Kerr spacetime. The first advantage is having an analytically exact result, which is valid

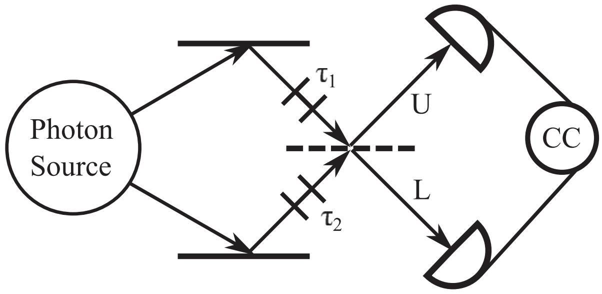

Figure 9.4.: *„Scheme of Hong-Ou-Mandel interference. Two photons are subject to optical delays $\tau_{1,2}$ and interfere on a common beam splitter to produce a joint detection statistic at the detectors U and L, which may be evaluated with a coincidence count (CC) logic" [2, quote & figure].*

for any angular momentum. Additionally, the validity of the perturbation theory approach presented in this thesis could be checked. In particular, special relativistic effects would be automatically taken into account. Furthermore, Krtouš et al. showed that the equations to be solved are separable [28]. Unfortunately, no analytical function has yet been found that solves them. This opens the possibility for further research, which applies to the Casimir effect and any electromagnetic effects in Kerr spacetime.

9.7. Quantum Optics in the presence of weak gravity

Already today, some experiments show the limits of the standard model [52]. For the „theory of everything", some unification of quantum and gravitational theory is needed. This goal still seems to be a long way off today. Therefore, quantum optics in curved spacetimes, i.e., quantum optics for (weak) gravity, would be a first step in the right direction. The Casimir effect is only one possible experimental setup to investigate this in more detail, and hopefully, the results gained in this thesis can help in the long term. An exciting question relating to quantum statistics and gravitational effects, would lead to a gravitational-influenced Hong-Ou-Mandel effect. Since bosons show bunching and fermions anti-bunching, an analog is possible with photons by controlling, for instance, their phases in the following setup: Consider a Hong-ou-Mandel setup, as shown in figure 9.4, in an asymptotically flat spacetime, see figure 3.3. Starting at the limit where the metric $g_{\mu\nu}$ is equal to the Minkowski metric $\eta_{\mu\nu}$, the results are well-known. Move the experimental setup closer and closer to the source of gravity, but do not touch or cross the event horizon. How will this affect the bunching and anti-bunching? Barzel et al. investigated „the influence of the relativistic redshift on Hong-Ou-Mandel interference" and concluded that their experimental setups is viable for a „genuine quantum test of gravity" [2]. Therefore, it is assumed that in the case of strong gravitational fields, measurable general relativistic influences will also occur and provide results at the limit between general relativity and quantum statistics. Thus, such an experiment might help to reveal the secrets behind quantum gravity.

10. Acknowledgement

I would first like to thank my thesis supervisor Priv.-Doz. Dr. Axel Pelster. Starting my thesis during the COVID-19 pandemic, I had to work from home and had less personal contact with him and the group members. Nevertheless, he took care of me highly and was always enthusiastically available for discussions. Whenever I ran into a trouble spot or had a question about my research or writing, emails were answered promptly, or zoom sessions were arranged spontaneously. He allowed this thesis to grow consistently, frequently inspired new ideas, helped me with his extensive knowledge, and did not lose sight of the goal. Furthermore, he has constantly encouraged me to attend various conferences or seminars.

I would also like to thank Prof. Dr. Michael Fleischhauer for allowing me to participate in his group seminar and being the second reviewer.

In addition, I like to acknowledge the second readers of this thesis, and I am gratefully indebted for their valuable comments on this thesis: M.Sc.-Phys. Christopher Mink, Dipl.-Phys. Martin Will, M.Sc.-Phys. Simon Ohler, Dipl.-Phys. Enrico Stein, and B.Sc.-Phys. Stefan Boschmann.

Finally, I must express my profound gratitude to my parents for providing me with unfailing support and continuous encouragement throughout my years of study, writing my Bachelor's thesis and this Master's thesis. This accomplishment would not have been possible without them. Thank you.

This page intentionally left blank.

Bibliography

[1] Ayzenberg, D., Yagi, K., Yunes, N. "Can the slow-rotation approximation be used in electromagnetic observations of black holes?" *Classical and Quantum Gravity* 33.10 (2016), p. 105006. ISSN: 0264-9381. DOI: 10.1088/0264-9381/33/10/105006.

[2] Barzel, R., Bruschi, D. E., Schell, A. W., Lämmerzahl, C. "Observer dependence of photon bunching: The influence of the relativistic redshift on Hong-Ou-Mandel interference." *Physical Review D* 105.10 (2022). ISSN: 1550-7998. DOI: 10.1103/PhysRevD.105.105016.

[3] Bezerra, V. B., Mota, H. F., Muniz, C. R. "Casimir effect due to a slowly rotating source in the weak-field approximation." *Physical Review D* 89.4 (2014). ISSN: 1550-7998. DOI: 10.1103/PhysRevD.89.044015.

[4] Bordag, M., ed. *The Casimir effect 50 years later: Proceedings of the Fourth Workshop on Quantum Field Theory Under the Influence of External conditions, 14 - 18 September 1998, Leipzig, Germany.* Singapore: World Scientific, 1999. ISBN: 981-02-3820-7.

[5] Brevik, I., Ellingsen, S. A., Milton, K. A. "Thermal corrections to the Casimir effect." *New Journal of Physics* 8.10 (2006), p. 236. DOI: 10.1088/1367-2630/8/10/236.

[6] Buhmann, S. Y. *Analytical Methods for Integrals and Differential Equations: Time-dependent pertubation theory and secular terms.* London, 2012. URL: https://www.sybuhmann.uni-freiburg.de/teaching.htm (visited on July 3, 2022).

[7] Butzer, P. L., Ferreira, P. J. S. G., Schmeisser, G., Stens, R. L. "The Summation Formulae of Euler–Maclaurin, Abel–Plana, Poisson, and their Interconnections with the Approximate Sampling Formula of Signal Analysis." *Results in Mathematics* 59.3-4 (2011), pp. 359–400. ISSN: 1422-6383. DOI: 10.1007/s00025-010-0083-8.

[8] Cabral, F., Lobo, F. S. N. "Electrodynamics and Spacetime Geometry: Foundations." *Foundations of Physics* 47.2 (2017), pp. 208–228. ISSN: 0015-9018. DOI: 10.1007/s10701-016-0051-6.

[9] Capasso, F., Munday, J. N., Iannuzzi, D., Chan, H. B. "Casimir Forces and Quantum Electrodynamical Torques: Physics and Nanomechanics." *IEEE Journal of Selected Topics in Quantum Electronics* 13.2 (2007), pp. 400–414. ISSN: 1077-260X. DOI: 10.1109/JSTQE.2007.893082.

[10] Cohen-Tannoudji, C., Diu, B., Laloë, F. *Quantenmechanik.* 4., durchges. und verb. Aufl. Berlin: de Gruyter, 2010. ISBN: 9783110224603.

[11] Cornejo, A. G. “A Lagrangian Solution for the Precession of Mercury’s Perihelion.” *International Journal of Astronomy* 3.2 (2014), pp. 31–34. DOI: 10.5923/j.astronomy.20140302.01.

[12] Cornish, N. J. *The Lagrange Points*. 1998. URL: https://map.gsfc.nasa.gov/ContentMedia/lagrange.pdf (visited on Sept. 25, 2022).

[13] Costas-Santos, R. S. “On the elementary symmetric functions of a sum of matrices.” *Journal of Algebra* (2006). DOI: Number. URL: http://arxiv.org/pdf/math/0612464v5.

[14] Fixsen, D. J. “THE TEMPERATURE OF THE COSMIC MICROWAVE BACKGROUND.” *The Astrophysical Journal* 707.2 (2009), pp. 916–920. ISSN: 0004-637X. DOI: 10.1088/0004-637x/707/2/916.

[15] Fließbach, T. *Allgemeine Relativitätstheorie*. Berlin, Heidelberg: Springer Berlin Heidelberg, 2016. ISBN: 978-3-662-53105-1. DOI: 10.1007/978-3-662-53106-8.

[16] Fosco, C. D., Lombardo, F. C., Mazzitelli, F. D. “Proximity force approximation for the Casimir energy as a derivative expansion.” *Physical Review D* 84.10 (2011). ISSN: 1550-7998. DOI: 10.1103/physrevd.84.105031.

[17] Gong, T., Corrado, M. R., Mahbub, A. R., Shelden, C., Munday, J. N. “Recent progress in engineering the Casimir effect – applications to nanophotonics, nanomechanics, and chemistry.” *Nanophotonics* 10.1 (2020), pp. 523–536. ISSN: 2192-8606. DOI: 10.1515/nanoph-2020-0425.

[18] Gradštejn, I. S., Ryžik, J. M., eds. *Table of integrals, series, and products*. 7. ed. Amsterdam: Elsevier Acad. Press, 2007. ISBN: 978-0-12-373637-6.

[19] Greiner, W., Reinhardt, J. *Field quantization: With 52 worked examples and problems*. Berlin et al.: Springer, 1996. ISBN: 3540591796.

[20] Gröbner, W., Hofreiter, N., eds. *Integraltafel: Zweiter Teil Bestimmte Integrale*. Vierte, verbesserte Auflage. Vienna and s.l.: Springer Vienna, 1966. ISBN: 978-3-211-80759-0. DOI: 10.1007/978-3-7091-3341-5.

[21] Gutzwiller, M. C. “Moon-Earth-Sun: The oldest three-body problem.” *Reviews of Modern Physics* 70.2 (1998), pp. 589–639. ISSN: 0034-6861. DOI: 10.1103/RevModPhys.70.589.

[22] Holstein, B. R. “The van der Waals interaction.” *American Journal of Physics* 69.4 (2001), pp. 441–449. ISSN: 0002-9505. DOI: 10.1119/1.1341251.

[23] Høye, J. S., Brevik, I. “Repulsive Casimir Force.” *Physical Review A* 98.2 (2018), p. 94. ISSN: 2469-9926. DOI: 10.1103/PhysRevA.98.022503. URL: http://arxiv.org/pdf/1805.06224v1.

[24] Intravaia, F., Reiche, D., Busch, K. “In der Unruhe liegt die Kraft.” *Physik Journal* (2022). URL: http://arxiv.org/pdf/2205.08351v1.

[25] Kah, P., Shrestha, M., Hiltunen, E., Martikainen, J. "Robotic arc welding sensors and programming in industrial applications." *International Journal of Mechanical and Materials Engineering* 10.1 (2015). ISSN: 1823-0334. DOI: 10.1186/s40712-015-0042-y.

[26] Kleinert, H. *Particles and quantum fields.* New Jersey et al.: World Scientific, 2016. ISBN: 9789814740906. DOI: Hagen.

[27] Korsch, H.-J. *Mathematische Ergänzungen zur Einführung in die Physik: Empfohlen für FiPS.* 4., überarb. und ergänzte Aufl. Barsinghausen: Binomi Verl., 2007. ISBN: 978-3-923923-61-8.

[28] Krtouš, P., Frolov, V. P., Kubizňák, D. "Separation of Maxwell equations in Kerr–NUT–(A)dS spacetimes." *Nuclear Physics B* 934 (2018), pp. 7–38. ISSN: 05503213. DOI: 10.1016/j.nuclphysb.2018.06.019.

[29] Lamoreaux, S. K. "Demonstration of the Casimir Force in the 0.6 to 6μm Range." *Physical Review Letters* 78.1 (1997), pp. 5–8. ISSN: 0031-9007. DOI: 10.1103/PhysRevLett.78.5.

[30] Lamoreaux, S. K. "Casimir forces: Still surprising after 60 years." *Physics Today* 60.2 (2007), pp. 40–45. ISSN: 0031-9228. DOI: 10.1063/1.2711635.

[31] Liebig, A., Peronio, A., Meuer, D., Weymouth, A. J., Giessibl, F. J. "High-precision atomic force microscopy with atomically-characterized tips." *New Journal of Physics* 22.6 (2020), p. 063040. DOI: 10.1088/1367-2630/ab8efd.

[32] Lifshitz, E. M. *The Theory of Molecular Attractive Foreces between Solids.* Ed. by Soviet Phys. JETP USSR 29, 94-110. 1956. URL: https://www.mit.edu/~kardar/research/seminars/Casimir/LifshitzTheory.pdf (visited on June 2, 2022).

[33] Marcus, M. "Determinants of Sums." *The College Mathematics Journal* 21.2 (1990), pp. 130–135. ISSN: 07468342. DOI: 10.1080/07468342.1990.11973297.

[34] Martinez, J. C., Chen, X., Jalil, M. B. A. "Casimir effect and graphene: Tunability, scalability, Casimir rotor." *AIP Advances* 8.1 (2018), p. 015330. DOI: 10.1063/1.5007787.

[35] Misner, C. W., Thorne, K. S., Wheeler, J. A., Kaiser, D. I. *Gravitation.* First Princeton University Press edition. Princeton and Oxford: Princeton University Press, 2017. ISBN: 978-0-691-17779-3.

[36] Mohideen, U., Roy, A. "Precision Measurement of the Casimir Force from 0.1 to 0.9μm." *Physical Review Letters* 81.21 (1998), pp. 4549–4552. ISSN: 0031-9007. DOI: 10.1103/PhysRevLett.81.4549.

[37] Mueller, T., Grave, F. *Catalogue of Spacetimes.* 2009. DOI: 10.48550/ARXIV.0904.4184.

[38] Nayfeh, A. H. *Perturbation methods.* A Wiley-Interscience publication. New York: Wiley, 1973. ISBN: 0-471-63059-4.

[39] Nazari, B. "Casimir effect of two conducting parallel plates in a general weak gravitational field." *The European Physical Journal C* 75.10 (2015). ISSN: 1434-6044. DOI: 10.1140/epjc/s10052-015-3732-y.

[40] Pelster, A. "Quantum Field Theory." Kaiserslautern, 2021. URL: https://www-user.rhrk.uni-kl.de/~apelster/Manuscripts/qft.pdf.

[41] Pelster, A. "Quantum Optics." Kaiserslautern, 2022. URL: https://www-user.rhrk.uni-kl.de/~apelster/Manuscripts/manuscripts.html.

[42] Pelster, A., Kleinert, H., Schanz, M. "High-Order Variational Calculation for the Frequency of Time-Periodic Solutions" (2002). DOI: 10.48550/arXiv.math-ph/0208032.

[43] Pieth, S., Köhler, U. *Our Solar System: A Short Introduction to the Bodies of our Solar System and their Exploration.* Ed. by German Aerospace Center. 2013. URL: http://europlanet.dlr.de/fileadmin/brochure_Solarsystem_2013_en_web.pdf (visited on July 21, 2022).

[44] Plebanski, J., Krasiński, A. *An introduction to general relativity and cosmology.* First paperback edition. Cambridge, New York, and Melbourne: Cambridge University Press, 2012. ISBN: 9780521856232. DOI: Jerzy.

[45] Prange, D. "Epstein-Glaser renormalization and differential renormalization." *Journal of Physics A: Mathematical and General* 32.11 (1999), pp. 2225–2238. ISSN: 0305-4470. DOI: 10.1088/0305-4470/32/11/015.

[46] Sicardy, B. "Stability of the triangular Lagrange points beyond Gascheau's value." *Celestial Mechanics and Dynamical Astronomy* 107.1-2 (2010), pp. 145–155. ISSN: 0923-2958. DOI: 10.1007/s10569-010-9259-5.

[47] Sorge, F. "Casimir effect in a weak gravitational field." *Classical and Quantum Gravity* 22.23 (2005), pp. 5109–5119. ISSN: 0264-9381. DOI: 10.1088/0264-9381/22/23/012.

[48] Stange, A., Campbell, D. K., Bishop, D. J. "Science and technology of the Casimir effect." *Physics Today* 74.1 (2021), pp. 42–48. ISSN: 0031-9228. DOI: 10.1063/PT.3.4656.

[49] Stange, A., Imboden, M., Javor, J., Barrett, L. K., Bishop, D. J. "Building a Casimir metrology platform with a commercial MEMS sensor." *Microsystems & nanoengineering* 5 (2019), p. 14. DOI: 10.1038/s41378-019-0054-5.

[50] The Johns Hopkins University Applied Physics Laboratory, ed. *THE MISSION: NASA's Parker Solar Probe mission will revolutionize our understanding of the Sun.* 2019. URL: http://parkersolarprobe.jhuapl.edu/The-Mission/index.php#Journey-to-the-Sun (visited on July 21, 2022).

[51] Verwey, E. J. W. *Theory of the stability of lyophobic colloids.* Mineola, N.Y: Dover Publications, 1948. ISBN: 9780486409290. URL: `http://www.loc.gov/catdir/description/dover031/99049862.html`.

[52] Virdee, T. S. “Beyond the standard model of particle physics.” *Philosophical transactions. Series A, Mathematical, physical, and engineering sciences* 374.2075 (2016). ISSN: 1364-503X. DOI: `10.1098/rsta.2015.0259`.

[53] Weber, A. “Interplay between Geometry and Temperature In the Casimir Effect.” Dissertation. Heidelberg: University of Heidelberg, 2010. URL: `https://www.osti.gov/etdeweb/servlets/purl/21403558` (visited on June 24, 2022).

[54] Weinberg, S. *Gravitation and cosmology: Principles and applications of the general theory of relativity.* New York, NY: Wiley, 1972. ISBN: 9780471925675.

[55] Weisstein, E. W. *CRC concise encyclopedia of mathematics.* 2. ed. Boca Raton, Fla.: Chapman & Hall/CRC, 2003. ISBN: 9781584883470. URL: `http://www.loc.gov/catdir/enhancements/fy0646/2002074126-d.html`.

[56] White, H., Vera, J., Han, A., Bruccoleri, A. R., MacArthur, J. “Worldline numerics applied to custom Casimir geometry generates unanticipated intersection with Alcubierre warp metric.” *The European Physical Journal C* 81.7 (2021). ISSN: 1434-6044. DOI: `10.1140/epjc/s10052-021-09484-z`.

[57] Wikipedia. *Lagrange-Punkte.* 2022. URL: `https://de.wikipedia.org/wiki/Lagrange-Punkte` (visited on Sept. 24, 2022).

This page intentionally left blank.

A. Secular terms in perturbation theory

Perturbation theory is a standard approximation method in physics. Moreover, such an approach often yields quite good results, although convergence is not given in general [10, chapter 11]. Exceedingly (ordinary) differential equations can often not be solved exactly, but applying perturbation theory yields an approximate result. The upcoming secular terms are examined based on a toy model from classical mechanics, where one considers some mass m at position x, which moves under the influence of a weakly non-linear force. Let us assume the anharmonic potential reads [6]

$$V(x) = \frac{1}{2}kx^2\left[1 + \frac{\varepsilon}{2}\frac{x^2}{{a_0}^2}\right] \,, \tag{A.1}$$

where k denotes Hooke's constant, a_0 is a characteristic length scale of the anharmonic potential, and ε stands for a small, dimensionless, positive parameter that describes the strength of the anharmonic potential. The Newtonian equation of motion for this system is given by [6]

$$m\ddot{x}^2 = -\frac{\mathrm{d}V(x)}{\mathrm{d}x} = -kx\left[1 + \varepsilon\frac{x^2}{{a_0}^2}\right] \,. \tag{A.2}$$

Assume the particle to be initially at some position $x(0) = x_0$ and at rest $\dot{x}(0) = 0$. Note that this differential equation should lead to a bounded solution, which satisfies energy conservation. The differential equation at hand is known as the Duffing equation, which can be solved by introducing the dimensionless variable $u = x/a_0$ and defining $\omega_0 = \sqrt{k/m}$ as the unperturbed frequency. The equation of motion (A.2) then reduces to [38, eq. (2.1.1)][6]

$$\ddot{u} + \omega_0^2 u + \varepsilon\omega_0^2 u^3 = 0 \quad \text{with } u(0) = a = \frac{x_0}{a_0}, \quad \dot{u}(0) = 0 \,. \tag{A.3}$$

To find a perturbative solution consider a divergent series in powers of the smallness parameter ε [6][38, eq. (2.1.3)]

$$u(t) = \sum_{n=0}^{\infty} u_n(t)\varepsilon^n \,, \tag{A.4}$$

and substitute this expression into (A.3). After expanding and ordering the terms in powers of ε, the zero-order equation is

$$\ddot{u}_0 + \omega_0^2 u_0 = 0 \quad \text{with } u_0(0) = a, \quad \dot{u}_0(0) = 0 \,. \tag{A.5}$$

The according first-order correction reads

$$\ddot{u}_1 + \omega_0^2 u_1 = -\omega_0^2 {u_0}^3 \quad \text{with } u_1(0) = 0, \quad \dot{u}_0(0) = 0 \;. \tag{A.6}$$

The solution of (A.5), which describes an unperturbed harmonic oscillator, reads [6][38, eq. (2.1.6)]

$$u_0(t) = a\cos(\omega_0 t) \;. \tag{A.7}$$

Inserting this into (A.6) and using the trigonometric identity $\cos^3(\theta) = \frac{3}{4}\cos(\theta) + \frac{1}{4}\cos(3\theta)$ leads to [6][38, eq. (2.1.7)]

$$\ddot{u}_1(t) + \omega_0^2 u_1(t) = -\frac{\omega_0^2 a^3}{4}\left[3\cos(\omega_0 t) + \cos(3\omega_0 t)\right] \quad \text{with } u_0(0) = 0, \quad \dot{u}_0(0) = 0 \;. \tag{A.8}$$

The solution to this inhomogeneous second-order differential equation, that satisfies the initial conditions, can be obtained via the method of variation of parameters. It reads [38]

$$u_1(t) = -\frac{a^3}{32}\left[\cos(\omega_0 t) - \cos(3\omega_0 t)\right] - \frac{3a^3}{8}\omega_0 t\sin(\omega_0 t) \;. \tag{A.9}$$

Thus [38, eq. (2.1.9)]

$$u(t) = a\cos(\omega_0 t) + \varepsilon a^3\left\{\frac{1}{32}\left[\cos(3\omega_0 t) - \cos(\omega_0 t)\right] - \frac{3}{8}\omega_0 t\sin(\omega_0 t)\right\} + \mathcal{O}\left(\varepsilon^2\right) \;, \tag{A.10}$$

seems to be the perturbative first-order solution of the anharmonic oscillator. This is not the case because, for $t \to \infty$, the term $t\sin(t)$ yields $u_1/u_0 \to \infty$ and would lead to an unbounded solution. Hence, $t\sin(t)$ is called a secular term. This kind of term often appears in the case of nonlinear oscillation problems and has the general form $t^n(\cos(t), \sin(t))$ [38, p. 25]. However, it is possible to generate a bounded solution from (A.10) by proceeding as follows.

First, combine the secular term with the zero-order contribution to write [6]

$$a\left[\cos(\omega_0 t) - \frac{3}{8}a^2\varepsilon\omega_0 t\sin(\omega_0 t)\right] \;. \tag{A.11}$$

Using first-order Taylor expansions for $\sin(\varepsilon t) \approx \varepsilon t$ and $\cos(\varepsilon t) \approx 1$ to rewrite this expression to

$$a\left[\cos(\omega_0 t)\cos\left(\frac{3}{8}a^2\varepsilon\omega_0 t\right) - \sin\left(\frac{3}{8}a^2\varepsilon\omega_0 t\right)\sin(\omega_0 t)\right] + \mathcal{O}\left(\varepsilon^2\right) \;. \tag{A.12}$$

Now apply the trigonometric addition theorem $\cos(x \mp y) = \cos(x)\cos(y) \pm \sin(x)\sin(y)$ and get

$$a\cos\left(\omega_0 t + \frac{3}{8}a^2\varepsilon\omega_0 t\right) + \mathcal{O}\left(\varepsilon^2\right) = a\cos(\omega t) + \mathcal{O}\left(\varepsilon^2\right) \;, \tag{A.13}$$

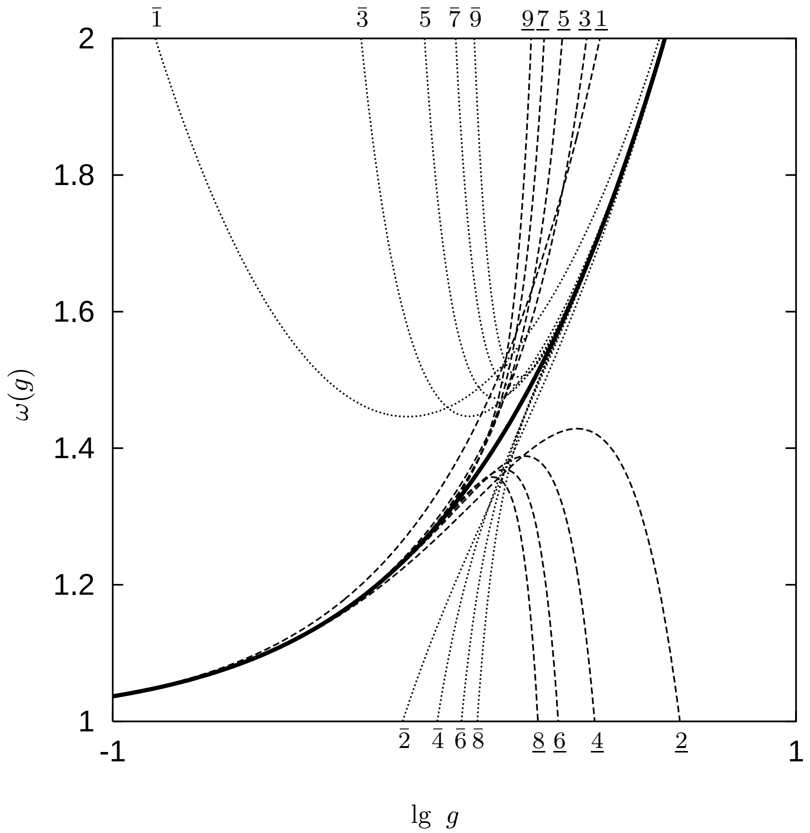

Figure A.1.: *Logarithmic plot of* (A.14) *where the solid curve represents the exact result. The dashed curves show the perturbative expansions in orders of the coupling constant $g = \varepsilon$ from $\underline{1}$ to $\underline{9}$ and their according partial sums marked with dotted curves from $\bar{1}$ to $\bar{9}$ [42].*

with $\omega = \omega_0 \left(1 + \frac{3}{8}a^2\varepsilon\right)$. Except for the generation of higher harmonics, the anharmonic oscillator behaves like a harmonic one with a new frequency ω that slightly differs from its original one ω_0. The essence of this type of perturbative renormalization, also called Poincaré-Lindstedt method, for removing secular terms is the combination of Taylor expansions and addition theorems. Reading [6, short and pedagogically prepared] or [38, chapter 2.1 & 3.1.1] are recommended for further mathematical details and other examples.

At first glance, such an expansion is only feasible for small coupling constants ε. However, it is possible to give an analytically exact result [42, eq. (21)]

$$\omega = \frac{\pi\sqrt{\omega_0^2 + \varepsilon}}{2F\left(\frac{\pi}{2}, \sqrt{\frac{\varepsilon}{2\left(\omega_0^2+\varepsilon\right)}}\right)}\,, \tag{A.14}$$

where F represents the elliptical integral of the first kind. This even allows statements to be made in the strong-coupling regime $\varepsilon \to \infty$. The essence of this investigation is „that the full function represents the envelope to all weak- and strong-coupling expansions“ [42], which is shown in figure A.1.

This page intentionally left blank.

B. Casimir calculus

In the thesis, the derivation of the Casimir energy in the case of Minkowski spacetime is performed in chapter 2. The renormalization of the upcoming difference between a series and an integral in equation (2.25) is solved using the Abel-Plana Summation Formula (APSF) in section 2.3.2. This chapter completes the derivation of the Casimir energy by applying the Euler-Maclaurin Summation Formula (EMSF) and Poisson Summation Formula (PSF), which can replace the APSF in the previous calculation. This shows concretely what Butzer et al. have proven in a mathematically correct way: „All the [three mentioned] formulae are equivalent to each other" [7, p. 364].
Due to the mathematical structure of perturbation theory in section 5.2, where the first-order inhomogeneities are given by the zeroth-order electromagnetic fields, the methods shown here can be used even for weakly curved spacetimes.

B.1. Casimir energy via Euler-Maclaurin Summation Formula

The starting point of this calculation is (2.34), where the integral

$$f(n) = \int_{|n|}^{\infty} u^2 \,\mathrm{d}u \tag{B.1}$$

appears. For suitable functions, the EMSF reads [7, eq. (1.1)]

$$\begin{aligned} \sum_{k=0}^{n} f(k) = \int_0^n f(x)\,\mathrm{d}x + \frac{1}{2}\left[f(0) + f(n)\right] + \sum_{k=1}^{r} \frac{B_{2k}}{(2k)!}\left[f^{(2k-1)}(n) - f^{(2k-1)}(0)\right] \\ + (-1)^r \sum_{k=1}^{\infty} \int_0^n \frac{\exp(\mathrm{i}2\pi kt) + \exp(-\mathrm{i}2\pi kt)}{(2\pi k)^{2r}} f^{2r}(t)\,\mathrm{d}t \ , \end{aligned} \tag{B.2}$$

where B_{2k} denotes the Bernoulli numbers. Formula (B.2) can be specialized to

$$\left(\sum_{n=0}^{\infty}{}' - \int_0^{\infty} \mathrm{d}n\right) f(n) = \frac{1}{2} f(\infty) - \sum_{p=1}^{\infty} \frac{B_{2p}}{(2p)!}\left[f^{(2p-1)}(0) - f^{(2p-1)}(\infty)\right] \ . \tag{B.3}$$

First, calculate the expression $f(\infty)$ for the integral (B.1) by inserting what is known:

$$f(\infty) = \left.\int_{|n|}^{\infty} u^2 \,\mathrm{d}u\right|_{n=\infty} = \int_{\infty}^{\infty} u^2 \,\mathrm{d}u = 0 \ . \tag{B.4}$$

Because the lower and upper boundaries coincide, the integral vanishes.

Second, derivatives of the integral with respect to the lower boundary, especially the parameter n, are needed. To this end, the relation

$$\begin{aligned}\frac{\mathrm{d}}{\mathrm{d}x}\int_{f(x)}^{a} g(t)\,\mathrm{d}t &= -\frac{\mathrm{d}}{\mathrm{d}x}\int_{a}^{f(x)} g(t)\,\mathrm{d}t \\ &= -\frac{\mathrm{d}}{\mathrm{d}x}\left[G\left(f(x)\right) - G\left(a\right)\right] \\ &= -\frac{\mathrm{d}}{\mathrm{d}x}G\left(f(x)\right) - \frac{\mathrm{d}}{\mathrm{d}x}G\left(a\right) \\ &= -g\left(f(x)\right)\frac{\mathrm{d}}{\mathrm{d}x}f(x)\;,\end{aligned} \tag{B.5}$$

that combines the theorem of integral calculus with the chain rule of differentiation, could be applied. The derivatives $f^{(2p-1)}(0)$ appearing in (B.3) are then calculated by using (B.5):

$$\begin{aligned}f^{(2p-1)}(0) &= \frac{\mathrm{d}^{2p-1}}{\mathrm{d}n^{2p-1}}\int_{|n|}^{\infty} u^2\,\mathrm{d}u\bigg|_{n=0} \\ &= -\frac{\mathrm{d}^{2p-2}}{\mathrm{d}n^{2p-2}}\left(|n|^2\frac{\mathrm{d}|n|}{\mathrm{d}n}\right)\bigg|_{n=0}\;.\end{aligned} \tag{B.6}$$

The absolute value function $|n|$ is not fundamentally differentiable in the point $n=0$. Remember that n is a natural number by the conditions given in (2.12) and (2.14). So, it is reasonable to drop the absolute value, which simplifies the derivative in (B.6) to one. Mathematically more correct would be the usage of the limit $\lim\limits_{n\to 0^+} \mathrm{d}|n|/\mathrm{d}n$, which leads to the following definition of the sign function

$$\operatorname{sgn}(x) = \begin{cases} -1 & ,\forall x<0 \\ +1 & ,\forall x\geq 0\;. \end{cases} \tag{B.7}$$

Inserting (B.7) into (B.6) yields

$$\begin{aligned}f^{(2p-1)}(0) &= -\frac{\mathrm{d}^{2p-2}}{\mathrm{d}n^{2p-2}}\left[n^2\operatorname{sgn}(n)\right]\bigg|_{n=0} \\ &= \begin{cases} 0 & ,p\neq 2 \\ -2 & ,p=2 \end{cases}\;.\end{aligned} \tag{B.8}$$

So, equation (B.3) has one non-vanishing derivative that corresponds to B_4 in (D.7). This leads, apart from a prefactor, to the Casimir energy

$$\begin{aligned}\left(\sum_{n=0}^{\infty}{}' - \int_0^{\infty}\mathrm{d}n\right)\int_{|n|}^{\infty}u^2\,\mathrm{d}u &= \frac{1}{2}f(\infty) - \sum_{p=1}^{\infty}\frac{B_{2p}}{(2p)!}\left[f^{(2p-1)}(0) - f^{(2p-1)}(\infty)\right] \\ &= -f^{(3)}(0)\frac{B_4}{4!} = -2\frac{1}{30}\frac{1}{4!} = -\frac{1}{360}\;.\end{aligned} \tag{B.9}$$

This result coincides with (2.39). Adding the appropriate physical prefactor leads to the Casimir energy

$$E_C = \hbar c A \frac{1}{2}\frac{\pi^2}{d^3}\left(-\frac{1}{360}\right) = -\frac{\hbar c \pi^2 A}{720 d^3} \ , \tag{B.10}$$

which is the same as in (1.3).

B.2. Poisson Summation Formula

The Poisson summation formula is a unique formula that uses a Fourier transformation to evaluate the difference between a series and an integral. Because the function $f(n)$ is even due to the absolute value in the lower boundary in (B.1), it is convenient to specify the PSF for even functions first.

B.2.1. Poisson Summation Formula for even functions

The PSF for suitable functions reads [7, eq. (1.6)]

$$\sum_{n=-\infty}^{\infty} f(n) = \sum_{m=-\infty}^{\infty} \int_{-\infty}^{\infty} f(x) e^{-2\pi \mathrm{i} m x} \, \mathrm{d}x \ . \tag{B.11}$$

An even function has the property $f(x) = f(-x)$. The left-hand side of (B.11) is then given by

$$\begin{aligned}
\sum_{n=-\infty}^{\infty} f(n) &= \sum_{m=-\infty}^{-1} f(n) + \sum_{m=1}^{\infty} f(n) + f(0) \\
&= \sum_{m=+\infty}^{+1} f(-n) + \sum_{m=1}^{\infty} f(n) + f(0) \\
&= \sum_{m=1}^{\infty} f(n) + \sum_{m=1}^{\infty} f(n) + f(0) \\
&= 2\sum_{m=1}^{\infty} f(n) + f(0) \ ,
\end{aligned} \tag{B.12}$$

whereas the right-hand side is represented by

$$
\begin{aligned}
&\sum_{m=-\infty}^{\infty} \int_{-\infty}^{\infty} f(x) e^{-2\pi \mathrm{i} m x} \, \mathrm{d}x \\
&= \sum_{m=-\infty}^{\infty} \int_{-\infty}^{\infty} f(x) \left[\cos(2\pi m x) - \mathrm{i} \sin(2\pi m x)\right] \mathrm{d}x \\
&= \sum_{m=-\infty}^{\infty} \left[\int_{-\infty}^{\infty} \underbrace{f(x)\cos(2\pi m x)}_{\text{even}} \, \mathrm{d}x - \mathrm{i} \int_{-\infty}^{\infty} \underbrace{f(x)\sin(2\pi m x)}_{\text{odd}} \, \mathrm{d}x \right] \\
&= \sum_{m=-\infty}^{\infty} \left[\underbrace{\int_{-\infty}^{\infty} f(x)\cos(2\pi m x) \, \mathrm{d}x}_{\equiv I(m)} - 0 \right] \\
&= \sum_{m=-\infty}^{-1} I(m) + I(0) + \sum_{m=1}^{\infty} I(m) \\
&= \sum_{m=-\infty}^{-1} I(-m) + \sum_{m=1}^{\infty} I(m) + I(0) \\
&= 2 \sum_{m=1}^{\infty} I(m) + I(0) \, .
\end{aligned}
\tag{B.13}
$$

Here it was used that

$$
I(m) = \int_{-\infty}^{\infty} f(x)\cos(2\pi m x) \, \mathrm{d}x = \int_{-\infty}^{\infty} f(x) \cos(-2\pi m x) \, \mathrm{d}x = I(-m) \tag{B.14}
$$

is an even function for the parameter m.
Equating the left- and right-hand results (B.12) and (B.13) gives rise to [41, eq. (2.218)]:

$$
\begin{aligned}
2 \sum_{m=1}^{\infty} f(n) + f(0) &= 2 \sum_{m=1}^{\infty} I(m) + I(0) \\
\Leftrightarrow \sum_{m=1}^{\infty} f(n) + \frac{f(0)}{2} &= \sum_{m=1}^{\infty} \underbrace{\int_{-\infty}^{\infty} f(x)\cos(2\pi m x) \, \mathrm{d}x}_{=\mathrm{Re}\left\{\int_{-\infty}^{\infty} f(x)\exp(-2\pi i m x)\right\}} + \underbrace{\frac{1}{2} \int_{-\infty}^{\infty} f(x) \, \mathrm{d}x}_{=\int_0^{\infty} f(x) \mathrm{d}x} \\
\Leftrightarrow \sum_{m=1}^{\infty} f(n) + \frac{f(0)}{2} - \int_0^{\infty} f(x) \, \mathrm{d}x &= \sum_{m=1}^{\infty} \mathrm{Re}\left\{ \int_{-\infty}^{\infty} f(x) \exp(-2\pi \mathrm{i} m x) \, \mathrm{d}x \right\} \\
\Leftrightarrow \left({\sum_{n=0}^{\infty}}' - \int_0^{\infty} \mathrm{d}n \right) f(n) &= \sum_{m=1}^{\infty} \mathrm{Re}\left\{ \int_{-\infty}^{\infty} f(x) \exp(-2\pi \mathrm{i} m x) \, \mathrm{d}x \right\} \, ,
\end{aligned}
\tag{B.15}
$$

which represents the final formula.

B.2.2. Casimir energy via Poisson Summation Formula

This case is a bit more mathematically involved than the ones before. The basis are special integrals from appendix D.2 and the symmetry of the function $f(n)$ itself in combination with trigonometric functions like $\sin(x)$ and $\cos(x)$. Moreover, the delta distribution $\delta(x)$, often called the delta function, is also necessary. To avoid a complete introduction in distribution theory, the axiomatically given properties are [27, eqs. (10.20) to (10.37)]:

$$\frac{1}{2\pi}\int_{-\infty}^{\infty}\exp(\mathrm{i}kx)\,\mathrm{d}k = \delta(x)\ , \tag{B.16}$$

$$\Rightarrow \frac{1}{2\pi}\int_{-\infty}^{\infty}\exp(-2\pi\mathrm{i}mx)\,\mathrm{d}x = \frac{1}{2\pi}\int_{-\infty}^{\infty}\exp(\mathrm{i}zm)\,\mathrm{d}z = \delta(m)\ , \quad \text{where } z=-2\pi x \text{ and } \mathrm{d}x = -2\pi\,\mathrm{d}z\ , \tag{B.17}$$

$$\int_a^b f(x)\delta(x-x_0) = \begin{cases} f(x_0) & a<x_0<b \\ \frac{1}{2}f(x_0) & a=x_0 \ \vee\ b=x_0 \\ 0 & x_0<a<b \ \vee\ a<b<x_0 \end{cases}\ , \tag{B.18}$$

$$\Rightarrow \int_1^{\infty}\delta(m)\,\mathrm{d}m = 0 = \sum_{m=1}^{\infty}\delta(m)\ , \tag{B.19}$$

$$\int_{-\infty}^{\infty}\delta(x-x_0))\,\mathrm{d}x = 1\ . \tag{B.20}$$

Based on this, the exact calculus for the Casimir energy is as follows:

First, use the previously derived PSF for even functions (B.15). Second, put in the concrete function $f(n)$ from (B.1):

$$\left(\sum_{n=0}^{\infty}{}' - \int_0^{\infty}\mathrm{d}n\right) f(n) = \sum_{m=1}^{\infty}\mathrm{Re}\left\{\int_{-\infty}^{\infty}\left(\int_{|x|}^{\infty}u^2\,\mathrm{d}u\right)\exp(-2\pi\mathrm{i}mx)\,\mathrm{d}x\right\}\ . \tag{B.21}$$

Third, evaluate the innermost integral:

$$\left(\sum_{n=0}^{\infty}{}' - \int_0^{\infty}\mathrm{d}n\right) f(n) = \sum_{m=1}^{\infty}\mathrm{Re}\left\{\int_{-\infty}^{\infty}\left(\lim_{N\to\infty}\frac{1}{3}u^3\Big|_{|x|}^{N}\right)\exp(-2\pi\mathrm{i}mx)\,\mathrm{d}x\right\}\ . \tag{B.22}$$

Fourth, use the theorem of integral calculus and split terms up with respect to the boundaries:

$$\left(\sum_{n=0}^{\infty}{}' - \int_0^{\infty}\mathrm{d}n\right) f(n) = \frac{1}{3}\sum_{m=1}^{\infty}\mathrm{Re}\left\{\left[\lim_{N\to\infty}N^3\int_{-\infty}^{\infty}\exp(-2\pi\mathrm{i}mx)\,\mathrm{d}x - \int_{-\infty}^{\infty}|x|^3\exp(-2\pi\mathrm{i}mx)\,\mathrm{d}x\right]\right\}\ . \tag{B.23}$$

Fifth, apply the definition of the delta function to the first term (B.17) and use the symmetry of the integrand in the second term to shift the boundaries:

$$\left(\sum_{n=0}^{\infty}{}' - \int_0^{\infty}\mathrm{d}n\right) f(n) = \frac{1}{3}\sum_{m=1}^{\infty}\mathrm{Re}\left\{\lim_{N\to\infty}N^3\delta(m) - 2\int_0^{\infty}|x|^3\exp(-2\pi\mathrm{i}mx)\,\mathrm{d}x\right\}\ . \tag{B.24}$$

Sixth, evaluate the terms separately and recognize that the summation starts at $m = 1$, but the delta function is only non-zero at $m = 0$ according to (B.19), so the first term can be dropped. Further, prepare the second term for the „complex Schwinger trick“:

$$\left(\sum_{n=0}^{\infty}{}' - \int_0^{\infty} \mathrm{d}n \right) f(n) = -\frac{1}{3} \sum_{m=1}^{\infty} \mathrm{Re}\left\{ 2 \int_0^{\infty} x^{4-1} \exp(-\mathrm{i}(2\pi m)x)\, \mathrm{d}x \right\} . \tag{B.25}$$

Seventh, proceed to the Schwinger trick (D.15):

$$\left(\sum_{n=0}^{\infty}{}' - \int_0^{\infty} \mathrm{d}n \right) f(n) = -\frac{2}{3} \sum_{m=1}^{\infty} \frac{\Gamma(4)}{(2\pi m)^4} . \tag{B.26}$$

Eighth, use the definition of the zeta function (D.1) and put in the concrete values of the appearing gamma- and zeta functions from (D.2), (D.4):

$$\left(\sum_{n=0}^{\infty}{}' - \int_0^{\infty} \mathrm{d}n \right) f(n) = -\frac{2}{3} \frac{1}{16\pi^4} \Gamma(4)\zeta(4) = -\frac{2}{3} \frac{1}{16\pi^4}\, 6\, \frac{\pi^4}{90} = -\frac{1}{360} \tag{B.27}$$

Ninth, add the prefactor, and the whole Casimir energy is given by

$$E_C = \hbar c A \frac{1}{2} \frac{\pi^2}{d^3} \left(-\frac{1}{360} \right) = -\frac{\hbar c \pi^2 A}{720 d^3} , \tag{B.28}$$

which is the same as in previous calculations and in accordance with (1.3).

C. Determinants of Sums

Evaluating the expression $\det(A+B)$ for arbitrary $n \times n$ matrices A and B is challenging. For this reason, an expansion in elementary symmetric functions S_k, defined via [13, eq. (3)]

$$S_k(A) = \sum_{|\alpha|=k} \det(A(\alpha,\alpha)) \;, \tag{C.1}$$

is applied. Here $\alpha \subseteq \{1,\ldots,n\}$ denotes an index set, and $A(\alpha,\alpha)$ represents the submatrix that lies in the rows and columns of A indexed by α, and the sum goes over the cardinality $|\alpha|$ of the index set α, which involves several permutations. Recognize that the binomial $\binom{n}{k}$ gives the number of possibilities for the index set. Note two exceptional cases of these functions [13]:

$$\begin{aligned} S_1(A) &= \mathrm{Tr}(A) \;, \\ S_n(A) &= \det(A) \;. \end{aligned} \tag{C.2}$$

The important formula for the determinant of 4×4 matrices reads [13, p. 7]

$$\begin{aligned} S_4(A+B) = S_4(A) &+ S_4(B) - S_1(A^3B) - S_1(A^2B^2) - S_1(AB^3) \\ &+ S_1(A^2B)S_1(A) + S_1(A^2B)S_1(B) + S_1(AB^2)S_1(A) \\ &+ S_1(AB^2)S_1(B) - S_1(AB)S_1(A)S_1(B) + S_3(A)S_1(B) \\ &+ S_3(B)S_1(A) + S_2(A)S_2(B) - S_2(A)S_1(AB) - S_2(B)S_1(AB) + S_2(AB) \;. \end{aligned} \tag{C.3}$$

C.1. General formula for 4×4 matrices

In general relativity 4×4 matrices are the quantities of interest. Therefore, $S_2(A)$, $S_3(A)$, and $S_4(A) = \det(A)$ are computed for an arbitrary 4×4 matrix A

$$A = \begin{pmatrix} a_{11} & a_{12} & a_{13} & a_{14} \\ a_{21} & a_{22} & a_{23} & a_{24} \\ a_{31} & a_{32} & a_{33} & a_{34} \\ a_{41} & a_{42} & a_{43} & a_{44} \end{pmatrix} \;. \tag{C.4}$$

The calculation for $S_2(A)$ goes as follows:

First, $k=2$ leads to $\binom{4}{2} = 6$ different index sets α, namely $\{1,2\}$, $\{1,3\}$, $\{1,4\}$, $\{2,3\}$, $\{2,4\}$, $\{3,4\}$.

Second, the resulting submatrices and their corresponding determinants read

$$A(\{1,2\},\{1,2\}) = \begin{pmatrix} a_{11} & a_{12} \\ a_{21} & a_{22} \end{pmatrix} \implies \det(A(\{1,2\},\{1,2\})) = a_{11}a_{22} - a_{12}a_{21} \ , \tag{C.5}$$

$$A(\{1,3\},\{1,3\}) = \begin{pmatrix} a_{11} & a_{13} \\ a_{31} & a_{33} \end{pmatrix} \implies \det(A(\{1,3\},\{1,3\})) = a_{11}a_{33} - a_{13}a_{31} \ , \tag{C.6}$$

$$A(\{1,4\},\{1,4\}) = \begin{pmatrix} a_{11} & a_{14} \\ a_{41} & a_{44} \end{pmatrix} \implies \det(A(\{1,4\},\{1,4\})) = a_{11}a_{44} - a_{14}a_{41} \ , \tag{C.7}$$

$$A(\{2,3\},\{2,3\}) = \begin{pmatrix} a_{22} & a_{23} \\ a_{32} & a_{33} \end{pmatrix} \implies \det(A(\{2,3\},\{2,3\})) = a_{22}a_{33} - a_{23}a_{32} \ , \tag{C.8}$$

$$A(\{2,4\},\{2,4\}) = \begin{pmatrix} a_{22} & a_{24} \\ a_{42} & a_{44} \end{pmatrix} \implies \det(A(\{2,4\},\{2,4\})) = a_{22}a_{44} - a_{24}a_{42} \ , \tag{C.9}$$

$$A(\{3,4\},\{3,4\}) = \begin{pmatrix} a_{33} & a_{34} \\ a_{43} & a_{44} \end{pmatrix} \implies \det(A(\{3,4\},\{3,4\})) = a_{33}a_{44} - a_{34}a_{43} \ . \tag{C.10}$$

Third, sum up the determinants according to (C.1) and get

$$\begin{aligned} S_2(A) = a_{11}a_{22} - a_{12}a_{21} + a_{11}a_{33} - a_{13}a_{31} + a_{11}a_{44} - a_{14}a_{41} \\ + a_{22}a_{33} - a_{23}a_{32} + a_{22}a_{44} - a_{24}a_{42} + a_{33}a_{44} - a_{34}a_{43} \ . \end{aligned} \tag{C.11}$$

Specializing this for symmetric matrices $a_{ij} = a_{ji}$ yields

$$\begin{aligned} S_2(A) = a_{11}\left(a_{22} + a_{33} + a_{44}\right) + a_{22}\left(a_{33} + a_{44}\right) + a_{33}a_{44} \\ - a_{12}^2 - a_{13}^2 - a_{14}^2 - a_{23}^2 - a_{24}^2 - a_{34}^2 \end{aligned} \tag{C.12}$$

and for diagonal matrices $a_{ij} = a_{ji} = 0$, $a_{ii} \neq 0$

$$S_2(A) = a_{11}\left(a_{22} + a_{33} + a_{44}\right) + a_{22}\left(a_{33} + a_{44}\right) + a_{33}a_{44} \ . \tag{C.13}$$

In the same way, and using the rule of Sarrus for the 3×3 submatrices, it can be shown that

$$\begin{aligned} S_3(A) = \ & a_{11}a_{33}\left(a_{22} + a_{44}\right) + a_{22}a_{44}\left(a_{11} + a_{33}\right) \\ & + a_{12}a_{23}a_{31} + a_{13}a_{21}a_{32} + a_{12}a_{24}a_{41} + a_{14}a_{21}a_{42} \\ & + a_{13}a_{34}a_{41} + a_{14}a_{31}a_{43} + a_{23}a_{34}a_{42} + a_{24}a_{32}a_{43} \\ & - a_{11}\left(a_{23}a_{32} + a_{42}a_{24} + a_{43}a_{34}\right) \\ & - a_{22}\left(a_{31}a_{13} + a_{41}a_{14} + a_{43}a_{34}\right) \\ & - a_{33}\left(a_{21}a_{12} + a_{41}a_{14} + a_{42}a_{24}\right) \\ & - a_{44}\left(a_{21}a_{12} + a_{31}a_{13} + a_{32}a_{23}\right) \ , \end{aligned} \tag{C.14}$$

For symmetric matrices $a_{ij} = a_{ji}$ this leads to

$$\begin{aligned} S_3(A) = {} & a_{11}a_{33}\left(a_{22}+a_{44}\right) + a_{22}a_{44}\left(a_{11}+a_{33}\right) \\ & + 2a_{12}a_{23}a_{13} + 2a_{12}a_{24}a_{14} + 2a_{13}a_{14}a_{34} + 2a_{23}a_{24}a_{34} \\ & - a_{11}\left(a_{23}^2 + a_{24}^2 + a_{34}^2\right) - a_{22}\left(a_{13}^2 + a_{14}^2 + a_{34}^2\right) \\ & - a_{33}\left(a_{12}^2 + a_{14}^2 + a_{24}^2\right) - a_{44}\left(a_{12}^2 + a_{13}^2 + a_{23}^2\right) \ , \end{aligned} \tag{C.15}$$

and for diagonal matrices $a_{ij} = A_{ji} = 0$, $a_{ii} \neq 0$

$$S_3(A) = a_{11}a_{33}\left(a_{22}+a_{44}\right) + a_{22}a_{44}\left(a_{11}+a_{33}\right) \ . \tag{C.16}$$

The complete formula for $S_4(A+B) = \det(A+B)$ is obtained by following the rules of matrix calculus and inserting the expressions (C.2), (C.11), and (C.14) into (C.3). Because of the final formula is rather longish and not necessary for the thesis it is not explicitly shown here. The relevant expression is calculated in the next section C.2.

C.2. Application for the Slow-Rotation Approximation

To evaluate the vital expression in section 5.1, assume

$$A = \begin{pmatrix} 1 & 0 & 0 & 0 \\ 0 & -1 & 0 & 0 \\ 0 & 0 & -1 & 0 \\ 0 & 0 & 0 & -1 \end{pmatrix} = A^{-1}, \qquad B = \begin{pmatrix} b_{11} & b_{12} & b_{13} & 0 \\ b_{21} & b_{22} & b_{23} & b_{24} \\ b_{31} & b_{32} & b_{33} & b_{34} \\ 0 & b_{42} & b_{43} & b_{44} \end{pmatrix} . \tag{C.17}$$

The matrix A has the following important properties: $A = A^{-1}$, A is diagonal, $\det(A) = S_4(A) = -1$, $A^2 = I_4$ equals the 4×4 unity matrix. The elements of the determinant given in (C.3) read

$$
\begin{aligned}
S_1(A) = \mathrm{Tr}(A) &= -2 \;, && \text{(C.18)}\\
S_1(B) = \mathrm{Tr}(B) = S_1(A^2B) &= b_{11} + b_{22} + b_{33} + b_{44} \;, && \text{(C.19)}\\
S_1(AB) = \mathrm{Tr}(AB) &= b_{11} - b_{22} - b_{33} - b_{44} \;, && \text{(C.20)}\\
S_2(A) &= 0 \;, && \text{(C.21)}\\
S_2(B) &= b_{11}\left(b_{22} + b_{33} + b_{44}\right) + b_{22}\left(b_{33} + b_{44}\right) && \\
&\quad + a_{33}a_{44} - b_{12}^2 - b_{13}^2 - b_{23}^2 - b_{24}^2 - b_{34}^2 \;, && \text{(C.22)}\\
S_2(AB) &= b_{11}\left(b_{22} + b_{33} + b_{44}\right) - b_{22}\left(b_{33} - b_{44}\right) && \\
&\quad - a_{33}a_{44} + b_{12}^2 + b_{13}^2 + b_{23}^2 + b_{24}^2 + b_{34}^2 \;, && \text{(C.23)}\\
S_3(A) &= 2 \;, && \text{(C.24)}\\
S_3(B) &= b_{11}b_{33}\left(b_{22} + b_{44}\right) + b_{22}a_{44}\left(b_{11} + b_{33}\right) && \\
&\quad + 2b_{12}b_{23}b_{13} + 2b_{23}b_{24}b_{34} && \\
&\quad - b_{11}\left(b_{23}^2 + b_{24}^2 + b_{34}^2\right) - b_{22}\left(b_{13}^2 + b_{34}^2\right) && \text{(C.25)}\\
&\quad - b_{33}\left(b_{12}^2 + b_{24}^2\right) - b_{44}\left(b_{12}^2 + b_{13}^2 + b_{23}^2\right) \;, && \\
S_4(A) = \det(A) &= -1 \;, && \text{(C.26)}\\
S_4(B) = \det(B) &= b_{34}^2b_{12}^2 - b_{33}b_{44}b_{12}^2 + 2b_{13}b_{12}\left(b_{23}b_{44} - b_{24}b_{34}\right) && \\
&\quad - b_{11}b_{22}b_{34}^2 - b_{11}b_{24}^2b_{33} + b_{14}^2\left(b_{23}^2 - b_{22}b_{33}\right) && \\
&\quad + 2b_{11}b_{23}b_{24}b_{34} - 2b_{14}\big[b_{13}\left(b_{23}b_{24} - b_{22}b_{34}\right) && \text{(C.27)}\\
&\quad + b_{12}\left(b_{23}b_{34} - b_{24}b_{33}\right)\big] - b_{11}b_{23}^2b_{44} && \\
&\quad + b_{11}b_{22}b_{33}b_{44} + b_{13}^2\left(b_{24}^2 - b_{22}b_{44}\right) \;. &&
\end{aligned}
$$

Assume that the matrix B is proportional to a small parameter ε and only the first-order correction is relevant. Then, all terms proportional to any matrix entry b_{ij}^2 vanish. Especially terms proportional to B^2 can be dropped, which means that the only remaining terms are $S_4(A)$, $S_3(A)$, $S_1(A)$, $S_1(B)$, and $S_1(AB)$. Thus, equation (C.3) reduces to

$$
S_4(A+B) = \det(A+B) \approx S_4(A) - S_1(AB) + S_1(B)S_1(A) + S_3(A)S_1(B) - S_2(A)S_1(AB) + \mathcal{O}\big(\varepsilon^2\big) \;. \tag{C.28}
$$

The terms (C.18) to (C.27) simplify a lot, for just considering first-order terms and inserting those into (C.3) leads to

$$
\begin{aligned}
\det(A+B) &= -1 - \left(b_{11} - b_{22} - b_{33} - b_{44}\right) - 2\left(b_{11} + b_{22} + b_{33} + b_{44}\right) + 2\left(b_{11} + b_{22} + b_{33} + b_{44}\right) + \mathcal{O}\big(\varepsilon^2\big)\\
&= -1 - b_{11} + b_{22} + b_{33} + b_{44} + \mathcal{O}\big(\varepsilon^2\big)\\
&= \det(A) - \mathrm{Tr}\big(A^{-1}B\big) + \mathcal{O}\big(\varepsilon^2\big) \;.
\end{aligned} \tag{C.29}
$$

If necessary, higher orders can be obtained analogously.

D. Formulary

This section summarizes the most essential functions and numbers, which are not elementarily known, in a short collection of formulae.

D.1. Special functions/numbers

The zeta function ζ in this thesis always refers to Riemann's zeta function in the following way [18, eq. 9.522(1)]

$$\forall\,\mathrm{Re}(z) > 1 : \zeta(z) = \sum_{n=1}^{\infty} \frac{1}{n^z} \; . \tag{D.1}$$

Some important values are [55, p. 2564]:

$$\begin{aligned} &\zeta(1) = \infty \; , \quad \zeta(2) = \frac{\pi^2}{6} \; , \quad \zeta(3) \approx 1.202 \; , \\ &\zeta(4) = \frac{\pi^4}{90} \; , \quad \zeta(5) \approx 1.037 \; , \quad \zeta(6) = \frac{\pi^6}{945} \; . \end{aligned} \tag{D.2}$$

The gamma function Γ for natural numbers n is given by [18, eq. 8.339(1)]

$$\forall n \in \mathbb{N}^+ : \Gamma(n) = (n-1)! \; . \tag{D.3}$$

Some important values read:

$$\begin{aligned} &\Gamma(1) = 1 \; , \quad \Gamma(2) = 1 \; , \quad \Gamma(3) = 2 \; , \\ &\Gamma(4) = 6 \; , \quad \Gamma(5) = 24 \; , \quad \Gamma(6) = 120 \; . \end{aligned} \tag{D.4}$$

Special numbers, that appear due to the integrals or the formulae itself, e.g. (B.2), are the Bernoulli numbers B_n that are defined via [18, eq. 9.610]

$$\frac{t}{\exp(t) - 1} = \sum_{n=0}^{\infty} B_n \frac{t^n}{n!} \quad \text{for } 0 < |t| < 2\pi \; . \tag{D.5}$$

For even Bernoulli numbers there exists a representation via the following integral [18, eq. 9.611(1)]

$$\forall n \in \mathbb{N}^+ : B_{2n} = (-1)^{n-1} 4n \int_0^{\infty} \frac{x^{2n-1}}{\exp(2\pi x) - 1}\, \mathrm{d}x \;\; , \tag{D.6}$$

which is equal to (D.10). The first four even Bernoulli numbers, that are sufficient for this thesis, read [18, eq. 9.71]

$$B_0 = 1, \qquad B_2 = \frac{1}{6}, \quad B_4 = -\frac{1}{30}, \quad B_6 = \frac{1}{42}\,. \tag{D.7}$$

D.2. Integrals

The following integrals are useful in this thesis and appear in general using the APSF for renormalization.
The first six expressions are related to either the gamma function Γ, the zeta function ζ, or the even Bernoulli numbers B_{2n} [20, p. 60, 61] [these and further formulae 18, p. 353 et seqq. & p. 1040 et seq.].
The last two integrals are sometimes called the „(complex) Schwinger trick“ and can be obtained using the residue theorem for a closed contour over a quarter circle with radius R around the origin of the coordinate system [18, eq. 3.381(4), 3.381(7)][41, chapter 2.16].

$$\forall \kappa \in \mathbb{R}^+ \, \forall \alpha \in \mathbb{R}^+ : \int_0^\infty \frac{x^\kappa}{e^{\alpha x} - 1}\,\mathrm{d}x = \alpha^{-\kappa-1}\Gamma(\kappa+1)\zeta(\kappa+1) \tag{D.8}$$

$$\forall n \in \mathbb{N}^+ \, \forall \alpha \in \mathbb{R}^+ : \int_0^\infty \frac{x^{2n-1}}{e^{\alpha x} - 1}\,\mathrm{d}x = \frac{|B_{2n}|}{4n}\left(\frac{2\pi}{\alpha}\right)^{2n} \tag{D.9}$$

$$\forall n \in \mathbb{N}^+ : \int_0^\infty \frac{x^{2n-1}}{e^{2\pi x} - 1}\,\mathrm{d}x = \frac{|B_{2n}|}{4n} \tag{D.10}$$

$$\forall \kappa \in \mathbb{R}_{>\text{-}1} \, \forall \alpha \in \mathbb{R}^+ : \int_0^\infty \frac{x^\kappa}{e^{\alpha x} + 1}\,\mathrm{d}x = \alpha^{-\kappa-1}(1-2^{-\kappa})\Gamma(\kappa+1)\zeta(\kappa+1) \tag{D.11}$$

$$\forall n \in \mathbb{N}^+ \, \forall \alpha \in \mathbb{R}^+ : \int_0^\infty \frac{x^{2n-1}}{e^{\alpha x} + 1}\,\mathrm{d}x = \frac{2^{2n-1}-1}{2n}|B_{2n}|\left(\frac{\pi}{\alpha}\right)^{2n} \tag{D.12}$$

$$\forall n \in \mathbb{N}^+ : \int_0^\infty \frac{x^{2n-1}}{e^{2\pi x} + 1}\,\mathrm{d}x = \frac{2^{-2n-2}\left(2^{2n}-2\right)}{n}|B_{2n}| \tag{D.13}$$

$$\forall\, \mathrm{Re}\{\mu\} > 0 \, \forall\, \mathrm{Re}\{\nu\} > 0 : \int_0^\infty x^{\nu-1} e^{-\mu x}\,\mathrm{d}x = \frac{\Gamma(\nu)}{\mu^\nu} \tag{D.14}$$

$$\forall 0 < \mathrm{Re}\{k\} < 1 \, \forall \mu \in \mathbb{R}\backslash\{0\} : \int_0^\infty x^{k-1} e^{\mathrm{i}\mu x}\,\mathrm{d}x = \frac{\Gamma(k)}{(-\mathrm{i}\mu)^k} \tag{D.15}$$